FINAL REPORT

(NASA-CR-169130) STUDY OF BOUNDARY-LAYER TRANSITION USING TRANSONIC CONE PRESTON TUBE DATA Final Report (Oklahoma State Univ., Stillwater.) 127 p HC A07/MF A01 CSCL 20D

N82-28579

Unclas

G3/34 28412

FINAL REPORT

STUDY OF BOUNDARY-LAYER TRANSITION USING TRANSONIC-CONE PRESTON-TUBE DATA

Research Grant Number NSF-2396

Principal Investigators

T. D. Reed and P. M. Moretti

Prepared by

T. D. Reed and A. Abu-Mostafa

July 1982

School of Mechanical and Aerospace Engineering

Oklahoma State University

Stillwater, Oklahoma 74078

The NASA Technical Officer for this Grant is:

F. W. Steinle, Jr.

Experimental Investigations Branch, 227-5

NASA Ames Research Center

Moffett Field, California 94035

ABSTRACT

Preston-tube data have been obtained on a sharp-nose, ten-degree cone in the NASA Ames 11-ft TWT and in flight tests. During analyses of the laminar-boundary-layer data , errors were discovered in both the wind-tunnel and the flight data. The apparent errors in the 11-ft TWT data are relatively minor and were easily corrected. However, the errors in the flight data are much more severe. A great deal of effort was expended in the search for a rational procedure for correcting this data. A correction procedure is recommended which forces the flight data to exhibit some of the orderly characteristics of the wind-tunnel data.

Subsequent to correcting the wind-tunnel data, a correlation is developed between Preston-tube pressures and the corresponding values of theoretical laminar skin friction. Because of the uncertainty in correcting the flight data, a correlation for the unmodified data is developed, and, in addition, three other correlations are developed based on different correction procedures. Each of these correlations are used in conjunction with the wind-tunnel correlation to define "effective" freestream unit Reynolds numbers for the 11-ft TWT over a Mach number range of 0.30 to 0.95. Using the preferred correlation, based on the recommended rearrangement of the flight data, the maximum effective Reynolds numbers are approximately 6.5% higher than the normal values over a unit Reynolds number range of 9.8 to 16.4 million per meter. These maximum values occur between freestream Mach numbers of 0.60 and 0.80. Smaller values are found outside this Mach number range. These results indicate wind-tunnel noise effects the average laminar skin friction much less than it effects boundary-layer transition.

Data on the onset, extent, and end of boundary-layer-transition are also summarized for these tests. The wind-tunnel data indicate a Reynolds number, based on distance to end-of-transition, is a unique function of noise and Mach number.

Finally, a procedure is described for studying the relative effects of varying nose radius on a ten-degree cone at supercritical speeds. Preliminary results indicate increasing nose radius promotes boundary-layer transition and separation of laminar boundary layers.

TABLE OF CONTENTS

LIST OF ILLUSTRATIONS

NOMENCLATURE

C_f	Skin-friction coefficient ($2\tau_w/\rho_e U_e^2$)
$\bar{C}_f$	Nondimensional difference between theoretical and correlated skin-friction coefficient $[(C_{f,t} - C_{f,c})/C_{f,t}]$
C_p	Pressure coefficient based on the difference between a Pitot and static pressure reading $[(P_p - P_w)/q_\infty]$
$(C_p)_c$	Pressure coefficient on surface of cone $[(P_w - P_\infty)/q_\infty]$
$(C_p)_{rms}$	Fluctuating pressure coefficient based on microphone data
d	External diameter of a round Pitot probe
D	Internal diameter of a pipe; in Appendix B, denotes diameter of base of cone
h	External height of face of a flattened Pitot probe
H	Boundary layer shape factor (δ^*/θ)
K_{eff}	Nondimensional effective height of Preston tube ($2Y_{eff}/h$)
L	Axial length of cone, 44.5 in.
M	Mach number
M_τ	Friction Mach number, $(\tau_w/\gamma P_w)^{\frac{1}{2}}$
P_e	Static pressure at outer edge of boundary layer
P_p	Preston tube pressure
P_w	Static pressure at wall
ΔP_p	Difference in pressure between a Preston tube and wall pressure
q_∞	Freestream dynamic pressure ($\rho U_\infty^2/2$)
R_d	Reynolds number based on U_p and external diameter of a circular Preston tube ($U_p d/\nu_e$) or height of a flattened probe ($U_p h/\nu_e$)
R_D	Reynolds number based on diameter of a sphere and freestream conditions
R_s^*	Reynolds number based on surface length from stagnation point and ν evaluated at the reference temperature of Sommer and Short ($U_e S/\nu'$)
R_τ	Reynolds number, based on probe height and wall properties, $U_\tau h/\nu_w$
Re_c	Critical Reynolds number for a sphere
Re_d	Reynolds number based on external diameter of a circular Preston tube and properties at outer edge of boundary layer, $U_e d/\nu_e$

Re_D	Reynolds number for incompressible flow thru a pipe of diameter D, $(U_m D/\nu)$
Re_m	Freestream unit Reynolds number per meter (U_∞/ν_∞)
$(Re_m)_{eff}$	Effective freestream unit Reynolds number per meter
Re_t	Reynolds number based on properties at outer edge of boundary layer and X_t
Re_T	Reynolds number based on freestream properties and X_T
S	Surface distance measured from a stagnation point
T	Temperature
u	Velocity parallel to bounding surface
u^+	Nondimensional velocity used in the law-of-the-wall (u/U_τ)
U	Velocity parallel to axis of cone
U_e	Velocity at outer edge of boundary layer
U_m	Mean or average velocity in a pipe flow
U_p	Velocity calculated from Preston-tube data and P_w
U_τ	Classical wall-shear-stress velocity $(\tau_w/\rho)^{0.5}$
U_∞	Freestream velocity
w	External width of face of a flattened Pitot probe in a direction parallel to the wall but normal tot he undisturbed streamlines
x	Distance along axis of cone
x*	Dimensionless pressure difference for incompressible flow $\log_{10}[\Delta P_p\ d^2/4\ \rho\nu^2]$
X	Distance along surface of cone; Appendix B, distance along axis measured from apex of a sharp-nose cone
X_ℓ	Most forward station at which Preston-tube measurements began
X_t	Distance along surface of cone from apex to onset of boundary-layer transition
X_T	Distance along surface of cone from apex to end of boundary-layer transition
X*	Dimensionless pressure difference for compressible, nonadiabatic flow $\log_{10}(U_p\ Y_{eff}/\nu_w)^2$
X_A*	Allen's correlation parameter $\log_{10}(U_p\ d/\nu')$
ΔX	Length of boundary-layer-transition zone

y	Distance measured normal to the wall; Appendix B, denotes perpendicular distance from axis of cone
y_c	Distance of geometric center of Preston-tube from wall
y^+	Nondimensional distance from the wall as used in the law-of-the-wall ($U_\tau y/\nu$)
y^*	Dimensionless shear stress for incompressible, isothermal flow $\log_{10}[\tau_w d^2/4\rho\nu^2$ or $0.25(U_\tau d/\nu)^2]$
Y_{eff}	Effective height of face of Preston tube = height of an undisturbed streamline above the wall which has a total pressure equal to the measured Pitot pressure
Y^*	Dimensionless shear stress for compressible, nonadiabatic flow $\log_{10}(\tau_w Y_{eff}^2/\rho_w \nu_w^2)$
Y_A^*	Allen's correlation parameter $\log_{10}(\sqrt{2}\, U_\tau d/\nu')$

Greek Letters

α	Angle-of-attack, defined to be positive for nose up
β	Yaw angle, defined to be positive when nose is to portside
$\bar{\alpha}$	Total effective angle-of-attack, $(\alpha^2 + \beta^2)^{\frac{1}{2}}$
δ	Boundary layer thickness
δ^*	Displacement thickness for compressible boundary layer
θ	Momentum thickness for compressible boundary layer
μ	Molecular viscosity
ν	Kinematic viscosity
ρ	Density of fluid
τ_w	Shear stress at wall
τ_w	Nondimensional wall shear stress $(\tau_w d^2/\rho\nu_w^2)$
ϕ	Azimuthal angle, measured clockwise (looking forward) from the top of cone

I. INTRODUCTION

A. Background

Since the 1920's, it has been known that freestream turbulence within wind tunnels caused differences between ostensibly identical tests in different wind tunnels and in flight. It was discovered, during these early years, that these differences in low-speed wind-tunnel tests could be accounted for by defining an "effective" freestream unit Reynolds number which was higher than the corresponding flight unit Reynolds number. The now classical procedure for defining an "effective" freestream Reynold number was developed based on the drag of a sphere. This procedure is based on the well-known fact (even in the 1920's) that the drag coefficient of a sphere (and a circular cylinder) drops sharply at a critical Reynolds number of the order of 10^5. This sharp drop in drag coefficient is caused by transition from a laminar to a turbulent boundary layer near the shoulder of the sphere. The turbulent boundary layer remains attached over a longer distance along the surface of the sphere and thereby reduces form drag.

According to Pope and Harper[1], a convention was eventually adopted to define the critical Reynolds number as the one which corresponds to a sphere drag coefficient of 0.30, which occurs roughly at the maximum in $d(C_D)/d(R_D)$. Careful measurements in free-air showed that the critical Reynolds number was approximately 385,000. The values measured in wind tunnels were always found to be less. This led to the formulation of a turbulence factor defined as the ratio of the free-air critical Reynolds number divided by the corresponding wind-tunnel value, i.e.,

$$TF = 385{,}000/(Re_c)_{WT} \quad .$$

The "effective" tunnel unit Reynolds number is then defined by

$$(Re_{ft})_{eff} = (TF)\ (Re_m) \quad .$$

Additional details of this procedure can be found in Ref. 1. Unfortunately, this method becomes inaccurate above $M_\infty = 0.35$ as compressibility effects become important. In particular, the sphere generates a rather strong shock slightly downstream of the shoulder of the sphere at high subsonic Mach numbers. This phenomena changes the relation between drag and Reynolds number, e.g., see Lu[2].

In low-speed tunnels ($M_\infty < 0.50$) the freestream unsteadiness is predominantly vorticity which is controlled in modern tunnels by a carefully designed turbulence-management section upstream of the test section, e.g., Loehrke and Nagib[3] and Eckert, et al.[4] Whereas, in transonic tunnels the dominant source of flow unsteadiness is wall-generated noise caused by flow through and across the ventilated test-section walls which are required to establish steady flow near Mach one. The noise intensity levels in transonic tunnels typical peak between $M_\infty = 0.70$ and 0.80, e.g., Reed, et al.[5] The AEDC Boundary Layer Transition Cone (see Fig. 1) was designed to calibrate the effects of noise on boundary-layer transition. It is superior to a sphere because a sharp-nose cone does not generate a significant transonic shock.* The need for such a calibration device was indicated by discrepancies between numerous transonic wind-tunnel tests of models at ostensibly identical flow conditions. A particularly well-documented study of differences in static aerodynamic data has been obtained with the same model of a C-5A transport aircraft in three major transonic wind tunnels; the results have been reported by Treon, et al.[6] The differences between the three different sets of tunnel data were reduced by accounting for "relative" Reynolds number effects between facilities. The AEDC 10-deg cone was used to define the differences in "relative" Reynolds number. As noted by Dougherty and Steinle:

> "These results substantiated the need for developing a method for predicting these corrections to Reynolds number to improve the extrapolation of wind-tunnel test results to full-scale flight conditions, i.e., a "turbulence factor" for transonic tunnels. Although the "effect" associated with these differences in transition characteristics between tunnels is of prime importance in adjusting the data, the "cause" is of particular significance since it relates directly to predicting the "effect" in new and different facilities. This illustration of improvement in agreement of results between transonic facilities suggests the use of transition Reynolds number for such corrections to be both technically appropriate and productive."

In 1971, an extensive test program was begun in which the AEDC-BLT cone was tested with the same probe-traversing mechanism and instrumentation, see Fig. 1. (Additional details of the cone are given in Refs. 7 and 8.) In addition, the cone was accompanied by Dougherty from AEDC in order to assure test procedures were matched as closely as possible. The primary purpose of this program was to simply detect the location of the boundary-layer-transition-zone on the cone in different wind tunnels and in free-flight but at

*See Appendix B for further discussion of the effects of nose bluntness on transonic flow about cones.

NOTE: CS = Cone Station = Distance in inches aft of the nose

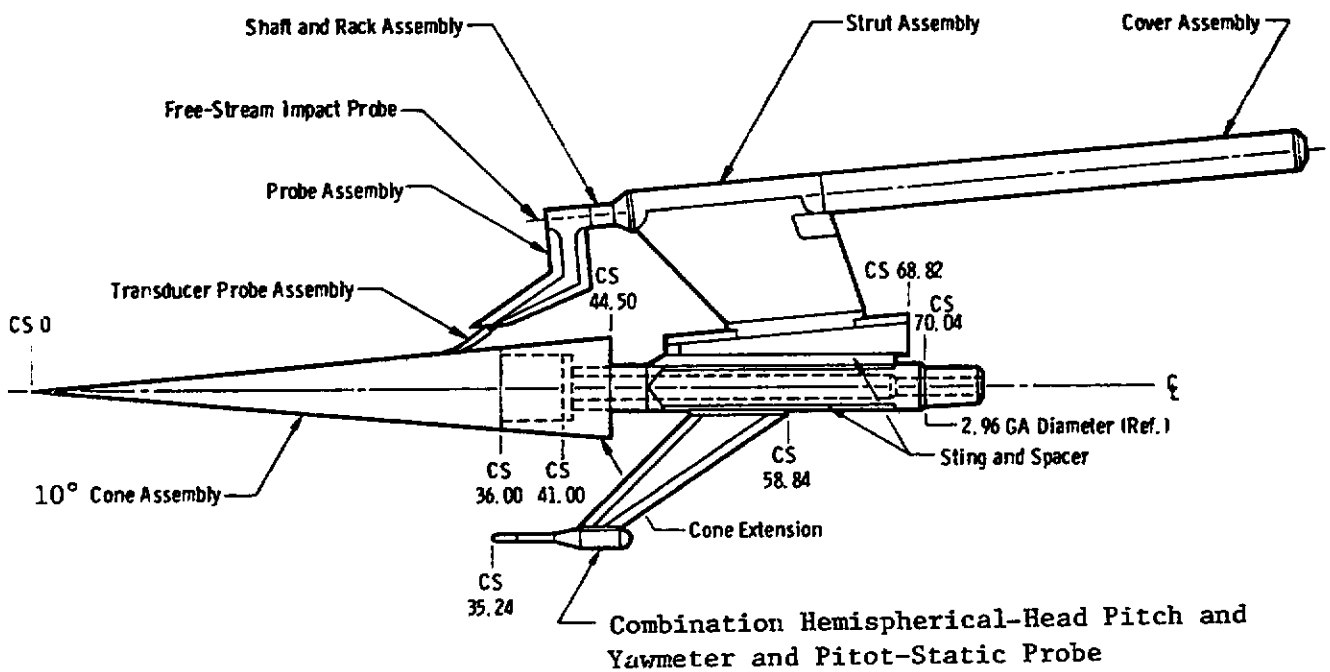

Figure 1. AEDC Boundary Layer Transition Cone

identical (or comparable) values of M_∞, Re_m and q_∞. The technique of using a traversing Pitot probe to detect boundary layer transition has been used since the 1930's. In fact, the first Wright Brothers' Lecture by Jones[9] in 1937 describes the utility of this technique in flight tests. Figure 2 is taken from this paper and shows clearly the change in total pressure across the transition zone along different paths parallel to the bounding surface.

The results of tests in six different tunnels is reported in Ref. 7, and a summary of results obtained in twenty three tunnels and a concluding flight test are reported by Dougherty and Fisher.[8] In this concluding report, Dougherty and Fisher found that the data for transition Reynolds number, based on the product of local unit Reynolds number and distance from nose to end-of-transition (X_T), was proportional to $(C_p)_{rms}^{-.25}$ with an error band of + 20%. This represents a significant step forward in the development of a procedure to calibrate flow quality in transonic wind tunnels.

The purpose of the work reported herein is to investigate the possibility of using the traversing-Pitot-probe data to derive more precise and/or additional information concerning the effects of noise on flow quality. The basic approach, which was selected to achieve this objective, is to interpret the surface Pitot-probe data as Preston-tube data, i.e., total pressures near the wall which can be related to skin friction. Unfortunately, four different probes were used during the series of wind-tunnel tests, and two were used during the flight tests. Replacement was necessary because of probe wear (along the underside of the probe where it made contact with the cone), damage and/or deterioration during use. This did not introduce any significant problem with regard to detection of transition but does become very important if the data are to be interpreted as Preston-tube data. In order to set the stage for this type of analysis of the data, the basics of Preston tubes and their use to measure skin friction is now introduced.

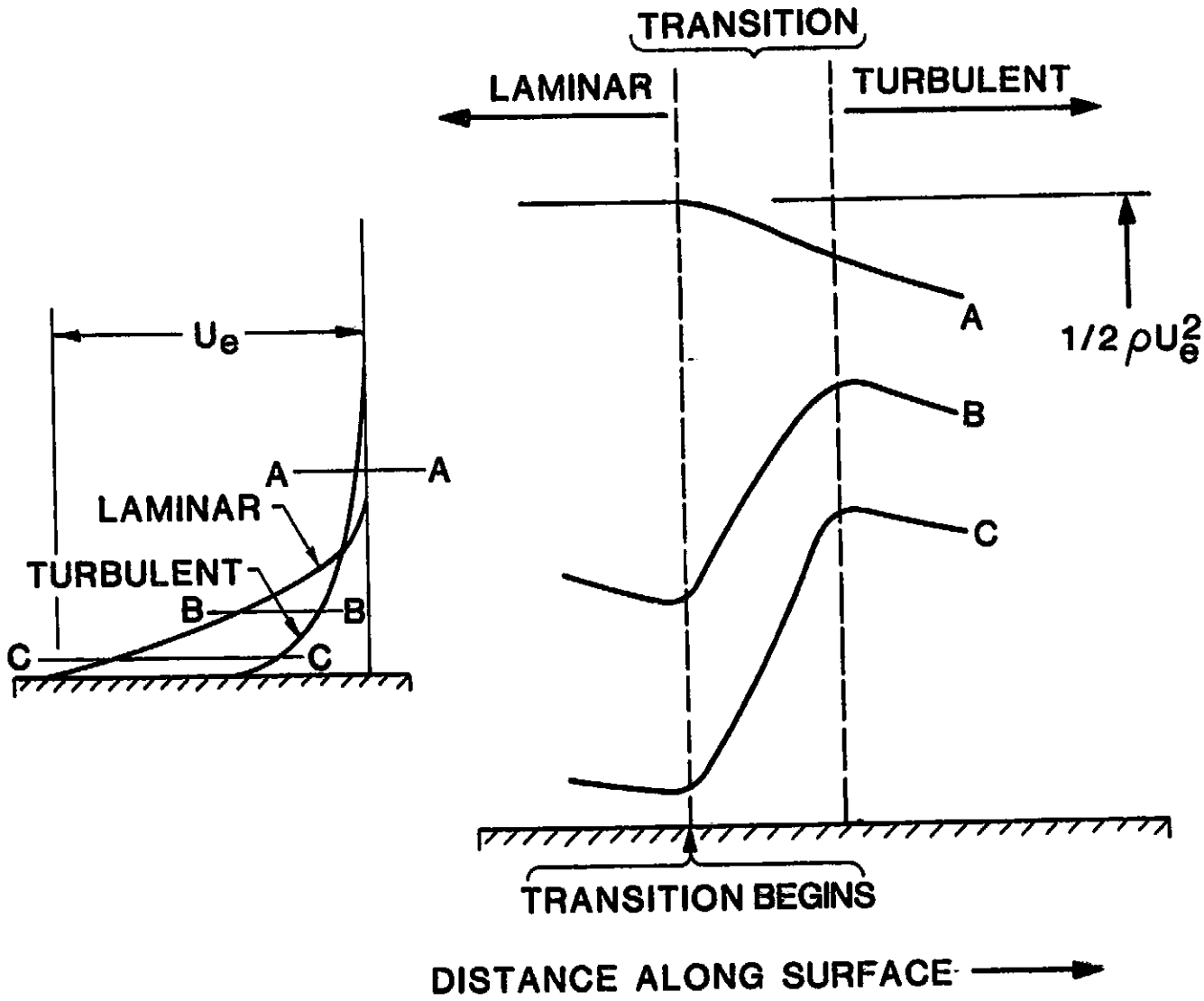

VARIATIONS OF
TOTAL PRESSURE THROUGH A REGION OF TRANSITION
FROM LAMINAR TO TURBULENT BOUNDARY-LAYER FLOW

Figure 2

B. Preston Tubes

According to Preston[10], the British engineers Stephens and Haslam[11] suggested in 1938 that it should be possible to use the data from a Pitot tube traversed along a surface to infer skin friction. Apparently, this idea was not pursued until Preston's work during the early 1950's. He developed a correlation between skin friction and the total pressure as measured with circular pitot tubes resting on the inside wall of a pipe.

In order to develop this correlation, Preston assumed the classical law-of-the wall is valid across the face of the probe and chose the characteristic length to be the height of the geometric center of the probe above the wall, i.e., d/2. As shown in Ref. 12, this leads to the following relation between Preston-tube pressure and skin friction.

$$\frac{(P_p - P_w)\, d/2}{\rho\nu^2} = G\left[\frac{\tau_w (d/2)^2}{\rho\nu^2}\right]$$

or inversely,

$$\frac{\tau_w\, d^2}{4\rho\nu^2} = F\left[\frac{\Delta P_p\, d^2}{4\rho\nu^2}\right] \qquad (1)$$

This relation suggest a convenient method to determine skin friction since the shear stress is uniquely related (for given fluid properties ρ and ν) to the difference in pressures between a Pitot tube (OD = d) and a static-pressure orifice at the wall. Using Eq. (1) as a guide, Preston obtained measurements inside a pipe flow with circular Pitot tubes having four different external diameters but constant ratios of internal to external diameters of 0.6. Pipe Reynolds number was varied over the range $10^4 < Re_D < 10^5$. Skin friction was determined via measurements of pressure drop over a known length of constant diameter pipe, viz., $\tau_w = (P_1 - P_2)D/4L$. An empirical fit of the data led to the following correlation.

$$y^* = -1.396 + \frac{7}{8}\, x^* \qquad \text{[Preston, 1954]} \qquad (2)$$

Where $y^* \equiv \log_{10} (\tau_w d^2/4\rho\nu^2)$ and $x^* \equiv \log_{10} (\Delta P_p d^2/4\rho\nu^2)$.
In this same paper, Preston also reported measurements with the tubes on the floor of a wind tunnel in slightly favorable and strong adverse pressure gradients. The use of Eq. (2) to convert the pressure measurements into skin friction coefficients led to a set of data that was consistent with

corresponding boundary-layer surveys with a minature, flattened Pitot probe.

Thus, in addition to the surface Pitot measurements with circular probes, Preston also used a small (h = 0.015 cm.) flattened Pitot probe to measure velocity profiles. In an effort to obtain accurate profiles, he employed an earlier estimate by Young and Maas[13] that the effective center of the probe would be displaced 0.25h toward the region of higher velocity. This correction is ostensibly to account for a velocity gradient across the height of the probe face. This is needed because as noted by Chue[14]:

> "Errors caused by the presence of a shear flow across the mouth of the pitot tube are due to the following two effects:
>
> (i) the stagnation pressure is proportional to the square of the velocity and when this is integrated over the orifice, it will have a higher value than the stagnation pressure calculated from the square of the velocity at the geometric centre of the orifice; and
>
> (ii) the presence of the probe in a velocity gradient causes deflection of the stream lines toward the region of lower velocity. This deflection causes the probe to indicate an impact pressure in excess of that existing at the same location in the absence of the probe.
>
> The existence of the second effect has been qualitatively demonstrated by smoke photographs. Both of these effects are therefore seen to cause the probe to read high, which explains the outward displacement of the effective from the geometric centre."

The net effect is the measured pressure corresponds to the total pressure of a streamline which is above the geometric center of the probe. Although Preston attempted to correct for this effect of shear, he noted that there is an additional effect associated with proximity to the wall. In particular, when the flattened probe was within a distance 3h of the wall, he found the displacement of the effective center was reduced and appeared to be a function of $U_\tau h/\nu$.

Preston did not attempt to define the functional relationship between y_c, h and Reynolds number. However, this was subsequently undertaken by MacMillan[15] for circular Pitot probes. His measurements indicated that when the geometric center of a <u>circular</u> probe is more than two diameters away from the wall, the effects of the wall on displacement of the effective center is nil, and the displacement due to shear alone is 0.15d (i.e., Y_{eff} = 0.65d), independent of Reynolds number. He also established that the effect of the wall is to reduce this displacement and move the effective

probe position closer to the wall. This is easily seen when one realizes that the downward flow across the face of the probe (caused by shear) is impeded as a probe approaches the wall. Furthermore, the oncoming streamlines (below the center of the probe) begin to lift upward and move over and around the probe instead of passing underneath between the probe and the wall. MacMillan proposed a single curve for a velocity correction which is to be added to the measured velocity in order to account for wall displacement effects. The correction is a function only of y_c/d and is 1.5% of the measured velocity when $y_c/d = 0.5$ and is zero when $y_c/d \geq 2.0$. This correction for wall effects is to be added to the displacement effects of shear. By expressing the wall effect in terms of a fraction of the measured velocity, MacMillan was able to define a correction which is independent of Reynolds number. However, since the measured velocity at a given value of y_c/d is a function of Re_D, the displacement caused by wall proximity is also a function of Re_D. Thus, MacMillan concluded that the total displacement of the effective center is a function of y_c/d and $U_\tau d/\nu$ when $0.5 \leq y_c/d < 2.0$. It is relevant to here note that any displacement effects, which occurred in Preston's data, are buried within the empirical coefficients of Eq. (2).

In 1964, Patel[16] published the results of an extensive set of tests with fourteen different circular Pitot probes and three different pipe diameters. He obtained a more accurate calibration for Preston tubes and established limits on the pressure-gradient conditions within which his calibration can be used with prescribed accuracy. Patel obtained empirical equations for $y^* = f(x^*)$ over three ranges of y^*: (1) $3.5 < y^* < 5.3$, (2) $1.5 < y^* < 3.5$, and (3) $y^* < 1.5$. These three regions correspond, respectively, to the fully-turbulent, the buffer or transition zone, and the viscous-sublayer regions of the classical law-of-the-wall. In incompressible flow, the normal Preston-tube Reynolds number range corresponds to the buffer zone, and for this region Patel obtained

$$y^* = 0.8287 - 0.1381\ x^* + 0.1437(x^*)^2 - 0.0060(x^*)^3, \qquad (3)$$

where: $1.5 < y^* < 3.5$ or $5.6 < U_\tau d/2\nu < 55$. Patel claims this correlates his data to within $\pm$ 1.5% of τ_w.

In the viscous-sublayer region, Patel found his data was correlated by

$$y^* = 0.5x^* + 0.037, \qquad (4)$$

when: $y^* < 1.5$ or $U_\tau d/2\nu < 5.6$.

In this near-wall region, the classical law-of-the-wall exhibits the linear relation

$$u^+ \equiv u/U_\tau = U_\tau y/\nu \equiv y^+ \ . \tag{5}$$

In order to relate Eqs. (4) and (5), Patel introduced K_{eff} and defined the "effective" center of a round Pitot tube to be at

$$Y_{eff} \equiv K_{eff}\, d/2 \ . \tag{6}$$

By definition of the effective center, the velocity recorded by a Preston tube, U_p, is the true velocity at Y_{eff}.

$$\therefore \ \Delta P_p = \frac{1}{2}\ \rho U_p^2 = \frac{1}{2}\,\rho(u^2)_{y=y_{eff}} \tag{7}$$

If this is substituted into Eq. (5), the results are

$$y^* = 0.5x^* - 0.5\ \log_{10}\ (0.5\ K_{eff}^2). \tag{8}$$

Now equating Eqs. (4) and (8) and solving for K_{eff}, a value of 1.3 is obtained.

Patel noted that this agrees "precisely" with the value determined by MacMillan. However, this value for K_{eff} is equivalent to MacMillan's results for displacement due to shear alone, i.e., when $y_c/d > 2.0$. Whereas, in the case of Patel's use of Pitot tubes resting on the bounding surface, the value of y_c/d is 0.5. Thus, Patel's results for K_{eff} appears to be fortuitous, but an argument can be made that makes this plausible. Firstly, MacMillan noted an additional displacement correction for viscous effects on Pitot probes in zero-shear leads to larger, positive displacements when $U_\tau d/\nu \leq 25$.** Secondly, as previously discussed, wall proximity effects result in a reduced or a negative displacement. Therefore, it appears (assuming no significant experimental errors) that Patel's value for K_{eff} occurs because viscosity and wall effects cancel each other.

**As noted in the review article by Chue[14], it is generally agreed that the pressure coefficient (C_p) for a Pitot probe is greater than one when $U_\infty d/2\nu < 300$. However, there is no concensus between existing experimental data and theoretical results as to precisely how C_p varies with Reynolds number.

II. RESULTS OF PRELIMINARY ANALYSES OF WIND-TUNNEL DATA

The traversing Pitot probes, used during the AEDC-BLT Cone tests, are of the flattened or oval-shaped type. Figure 3 shows typical dimensions of the probe used during flight tests of the cone. The probes used in wind-tunnel tests are geometrically similar. The particular probe, used during tests in the NASA Ames 11-ft Transonic Wind Tunnel (TWT), had a height of 0.0097 in.

Since Patel's results are for circular Preston tubes, they cannot be applied directly to the AEDC Cone tests. In addition, these tests were conducted at transonic speeds and compressibility effects are expected. With regard to flattened Preston tubes, Quarmby and Das[17] conducted an experimental study and calibration of six oval-shaped probes when used as Preston tubes. When $x^* > 4.6$, they found these probes gave exactly the same calibration relation between y^* and x^* as was obtained by Patel (Eq. 3) if the external height of the probe face is used in place of d. At lower values of x^*, the negative displacement of the effective center caused by wall proximity was larger (≈5%) for the flattened probes with aspect ratios between 1.5 and 1.9.** The following calibration equation correlated the measurements of Quarmby and Das to within 1.5% of τ_w.

$$y^* = 0.5152 + 0.1693\, x^* + 0.0651\, (x^*)^2$$

$$\text{for} \quad 3.38 < x^* < 6 \qquad (9)$$

Since these results for oval-shaped Preston tubes agree so closely with Patel's results and Patel's value for $K_{eff} = 1.3$ appeared to be appropriate in the viscous-sublayer of a turbulent wall-flow, it was initially decided to use this same value in an attempt to correlate the traversing Pitot probe data obtained within the laminar boundary layer on the AEDC Cone. This appeared to be reasonable in light of the fact that the x^*'s for the cone data were > 5.5. Although this is equivalent to assuming K_{eff} is independent of Mach number, Reynolds number, velocity gradient across the face, and aspect ratio, this assumption was attractive because it greatly simplified the analytical work.

Now turning our attention to compressibility and Mach number effects,

**This is consistent with the idea that flow about the face becomes more two-dimensional as aspect ratio increases and more of the flow passes up and over the face rather than around the sides.

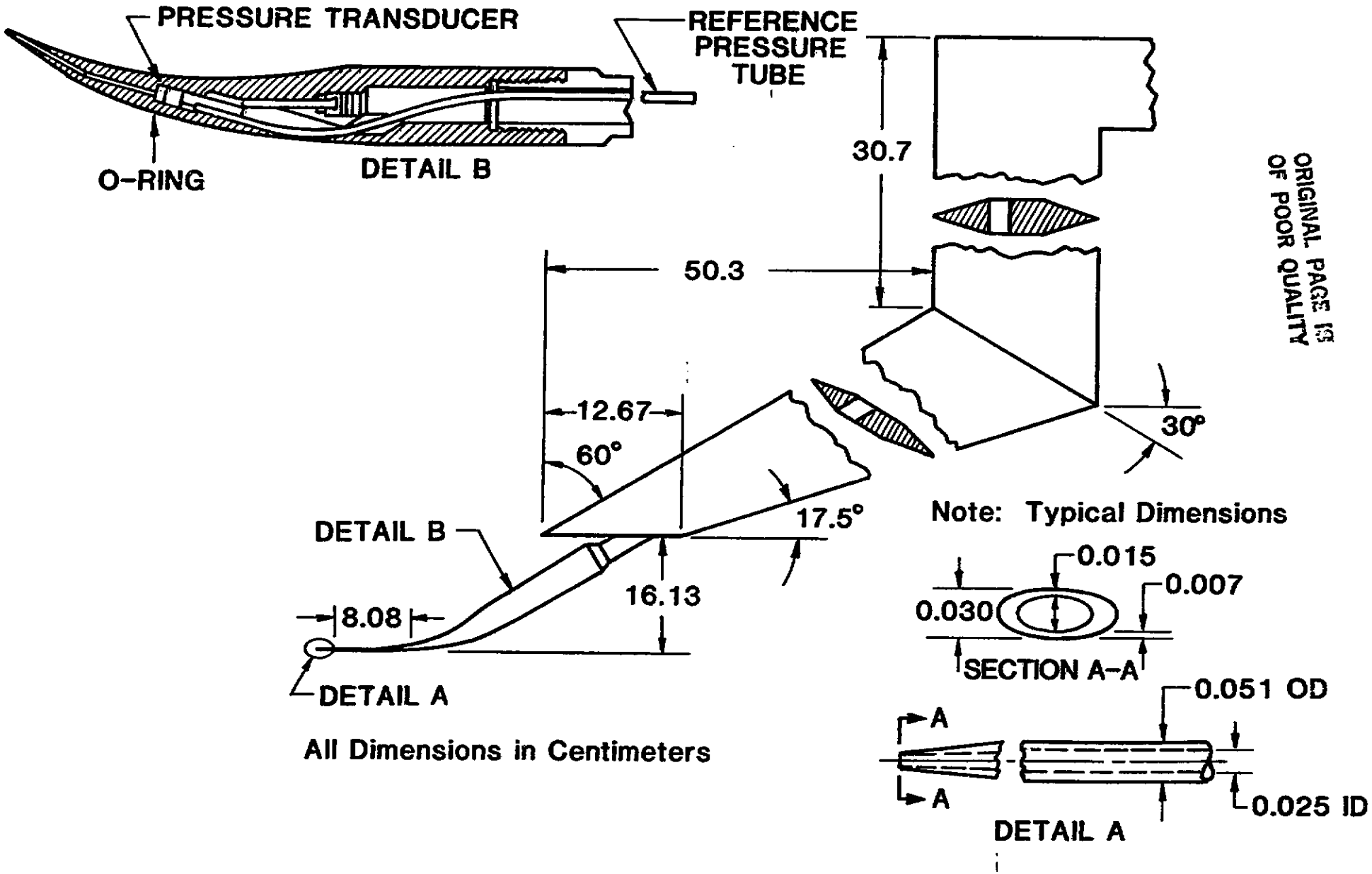

DIMENSIONS OF TRAVERSING PRESTON-TUBE PROBE USED DURING FLIGHT TESTS

Figure 3

Allen[18] has performed the most comprehensive analysis of Preston tubes in supersonic boundary layers. He developed a correlation using three independent sets of simultaneous measurements of Preston-tube pressures and skin friction via a floating-element force balance. These data were obtained within flat-plate, turbulent boundary layers and with Mach numbers in the range: $1.6 \leq M_\infty \leq 4.6$. Allen selected the same basic dimensionless parameters as Patel; except he chose to evaluate the fluid properties ρ and ν at a reference temperature developed by Sommer and Short[19], and the velocity U_p was calculated from P_p and the wall pressure P_w (= P_e) using standard compressible flow relations.**

$$X_A^* \equiv \log_{10}\left\{\frac{\rho'}{\rho_e}\,\frac{\mu_e}{\mu'}\,Re_d\,\frac{U_p}{U_e}\right\} = \log_{10}\,(U_p\, d/\nu') \qquad (10a)$$

$$Y_A^* \equiv \log_{10}\left\{\frac{\mu_e}{\mu'}\,Re_d(\rho' C_f/\rho_e)^{\frac{1}{2}}\right\} = \log_{10}\,(\sqrt{2}\,U_\tau d/\nu') \qquad (10b)$$

The primes denote properties evaluated at the Sommer and Short reference temperature, viz.,

$$T'/T_e = 0.55 + 0.035\,M_e^2 + 0.45\,T_w/T_e\ . \qquad (11)$$

The correlation derived by Allen is

$$Y_A^* = -0.4723 + 0.7814\,X_A^* + -0.01239(X_A^*)^2\ . \qquad (12)$$

[Allen, 1977]

Allen found that the majority of the skin-friction-coefficient data were within +15% to -12% of Eq. (12). This rather large scatter, compared to the incompressible pipe-flow calibrations of Patel[16] and Quarmby and Das[17], is at least partly associated with the much greater sensitivity and vulnerability of floating-element balances to extranneous errors.††

Obviously, the parameters used by Allen are logical candidates in any attempt to correlate the transonic cone data. However, the basic purpose of a reference temperature is to permit use of skin friction formulas for incompressible flow to estimate compressible skin friction by evaluating fluid properties at the reference temperature. Thus, the resulting reference properties represent an "average" value across a boundary layer. Whereas, small Preston tubes encounter only the flow near the wall. Therefore, it appeared to us that properties based simply on the wall temperature would be more apropo. The utility of evaluating properties at both of these tempera-

**The details can be found in the report by Allen[20] or Reed, et al.[12]

††Allen[21] has discussed the various error sources in floating-element force balances, and he has recently suggested an improved design for this type of instrument, Ref. 22.

tures was investigated, and the results are reported following a summary of the wind tunnel data.

Wind Tunnel Data

Although the AEDC-BLT Cone has been tested in twenty three different wind tunnels, only the analyses of subsonic data from the NASA Ames 11-ft Transonic Wind Tunnel (TWT) is reported herein. Suface Pitot-probe surveys were taken along the cone between axial stations 10 and 89 cm. aft of the nose. Table I lists the twenty one subsonic flow conditions at which the cone was tested.** The pattern of typical pressure surveys at high and low Reynolds numbers are shown, respectively, in Figures 4 and 5.

As a point of departure, this research seeks a correlation between the Preston-tube pressures, measured within the laminar portion of the cone's boundary layer, and the corresponding theoretical values of skin friction. If successful, the intent was, and is, to compare such a correlation with the corresponding correlation for flight data. It is thought that such a comparison can lead to the definition of an "effective" unit Reynolds number for the 11-ft TWT. However, a literature search for Preston-tube data within laminar boundary layers turned up only one reference, viz., Prozorov.[23]

Prozorov obtained surface Pitot-probe measurements within low-speed, flat-plate, laminar boundary layers. He used four circular Preston tubes and three rectangular-shaped probes with aspect ratios of 5.21, 5.21, and 5.00. Although his data exhibited considerable scatter, he concluded, based on his measurements, that K_{eff} is a universal function of $U_p d/\nu$ (or $U_p h/\nu$) for both laminar and turbulent boundary layers and is independent of probe geometry.++ Within the accuracy of his data, K_{eff} has nearly a constant value of 1.3 when $R_d > 100$ and approaches 1.8 when $R_d \simeq 32$. This essentially verifies the results of Preston for turbulent pipe flows. However, Prozorov found $\tau_w d^2/\rho\nu^2$ to be a different function of R_d for laminar boundary layers compared to what Preston found. The two calibration curves for $\tau_w d^2/\rho\nu^2$ diverge for $R_d > 100$. He explained this in terms of the following equation which was derived from a Maclaurin series expansion of U_p at small distances from the wall and the conservation of mass and momentum for steady, two-dimensional flow.

**Although surveys were also conducted at low supersonic speeds, the shock interactions between the traversing-probe assembly and the hemispherical Pitot-static probe were not completely calibrated, and thus the supersonic data were not included in this research.

++This is inconsistent with the results of MacMillan[15] which indicated K_{eff} for circular Preston tubes is a function of $U_\tau d/\nu$ and the results of Quarmby and Das[17] which indicated K_{eff} is also a function of aspect ratio.

Table 1. Wind Tunnel Cases Used To Develop Laminar Correlations

RUN NO.	M_∞	$Re_\infty \times 10^{-6}$	q_∞(kPa)	α°	β°
15.231	0.95	13.1	33.1	-0.05	0.02
19.289	0.8	13.1	29.5	-0.00	-0.02
21.318	0.7	13.1	26.2	-0.01	-0.03
23.346	0.6	13.1	22.8	-0.00	-0.03
25.376	0.5	13.1	19.3	-0.01	-0.03
27.411	0.4	13.1	19.3	-0.00	-0.03
29.440	0.3	13.1	11.0	-0.01	-0.03
39.545	0.4	8.2	19.0	0.02	0.02
40.547	0.6	16.4	28.1	0.02	0.02
41.548	0.7	16.4	32.6	0.02	0.02
42.549	0.8	16.4	36.4	0.01	0.02
43.550	0.9	16.4	40.3	0.01	0.02
44.551	0.95	16.4	41.8	0.01	0.02
56.631	0.9	9.8	23.6	0.06	0.01
57.632	0.8	9.8	21.7	0.07	0.01
58.633	0.7	9.8	19.5	0.07	0.01
59.634	0.6	9.8	17.1	0.08	0.01
60.635	0.5	9.8	14.5	0.07	0.01
61.636	0.4	9.8	11.8	0.07	0.01
70.726	0.7	13.1	25.8	0.04	0.02
72.748	0.8	13.1	29.0	0.03	0.02

PATTERN OF TYPICAL PRESTON TUBE DATA FOR HIGH UNIT REYNOLDS NUMBER

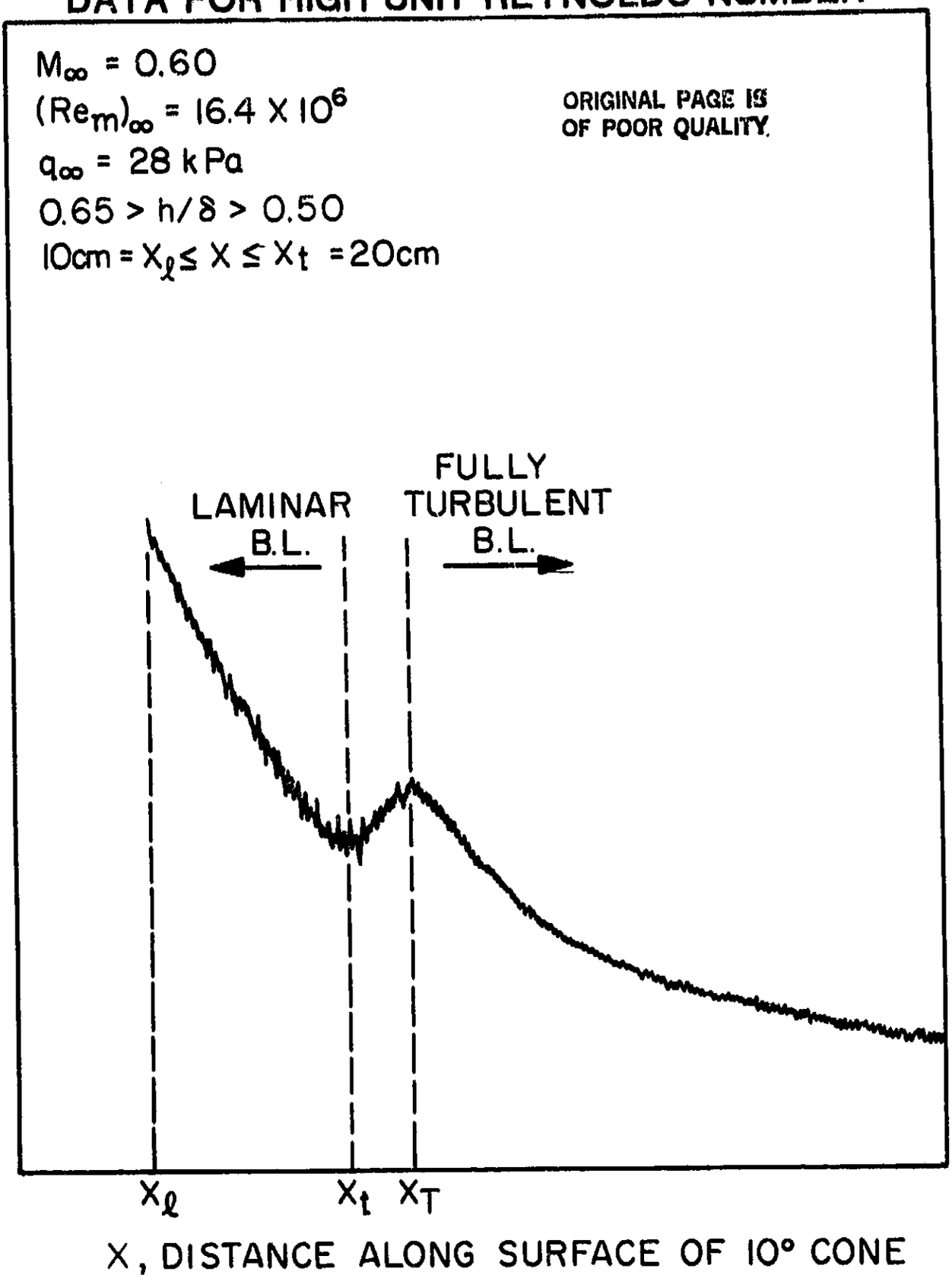

Figure 4

PATTERN OF TYPICAL PRESTON TUBE DATA FOR LOW UNIT REYNOLDS NUMBER

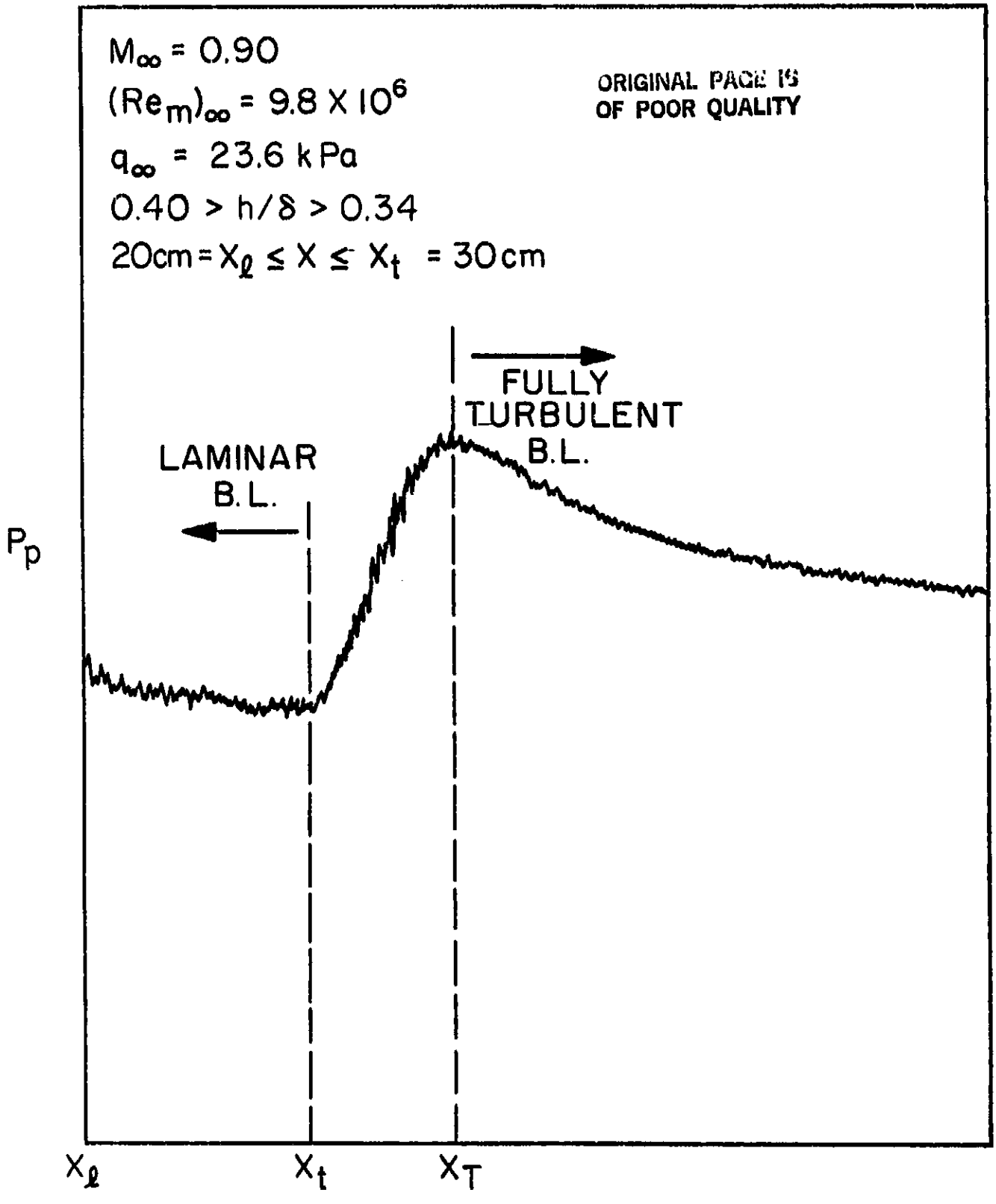

Figure 5

$$\bar{\tau}_w \equiv \frac{\tau_w d^2}{\rho\nu^2} = \frac{2R_d}{K_{eff}} - \frac{d}{4}\frac{d}{dx}\left(\frac{P_w d^2}{\rho\nu^2}\right) K_{eff} \qquad (13)$$

Prozorov claims this is valid in laminar, transitional and turbulent flows provided the probe height is within the viscous-sublayer. According to Eq. (13), $\bar{\tau}_w = fn(R_d)$ if and only if K_{eff} is also and the pressure gradient is negligible.

It was decided not to use Prozorov's equation [$\bar{\tau}_w = \bar{\tau}_w (R_d, K_{eff}, dP_w/dx)$] for the development of a correlation of laminar Preston-tube data for the following reasons.

1. It was not expected that the probes used in the subject tests would always be within the viscous sublayer.
2. For efficiency, it is desirable to have a common procedure for analysis of both the laminar and turbulent data. Use of the classical law-of-the-wall leads to a procedure which is applicable to both types of flow; provided pressure gradients are small.
3. The static pressure gradients along the cone surface were known to be small, and Patel's work[16] defined the errors to be expected when using calibrations of Preston tubes, based on the law-of-the-wall, in turbulent flows with small pressure gradients.

Thus, for analyses of the laminar data, it was decided to use the basic correlations parameters utilized by Patel and Allen for turbulent wall-flows.

Computation of Boundary Layer and Data Analysis

The distribution of static pressure along the surface of the sharp cone at subsonic speeds is assumed to be defined by the inviscid theory of Wu and Lock.[24] Predictions for pressure coefficient along the surface of a 10-degree cone are shown in Figure 6 as a function of freestream Mach number. This information and the known tunnel freestream conditions are used to calculate flow conditions along the outer edge of the boundary layer. The conical laminar boundary layer is then calculated using a computer program developed at Stanford University by Crawford and Kays[25] which they have labelled STAN-5. The resulting distributions of laminar skin friction and boundary layer properties are then matched with the corresponding values of surface - Pitot measurements.

It was arbitrarily decided to only use Preston-tube data at 1/2 in. intervals beginning with the most forward station at which data were obtained.

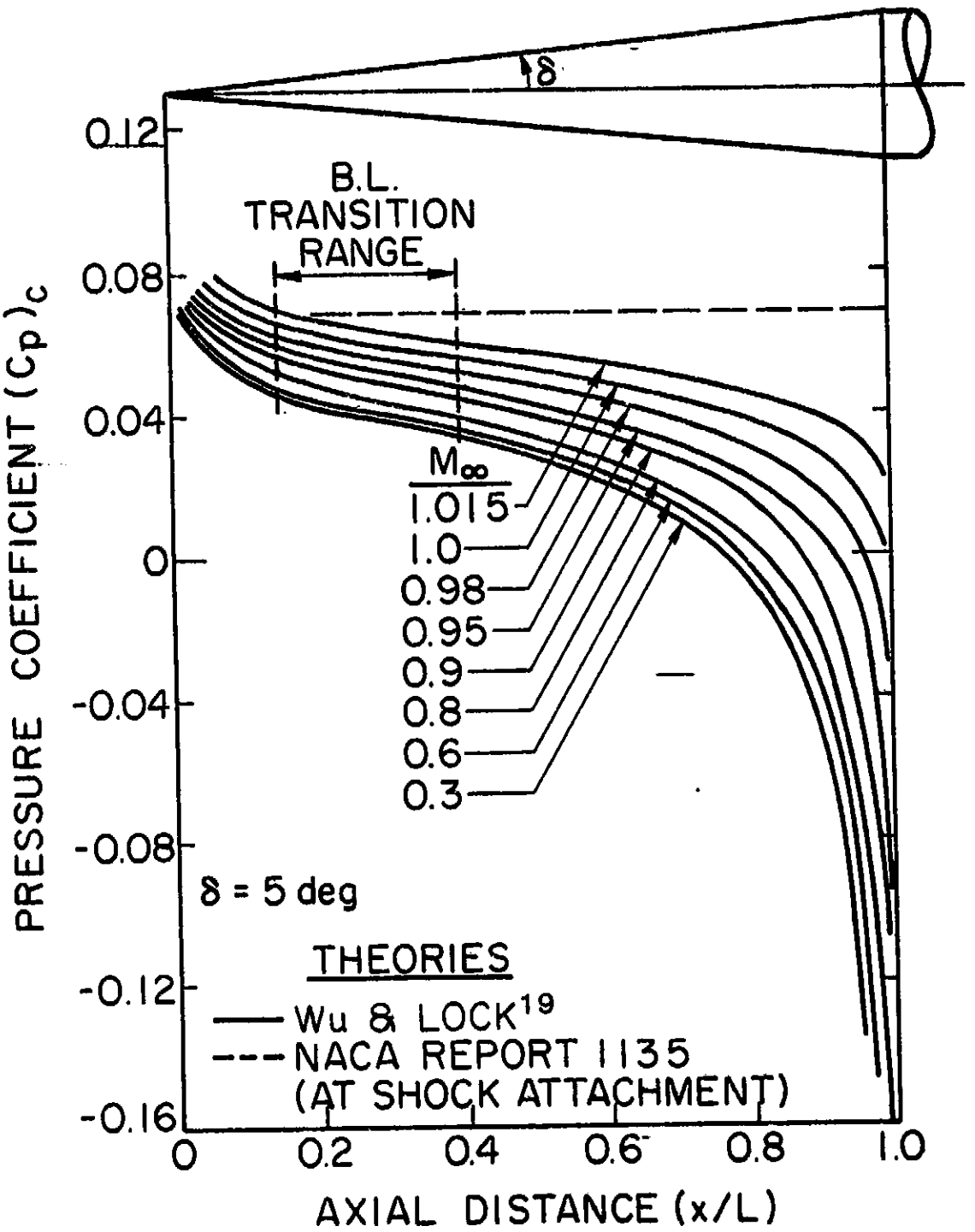

INVISCID PRESSURE DISTRIBUTION ABOUT A 10° CONE AT TRANSONIC SPEEDS

Figure 6

This resulted in a total of 148 data points along the cone at the various M_∞ and Re_m listed in Table 1. The following linear equation was first used to correlate the Preston-tube measurements with the corresponding values of theoretical skin friction.

$$Y^* = A\,X^* + B\,T^* + C \tag{14}$$

where

$$Y^* \equiv \log_{10}\left(\tau_w Y_{eff}^2/\rho_w \nu_w^2\right) = \log_{10}\left(U_\tau\, Y_{eff}/\nu_w\right)^2 \tag{15a}$$

$$X^* \equiv \log_{10}\left(U_p\, Y_{eff}/\nu_w\right)^2 \tag{15b}$$

$$T^* \equiv \log_{10}\left(T'/T_e\right) \tag{15c}$$

$$Y_{eff} = K_{eff}\, h/2 = 0.65\, h \tag{15d}$$

The reference temperature was introduced to account for small departures of the fluid properties ρ and ν from the wall values. The coefficients A, B, and C were determined by a least-squares fit of the data. This resulted in the following semi-empirical correlation.

$$Y^* = 0.655X^* + 2.095T^* - 0.895 \equiv Z^* - 0.895 \tag{16}$$

A plot of Eq. (16) is presented in Fig. 7 along with the individual data points. The corresponding differences in skin friction coefficient are shown in Figure 8. The rms value of $\overline{C}_f \equiv (C_{f,t} - C_{f,c})/C_{f,t}$ is 6.7%.

Next, an equation quadratic in X* was tried. The resulting correlation is

$$Y^* = 0.273(X^*)^2 - 2.618\,X^* + 1.645T^* + 8.92 \tag{17}$$

A plot of this equation and the associated data are shown in Fig. 9. The corresponding $\overline{C}_f$ is presented in Fig. 10. When the correlation parameters of Allen (Eq. 10) are used to fit the same data, the rms value of $\overline{C}_f$ is 8.6%. Thus, the parameters defined in Eqs. (15) appear to be superior for correlating this particular data. An examination of Fig. 10 reveals that the data in the upper left-hand corner is separated from the majority of the data. These six data points corresponds to Run No. 57 ($M_\infty = 0.80$, $Re_m = 9.8\times10^6$). When they are deleted, the rms value of $\overline{C}_f$ is reduced from 6.7% to 5.2%. Finally, the seven data points, which form almost a vertical line on the left of Fig. 9, correspond to Run No. 72 ($M_\infty = 0.80$, $Re_m = 13\times10^6$). When these points are also deleted, the correlation becomes

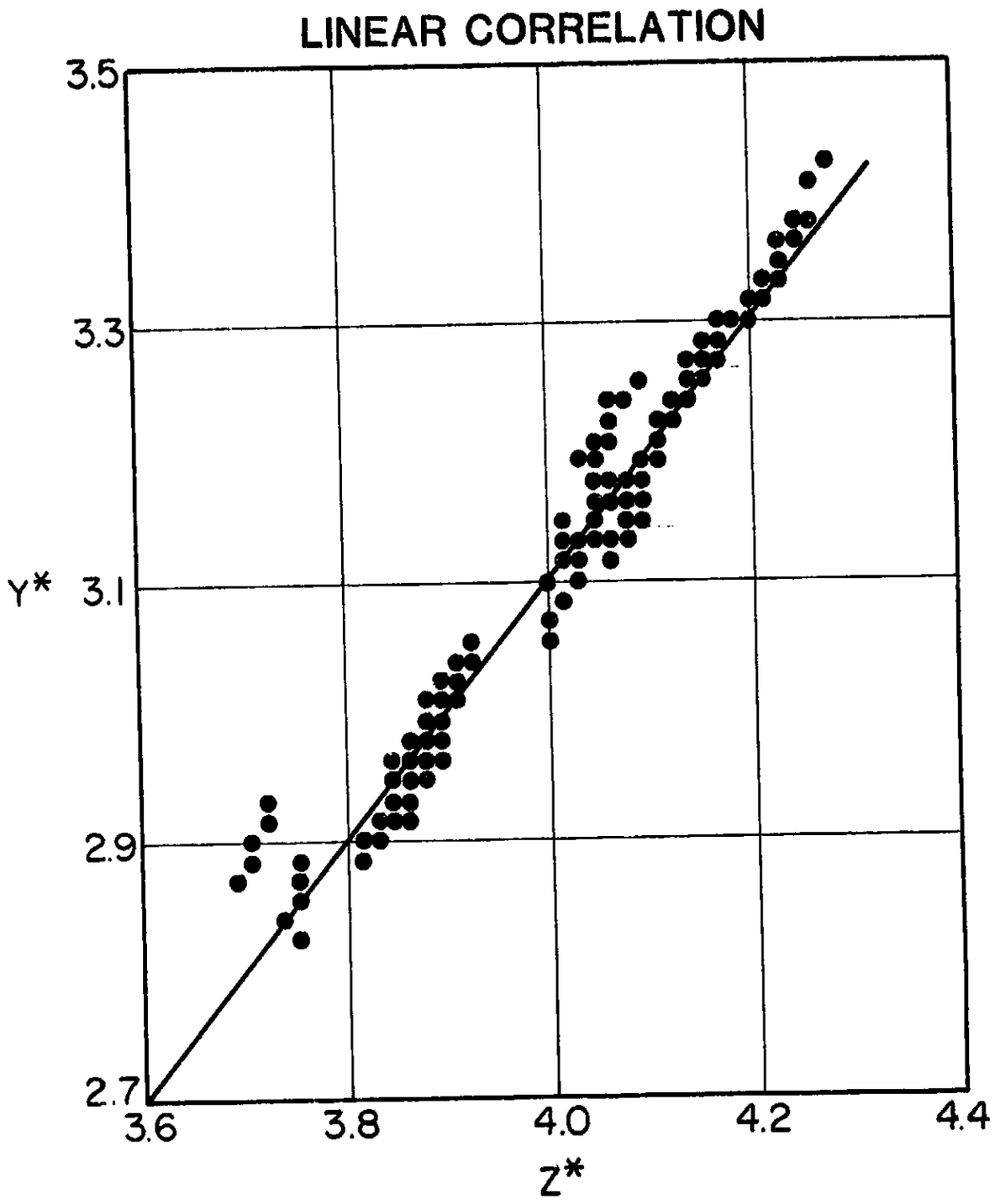

$$Y^* = Z^* - 0.895$$

Where

$$Z^* = 0.655\,X^* + 2.095 \log_{10}(T'/T_e)$$

$$Y_{eff} = 0.65\,h$$

Figure 7.

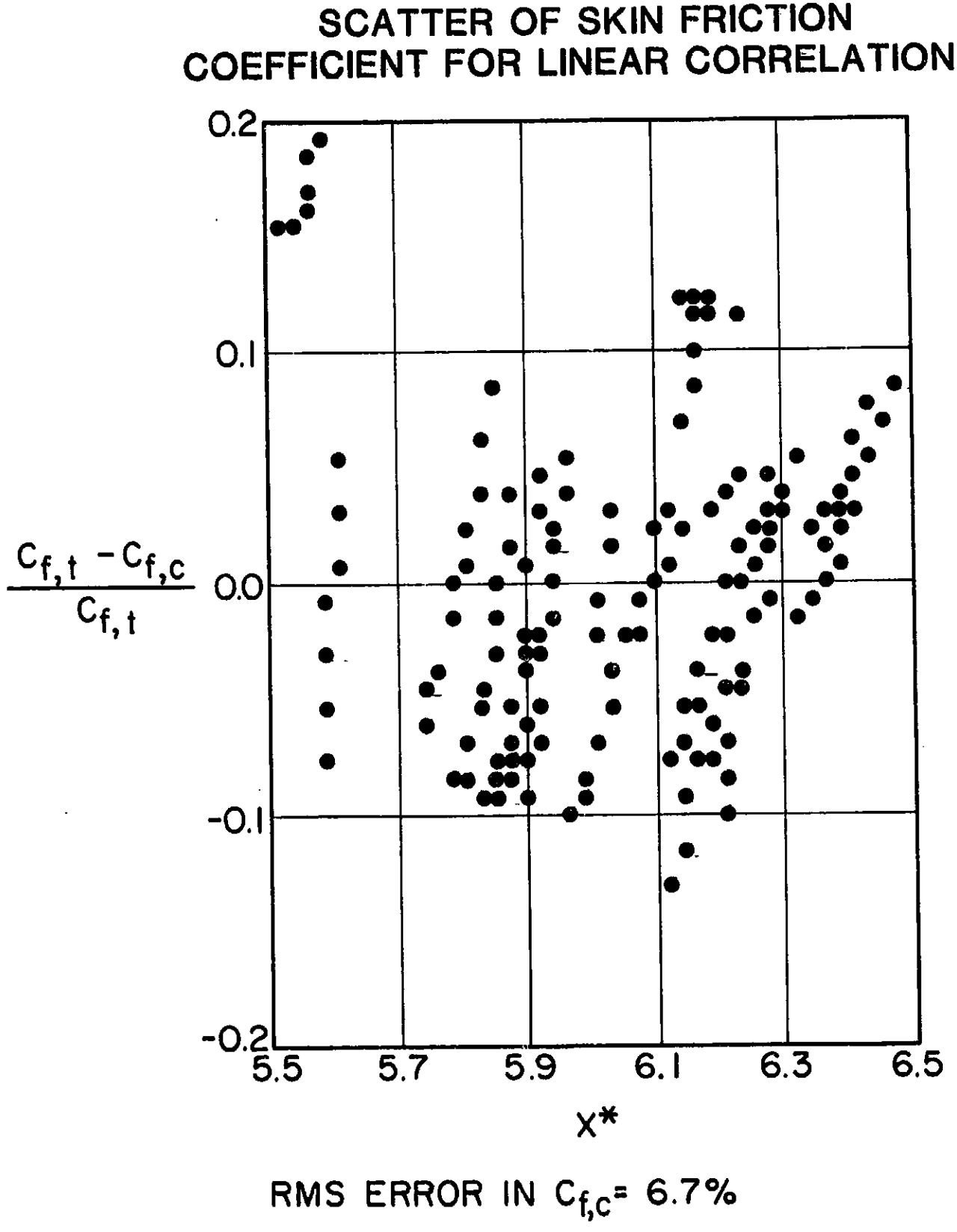
SCATTER OF SKIN FRICTION
COEFFICIENT FOR LINEAR CORRELATION
0.2
0.1
0.0
-0.1
-0.2
$\frac{C_{f,t} - C_{f,c}}{C_{f,t}}$
5.5
5.7
5.9
6.1
6.3
6.5
X*
RMS ERROR IN $C_{f,C}$= 6.7%

Figure 8.

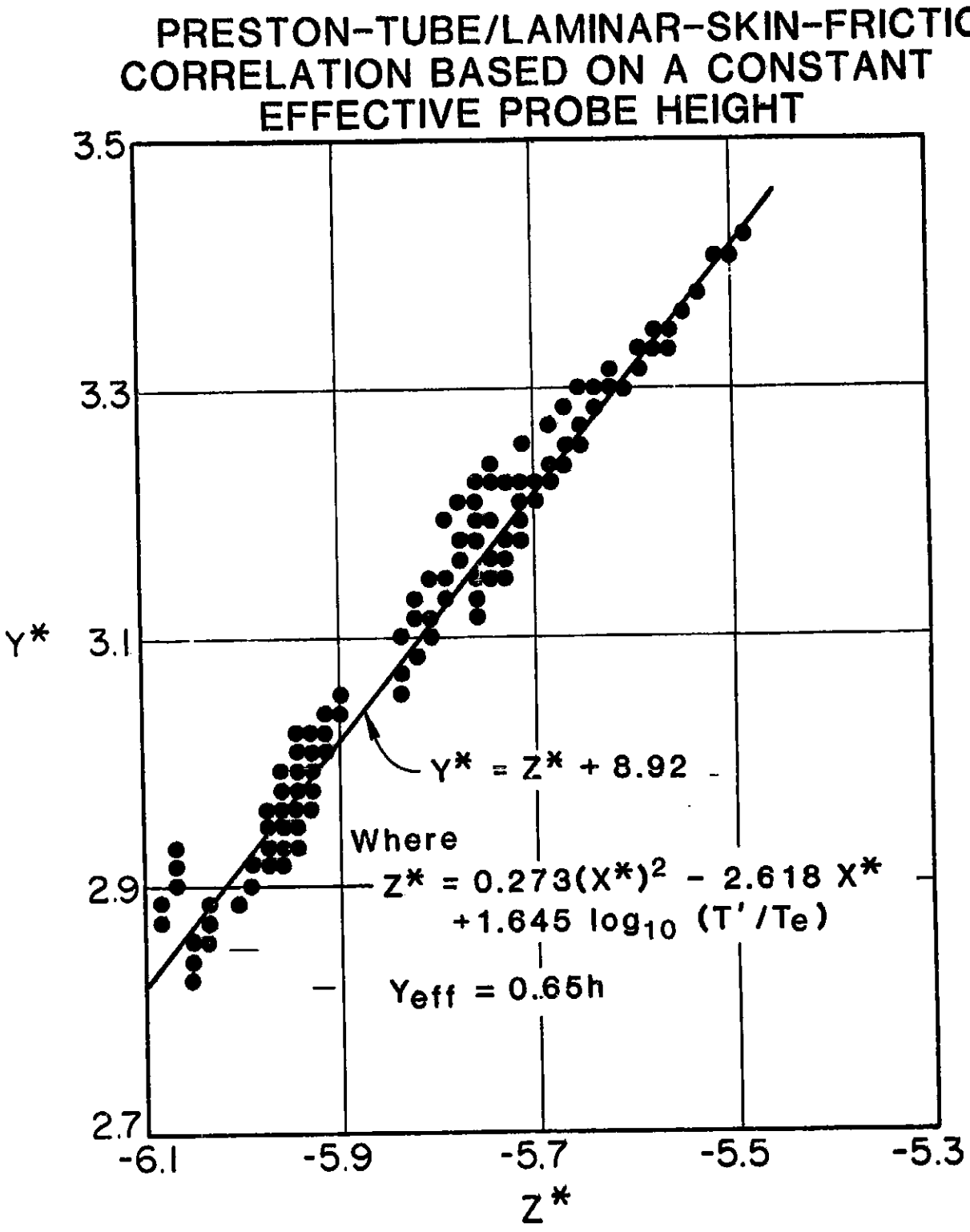

Figure 9

SCATTER OF SKIN FRICTION COEFFICIENT FOR QUADRATIC CORRELATION

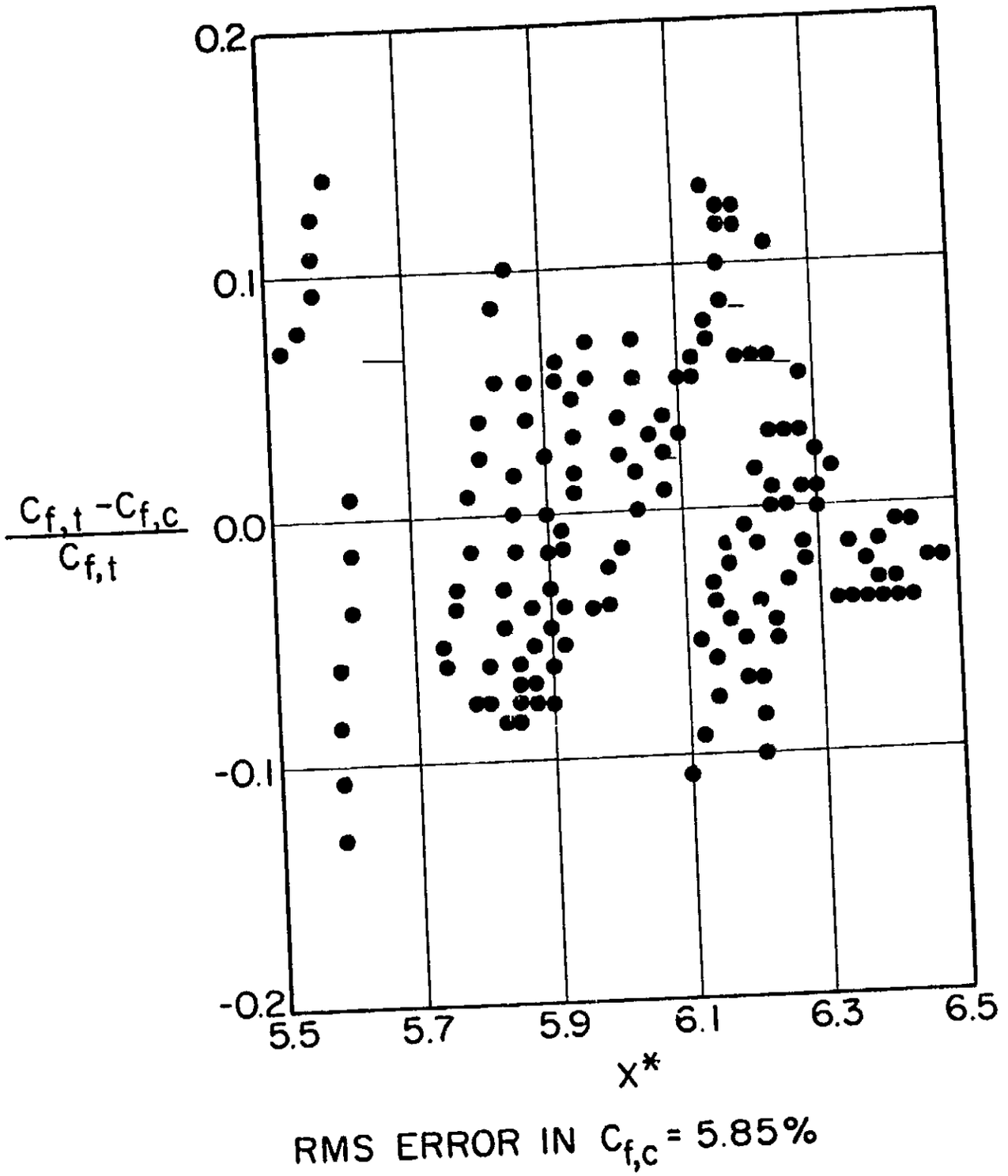

RMS ERROR IN $C_{f,c}$ = 5.85%

Figure 10.

$$Y^* = 0.0942(X^*)^2 - 0.438X^* + 2.023T^* + 2.272 \quad . \tag{18}$$

The associated rms value of $\bar{C}_f$ is 4.93%.

These results are good compared to the correlation of Allen[18] but are rather large compared to the very small scatter ($\simeq$ 1%) of the correlations for incompressible flow of Patel (Eq. 3) and Quarmby and Das (Eq. 9). Although greater scatter may be expected for compressible flows, somewhat less scatter is expected for a correlation of the subsonic cone data because errors associated with floating-element balances are not present as they are in the data considered by Allen. Thus, the question arises: how can the data be better correlated? This led to a reexamination of the data and the development of an improved correlation when K_{eff} is treated as a variable. The details of this second analysis of the wind tunnel data are discussed in the next section.

III. REANALYSIS OF WIND TUNNEL DATA USING VARIABLE K_{eff}

Reexamination of the papers by McMillan,[15] Patel,[16] and Quarmby and Das[17,26] led us to conclude that, in general, the effective center of a Pitot tube is a function of:

$$K_{eff} = K_{eff}\ (U_\tau h/\nu,\ y_c/h,\ w/h) \quad . \tag{19}$$

In the case of a Preston tube, $y_c/h = 0.5$, and aspect ratio (w/h) is a constant for a given probe. When these restrictions apply, Eq. (19) reduces to $K_{eff}(U_\tau h/\nu)$. Since, in general, wall shear stress is a function of Reynolds number, pressure gradient, Mach number and heat transfer, we can expect K_{eff} for a given Preston tube to also be a function of these variables. If this conclusion is true, it is necessary to interpolate K_{eff} from the STAN-5 boundary-layer profiles. This has been done by finding the position within the theoretical laminar profiles at which the total pressure is equal to the measured Pitoto pressures. Table II provides a summary of the results for each wind-tunnel flow condition.

It may be noticed that only nineteen cases appear in Table II as compared with twenty one in Table I. In the process of tabulating $(C_p)_{rms}$, it was discovered that the exact flow conditions for Run Nos. 27.411 and 39.545 were in doubt. After a brief attempt to ascertain the correct values it was decided to drop these two cases from further consideration.

In addition to K_{eff} and P_p, Table II also includes noise measurements of $(C_p)_{rms}$ as obtained with a 0.635 cm microphone mounted flush with the surface of the cone at a distance 45.7 cm aft of the nose and 135 degrees around from the Preston tube. As discussed in the introduction, Dougherty and Fisher[8] have correlated boundary layer transition with this type of noise data. Thus, it is anticipated that this data will be relevant to the definition of an "effective" unit Reynolds number for the 11-ft TWT.

TABLE II

WIND TUNNEL DATA USED IN DEVELOPMENT OF LAMINAR CORRELATION

R/m	M_∞	$Re_{ft} \times 10^{-6}$	q_∞(psf)	Tw/Taw	$\alpha°$	$\beta°$	$(C_p)_{rms}$	X_t(in)	X(in)	P_p (psf)	K_{eff}
39.330	0.30	4.0	230	1.0	-.006	-.026	0.400		6.5	3772.2	1.239
									7.0	3767.9	1.255
									7.5	3765.1	1.277
									8.0	3762.2	1.297
									8.5	3760.8	1.326
								9.5			
61.636	0.40	3.0	246	1.0	0.070	0.007	0.534		6.5	2298.6	1.225
									7.0	2297.2	1.263
									7.5	2294.4	1.284
									8.0	2292.9	1.314
									8.5	2291.5	1.343
									9.0	2290.1	1.369
									9.5	2288.7	1.394
									10.0	2285.8	1.406
									10.5	2284.4	1.425
									11.0	2281.5	1.438
								11.5			
60.635	0.50	3.0	302	1.0	0.068	0.007	0.862		6.5	1848.6	1.218
									7.0	1844.3	1.240
									7.5	1842.9	1.275
									8.0	1841.5	1.308
									8.5	1838.6	1.327
									9.0	1837.2	1.356
									9.5	1834.4	1.373
									10.0	1831.5	1.385
									10.5	1828.6	1.396
									11.0	1827.2	1.417
									11.5	1824.4	1.426
								11.75			
25.376	0.50	4.0	404	1.0	-.005	-.025	0.793		5.0	2524.3	1.106
									5.5	2518.6	1.140
									6.0	2510.0	1.159
									6.5	2502.9	1.179
									7.0	2497.2	1.200
									7.5	2491.5	1.218
									8.0	2487.2	1.240
									8.5	2482.9	1.259
									9.0	2480.1	1.282
								9.5			

TABLE II (CONT'D)

WIND TUNNEL DATA USED IN DEVELOPMENT OF LAMINAR CORRELATION

Run #	M_∞	$Re_{ft} \times 10^{-6}$	q_∞(psf)	Tw/Taw	$\alpha°$	$\beta°$	$(C_p)_{rms}$	X_t(in)	X(in)	P_p (psf)	γ_{eff}
59.634	0.60	3.0	357	1.0	0.075	0.006	1.468		6.5	1556.7	1.207
									7.0	1553.9	1.238
									7.5	1549.6	1.257
									8.0	1546.7	1.281
									8.5	1543.9	1.305
									9.0	1541.0	1.322
									9.5	1538.2	1.341
									10.0	1535.3	1.356
									10.5	1533.9	1.379
									11.0	1529.6	1.381
								11.5			
23.346	0.60	4.0	477	1.0	-.001	-.025	1.395		4.0	2179.6	1.079
									4.5	2163.9	1.101
									5.0	2145.3	1.109
									5.5	2131.1	1.120
									6.0	2121.1	1.137
									6.5	2114.0	1.161
									7.0	2108.3	1.186
									7.5	2102.6	1.206
									8.0	2096.9	1.226
								8.5			
40.547	0.60	5.0	586	1.0	0.021	0.021	1.583		4.5	2648.6	0.986
									5.0	2631.5	0.994
									5.5	2618.7	1.004
									6.0	2604.4	1.015
									6.5	2593.0	1.029
									7.0	2580.2	1.036
									7.5	2571.6	1.049
								8.0			
58.623	0.70	3.0	408	1.0	0.071	0.006	1.866		5.5	1351.1	1.126
									6.0	1345.4	1.154
									6.5	1341.1	1.182
									7.0	1336.8	1.206
									7.5	1332.6	1.228
									8.0	1328.3	1.245
									8.5	1325.4	1.268
									9.0	1322.6	1.289
									9.5	1318.3	1.299
									10.0	1315.5	1.317
									10.5	1312.6	1.331
								11.0			

[illegible]	[illegible]	[illegible]	q_∞ (psf)	Tw/Taw	α°	β°	$(C_D)_{min}$	X_t (in)	X(in)	P_{t_2} (psf)	[illegible]
[illegible]	[illegible]	4.0	548	1.0	-.006	-.025	1.807		4.5	1903.5	1.[illegible]
									5.0	1888.1	1.[illegible]
									5.5	1864.6	1.[illegible]
									6.0	1838.6	1.[illegible]
									6.5	1813.6	1.[illegible]
									7.0	1788.1	1.[illegible]
									7.5	1763.6	1.[illegible]
									8.0	1738.6	1.[illegible]
								8.5			
29,726	0.70	4.0	538	1.0	0.036	0.023	1.918		6.5	1788.5	1.[illegible]
									7.0	1780.0	1.101
									7.5	1774.[illegible]	1.121
									8.0	1768.6	1.139
									8.5	1764.3	1.159
								9.0			
41,548	0.70	5.0	680	1.0	0.018	0.021	1.970		4.5	2388.0	[illegible]
									5.0	2326.6	[illegible]
									5.5	2312.3	[illegible]
									6.0	2296.6	1.006
									6.5	2279.5	1.013
								7.0			
57,642	0.80	3.0	453	1.0	0.066	0.006	1.745		8.0	1156.4	1.219
									8.5	1153.6	1.[illegible]
									9.0	1152.1	1.271
									9.5	1149.[illegible]	1.[illegible]
									10.0	1146.4	1.[illegible]
									10.5	1143.6	1.[illegible]
								11.5			
19,289	0.80	4.0	617	1.0	-.003	-.022	1.706		5.5	1684.9	1.141
									6.0	1673.5	1.164
									6.5	1663.6	1.188
									7.0	1655.9	1.211
									7.5	1646.4	1.230
									8.0	1638.[illegible]	1.251
								9.0			
72,743	0.80	4.0	605	1.0	0.030	0.023	1.798		7.0	1572.4	1.070
									7.5	1566.[illegible]	1.091
									8.0	1562.[illegible]	1.115
									8.5	1558.1	1.135
								9.0			
42,549	0.80	5.0	761	1.0	0.013	0.021	1.793		4.5	2115.3	0.977
									5.0	2093.9	0.998
									5.5	2072.5	1.012
									6.0	2054.0	1.023
									6.5	2035.4	1.033
								7.25			

TABLE II (CONT'D)

WIND TUNNEL DATA USED IN DEVELOPMENT OF LAMINAR CORRELATION

Run #	M_∞	$Re_{ft} \times 10^{-6}$	q_∞(psf)	Tw/Taw	$\alpha°$	$\beta°$	$(C_p)_{rms}$	X_t(in)	X(in)	P_p (psf)	K_{eff}
56.631	0.90	3.0	492	1.0	0.062	0.006	1.488		8.5	1001.7	1.153
									9.0	1000.3	1.180
									9.5	998.9	1.205
									10.0	997.4	1.231
									10.5	996.0	1.254
									11.0	996.0	1.285
									11.5	996.0	1.315
								12.0			
42.550	0.90	5.0	842	1.0	0.010	0.021	1.512		5.0	1884.2	0.952
									5.5	1858.5	0.951
									6.0	1840.0	0.974
									6.5	1920.0	0.[illegible]
								7.25			
15.231	0.95	4.0	691	1.0	-.048	0.018	1.397		4.0	1462.0	1.011
									4.5	1437.7	1.029
									5.0	1419.2	1.057
									5.5	1402.1	1.075
									6.0	1387.8	1.091
									6.5	1376.4	1.110
									7.0	1367.9	1.132
									7.5	1359.3	1.150
									8.0	1350.8	1.166
									8.5	1340.8	1.176
								9.5			
44.551	0.95	5.0	873	1.0	0.008	0.021	1.391		5.0	1776.9	0.931
									5.5	1751.2	0.938
									6.0	1731.3	0.940
									6.5	1712.7	0.956
								7.25			

The method used to define K_{eff} has the effect of adjusting the height above the wall at which P_p is measured. This procedure is expected to lead to an improved correlation between P_p and C_f because the Preston-tube pressure is forced to be consistent with the theoretical boundary-layer profile and skin friction. However, a high or low value of P_p and K_{eff} for a given value of C_f and h leads to a numerically different relationship between X* and Y*. Higher values of P_p produce a more nonlinear correlation.

In order to make this point apparent, it is helpful to see a representative graph of the axisymmetric laminar boundary layers in standard law-of-the-wall coordinates, i.e., u^+ vs. y^+. Three typical velocity profiles are shown in Fig. 11 for $M_\infty = 0.60$ and three different unit Reynolds numbers. The key observation to note from this figure is that $Y_{eff}\ U_\tau/\nu_w$ is $\simeq 35$, and at this height the normalized velocity u^+ is only 7% below the linear relation $u^+ = y^+$. When a Preston tube is completely submerged in this linear region, Patel[16] has shown that a linear relation between y* and x* results, e.g., see Eq. (4). As the probe height increases and/or boundary layer thickness decreases, the relation between y* and x* becomes more nonlinear, e.g., see Eq. (3). In the case of the subject data, a relatively small nonlinearity is expected.

The above discussion of how a correlation is influenced by high or low values of P_p, naturally leads to the question of accuracy of the measured pressures, and how can erroneous data for a given wind-tunnel condition be identified? This can be qualitatively assessed by comparing the corresponding values of K_{eff} for a particular case with the distribution of K_{eff} for the majority of the data.** For this purpose, K_{eff} has been plotted as a function of $U_\tau h/\nu_w$, M_∞ and Re_m and is shown in Fig. 12. It is relevant to here note that the slightly favorable pressure gradients are negligible over the range $0.09 < X/L < 0.26$ for which laminar Preston-tube data are available, see Fig. 6 and Table II. Thus, the systematic variations in K_{eff} are apparently caused by changes in flow about the face of the probe with changes in: (1) Reynolds number, (2) Mach number, and (3) tunnel freestream disturbance levels. These variations in effective probe height must be properly accounted for if a single correlation equation, with constant coefficients, is to be uniformly valid with respect to Mach number.

The variations of Keff, shown in Fig. 12, show that the effective height of a probe decreases as $U_\tau h/\nu_w$ increases and/or Mach number increases. In either case, the pressure difference $\Delta P_p \equiv P_p - P_w$ increases. Since $U_\tau h/\nu_w$ increases as a given probe moves forward toward the nose, it is obvious that

**Here we assume the bulk of the data provides a valid reference.

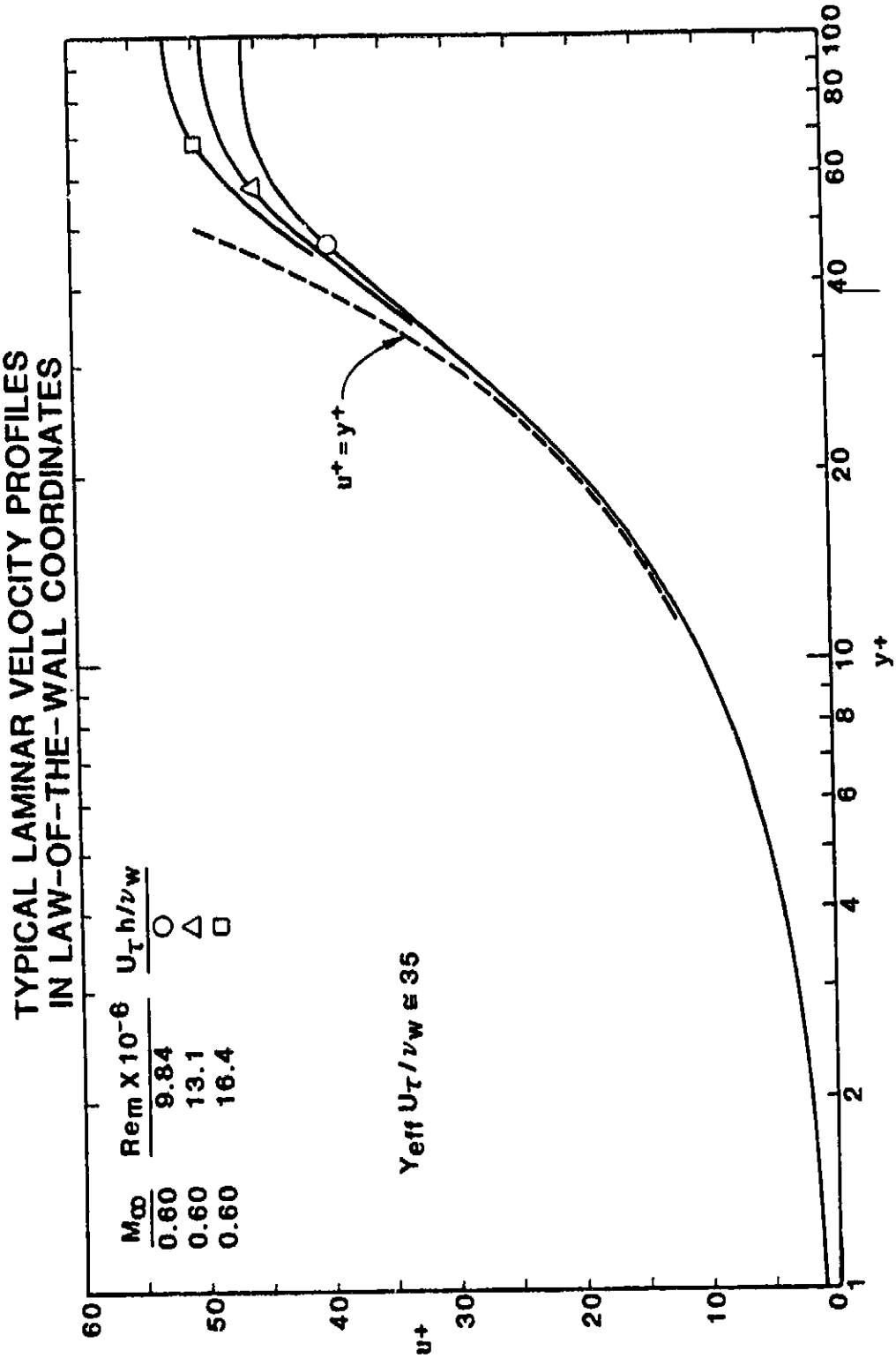

Figure 11

VARIATION OF EFFECTIVE HEIGHT OF PROBE.

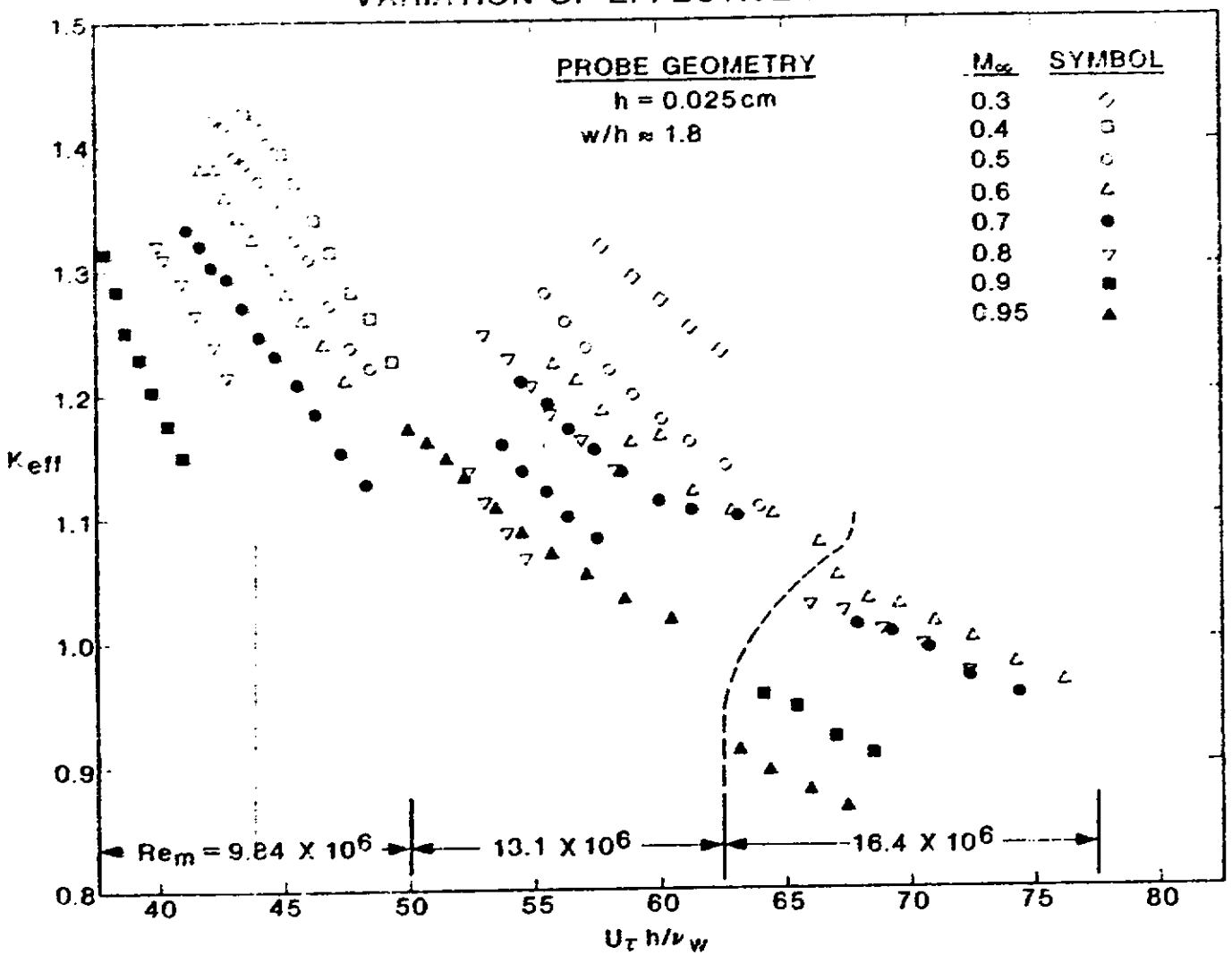

Figure 12

ΔP_p will increase also.† In the case of Mach number it is not quite so obvious that ΔP_p increases with M_∞. In order to illustrate this phenomena, Fig. 13 presents the effect of M_∞ on the distributions of total pressure across the calculated laminar boundary layers on a 10° cone. Here, we see that for a given wall shear stress the total pressure increases with M_∞. This is true for approximately the inner half of laminar boundary layers. Based on the theoretical boundary layer calculations and the given probe height (0.0246 cm) used during these wind tunnel tests, the range of the ratio of probe height to boundary layer thickness is $0.34 < h/\delta < 0.77$. However, the effective height varies in such a way that Y_{eff}/δ is always less than 0.5. In fact, for the three cases shown in Fig. 13, Y_{eff}/δ is ≤ 0.32. The individual values of Y_{eff}/δ and ΔP_p are listed in Table III.

The above described effects of Mach number have also been observed by Bradshaw and Unsworth[27] in their analyses of data for supersonic, flat-plate, turbulent boundary layers. In addition, the fact that the effective height of a probe is less than the actual height explains why Allen's[28] Preston-tube and turbulent skin friction data for supersonic turbulent boundary layers appeared to follow the logarithmic law-of-the-wall even when d/δ was as large as 0.70.

Only two subsonic wind-tunnel conditions were repeated, viz., $M_\infty = 0.7$ and 0.8 at a Reynolds number of 13×10^6. Comparisons of K_{eff} for each of these cases indicate a difference of 0.075 for $M_\infty = 0.7$ and 0.15 for $M_\infty = 0.80$. These differences translate, respectively, to differences in measured pressure of 1.1 kPa (0.16 psi) and 2.3 kPa (0.33 psi). Since the full-scale range of the pressure transducer used in the probe is 34.5 kPad (5 psid), the corresponding percent errors in pressure are 3.2% and 6.6%, respectively. These values are a measure of the repeatability and precision of the Preston-tube data.

Since the distribution of K_{eff} for a given M_∞ is expected to be continuous, the discontinuities between the data for unit Reynolds numbers of 9.8 and 13 are also a measure of precision. The 11-Ft TWT was shut down between the runs for different unit Reynolds number, and individual Mach number cases were run in the order listed in Table 1. However, there were two exceptions to this order. The tunnel was started for run numbers 44-47 and was shut down after wards. The second exception occurred for run numbers

*Only data from run number 44 is being used in this work.

†The Preston-tube measurements of Prozorov[23] for incompressible flat-plate boundary layers also exhibit a decreasing effective probe height with increasing $U_\tau h/\nu_w$, when $U_\tau h/\nu_w$ is less than 100.

THEORETICAL DISTRIBUTION OF TOTAL PRESSURE ACROSS COMPRESSIBLE LAMINAR BOUNDARY LAYERS ON A SHARP NOSE TEN DEGREE CONE

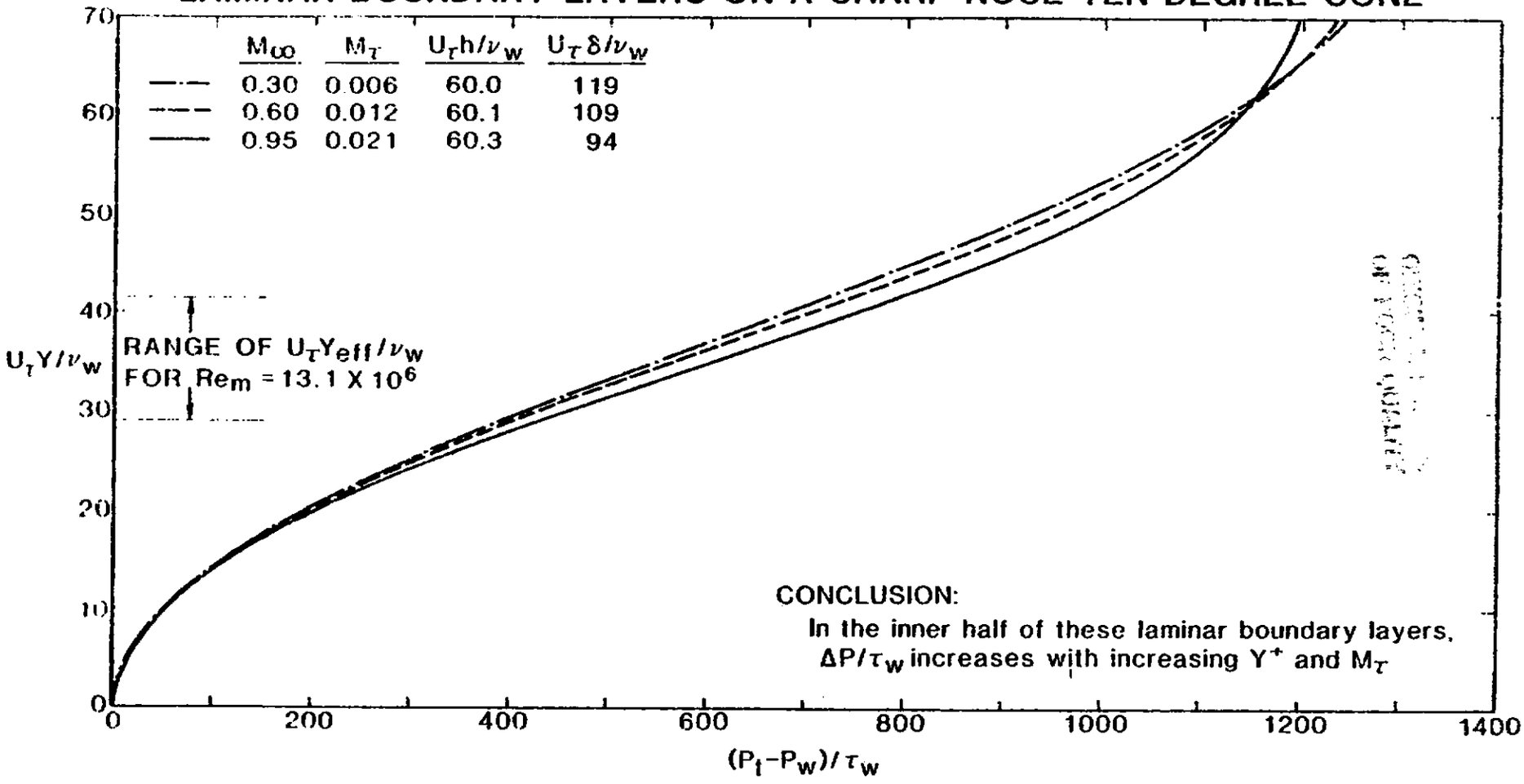

Figure 13

TABLE III

EFFECTS OF MACH NUMBER ON THE PRESSURE
DIFFERENCE ASSOCIATED WITH THE PRESTON TUBE USED IN 11-FT WIND TUNNEL TESTS

M_∞	$Re_m \times 10^{-6}$	$U_\tau Y_{eff}/\nu_w$	Y_{eff}/δ	$\Delta P_p/\tau_w$	τ_w(Pa)	P_p(kPa)
0.3	13.1	38.3	0.32	632.5	7.915	5.008
0.6	13.1	34.09	0.31	540	18.31	9.887
0.95	13.1	29.2	0.31	435	32.18	14.000

70 (M_∞ = 0.7, Re_m = 13 x 10^6) and 72 (M_∞ = 0.8, Re_m = 13 x 10^6) which were performed at a higher unit Reynolds number immediately after the preceeding runs (56-61) for a lower Reynolds number. Thus, for these two runs, it is suspected that the pressure transducer was being influenced by unsteady temperatures and may not have achieved an equilibrium temperature. This phenomenon may have also contributed to errors in pressure measurement for other cases. For example, the K_{eff} for run number 44 (M_∞ = 0.95 Re_m = 16.4 x 10^6) appear to be low.

Using the entire 136 values of K_{eff}, shown in Fig. 12, a correlation between Preston-tube pressures and theoretical, laminar skin friction can be calculated. The equation obtained from a least-squares fit of a quadratic to the data is

$$Y^* = 0.0174(X^*)^2 + 0.3274\ X^* - 0.0392\ T^* + 0.4333, \quad \text{for } 5.4 < X^* < 6.3 \text{ and } M_\infty < 1.0. \tag{20}$$

The rms error in $C_{f,c}$ is now 0.90%. This amount of scatter is comparable to the pipe flow calibrations of Patel[16] and Quarmby and Das[17,18].

However, the lack of continuity between the K_{eff} data for Re_m = 9.8 x 10^6 and the rest of the data is of concern. A reexamination of the data sheets for this Reynolds number indicate some confusion as to the correct gain factor for the X-Y plotter. For example, on the Preston-tube data sheet for Run No. 56 (M_∞ = 0.90, Re_m = 9.8 x 10^6), the listed gain factor is 0.289 psi/cm. Use of this gain factor results in a Preston-tube pressure higher than freestream total pressure! A review of the tunnel testing procedure led to the conclusion that Runs 56-61 should be shifted so that the distribution of K_{eff} for Run No. 58 (M_∞ = 0.70, Re_m = 9.8 x 10^6) forms a continuous curve with Run No. 21 (M_∞ = 0.70, Re_m = 13 x 10^6). In addition, Runs 70 and 72 were shifted, as a group, so as to align Run No. 70 with Run No. 21. A plot of the revised K_{eff}'s are shown in Fig. 14. The corresponding correlation is

$$Y^* = -0.0136\ (X^*)^2 + 0.6977(X^*) + 0.1051\ T^* + 0.6669, \quad \text{for } 5.4 < X^* < 6.3 \text{ and } M_\infty < 1.0. \tag{21}$$

The curves, which appear in Fig. 14, will be discussed in the following section on analyses of flight data.

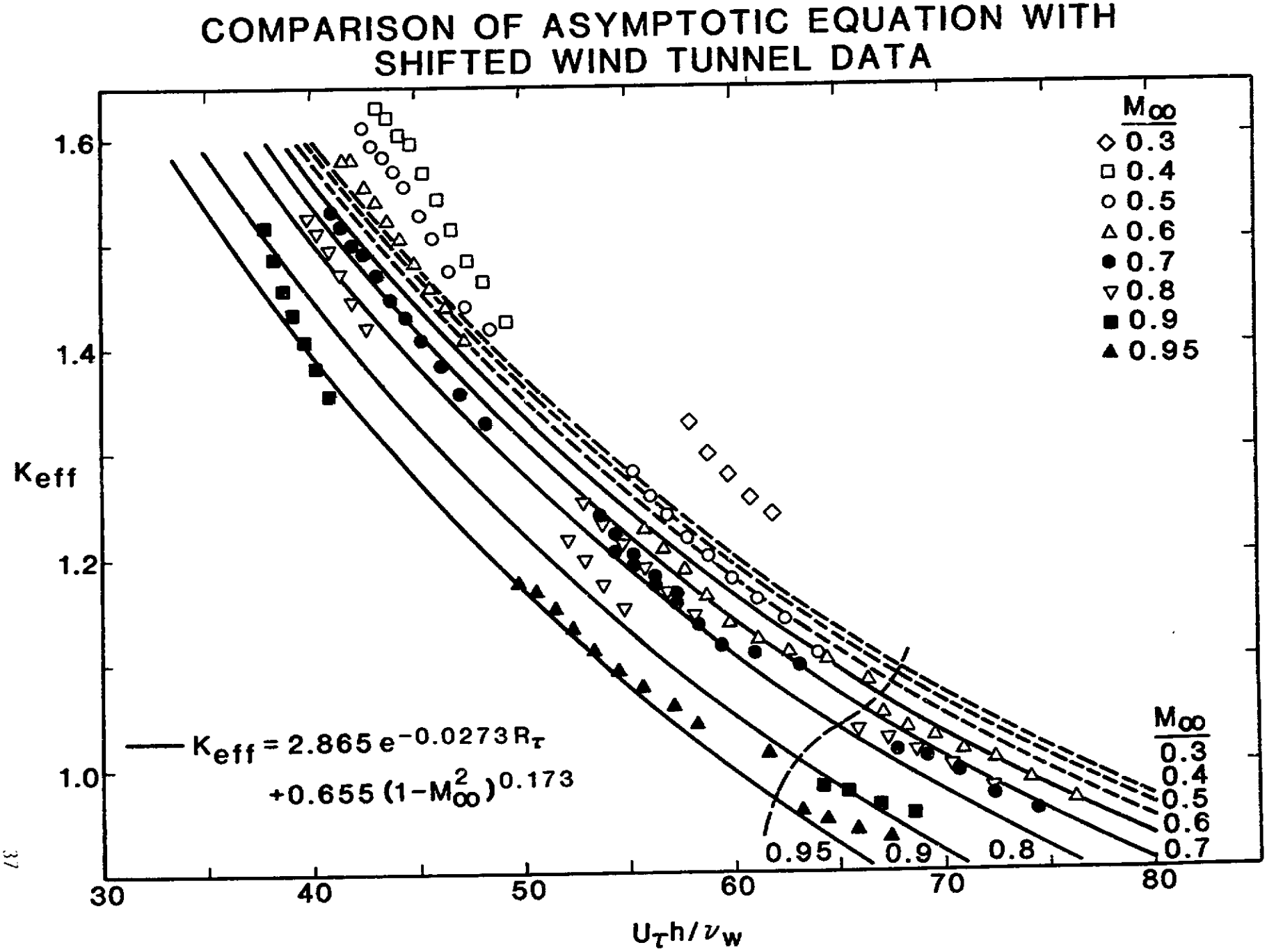

Figure 14

This equation is shown in Fig. 15 with the individual data points superimposed. The rms error in $C_{f,c}$ is now 0.97%, and the individual values of $\bar{C}_f$ are presented in Fig. 16. Equation (21) is considered to be our best estimate of a correct correlation for the 11-Ft TWT.

It may be noted that the contribution of the T* term is very small because the temperature ratio T'/T_e is near one and the log of 1 is zero. This simply indicates negligible departures of density (ρ) and viscosity (μ) from values based on wall temperature. In anticipation of the need to compare the wind-tunnel correlation with a correlation based on flight data, it is obvious that such a comparison will be easier if T* is dropped. Upon doing this and refitting the data, the following simplied correlation is obtained.

$$Y^* = -0.0103\ (X^*)^2 + 0.6653\ X^* - 0.5946, \qquad (22)$$

for $5.7 < X^* < 6.3$ and $M_\infty < 1$.

The rms error in $C_{f,c}$ has increased only slightly to 0.98%. Equation (22) is plotted on Fig. 17 and is compared with an analogous correlation for the unmodified wind tunnel data. It should be noted that the small increase in rms error of $C_{f,c}$, relative to the unmodified data, is caused by the fact that a given difference in K_{eff} leads to a greater difference in Preston-tube pressure as the height above the wall is increased, recall Fig. 13.

It is here emphasized that the numerical values of K_{eff} and the coefficients in Eqs. (21) and (22) are valid only for the Ames 11-Ft TWT and the particular probe used during these tests. The numbers are expected to be different for different wind-tunnel environments and for probes with significantly different aspect ratio and/or face geometry. In particular, the coefficients are believed to contain information on the freestream disturbance levels which are peculiar to the 11-Ft TWT. With the attainment of this objective, a corresponding analysis of the flight data was begun. This is reported in the next section.

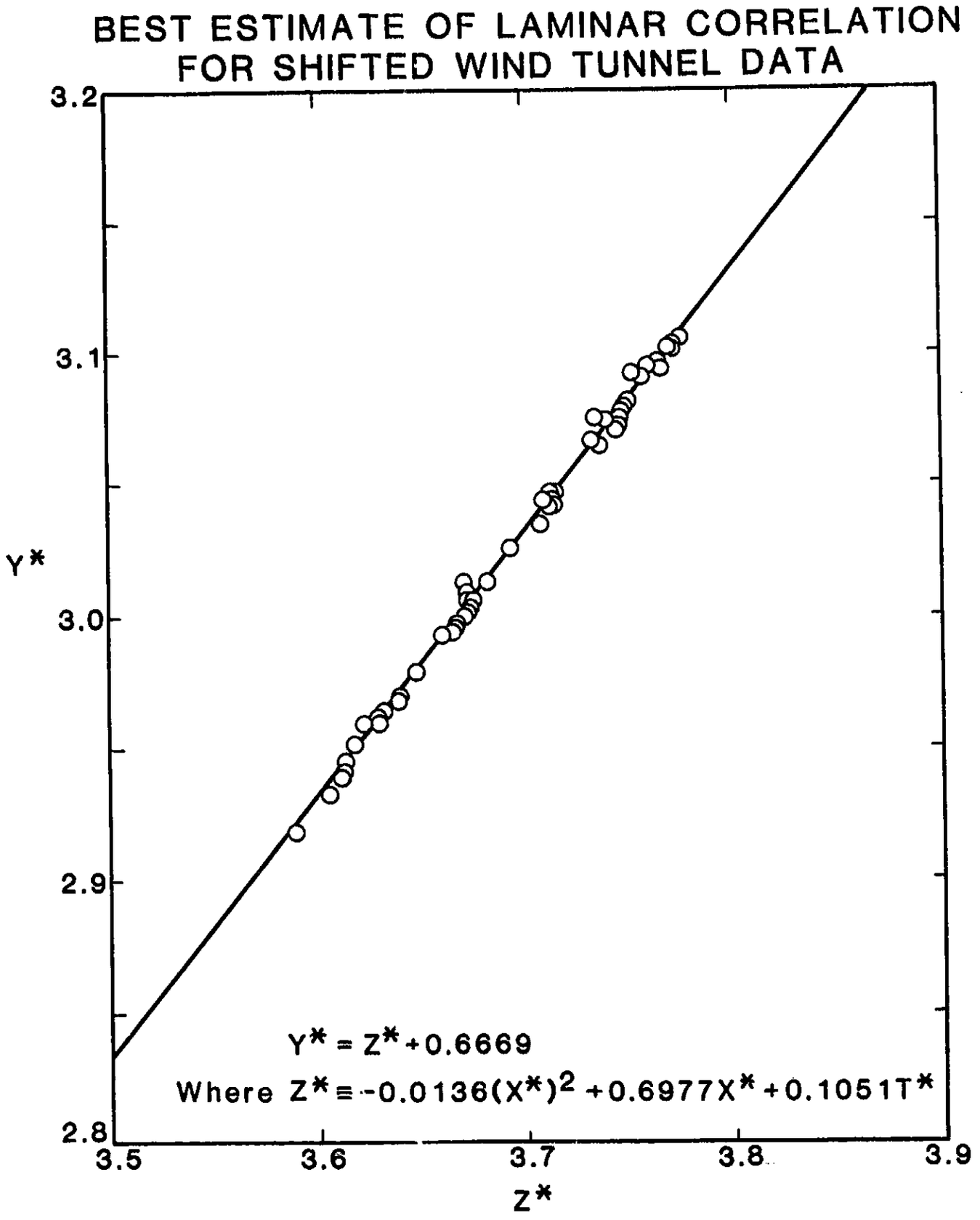

Figure 15

SCATTER OF LAMINAR SKIN FRICTION COEFFICIENT ABOUT THE BEST CORRELATION FOR WIND TUNNEL DATA

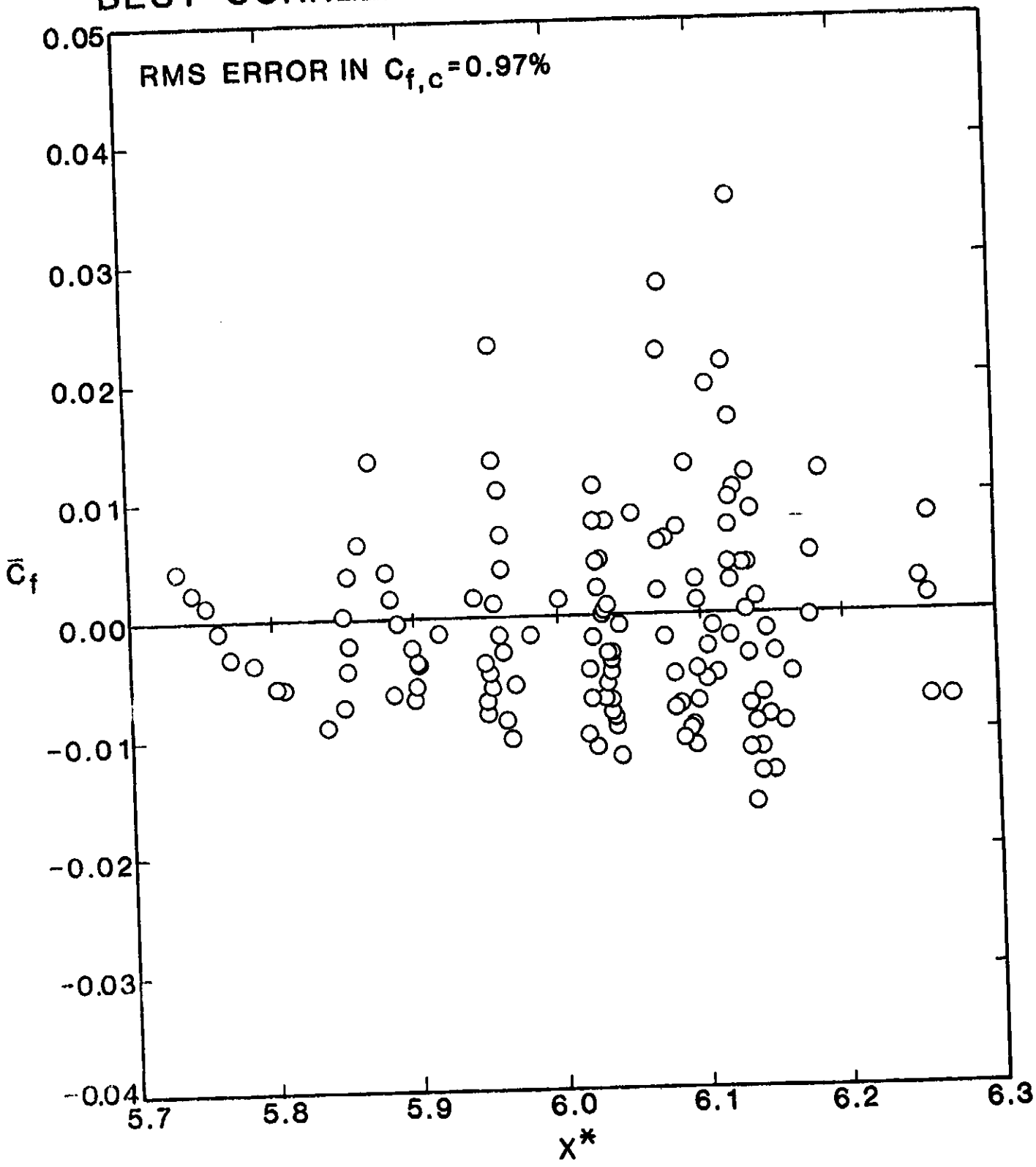

Figure 16

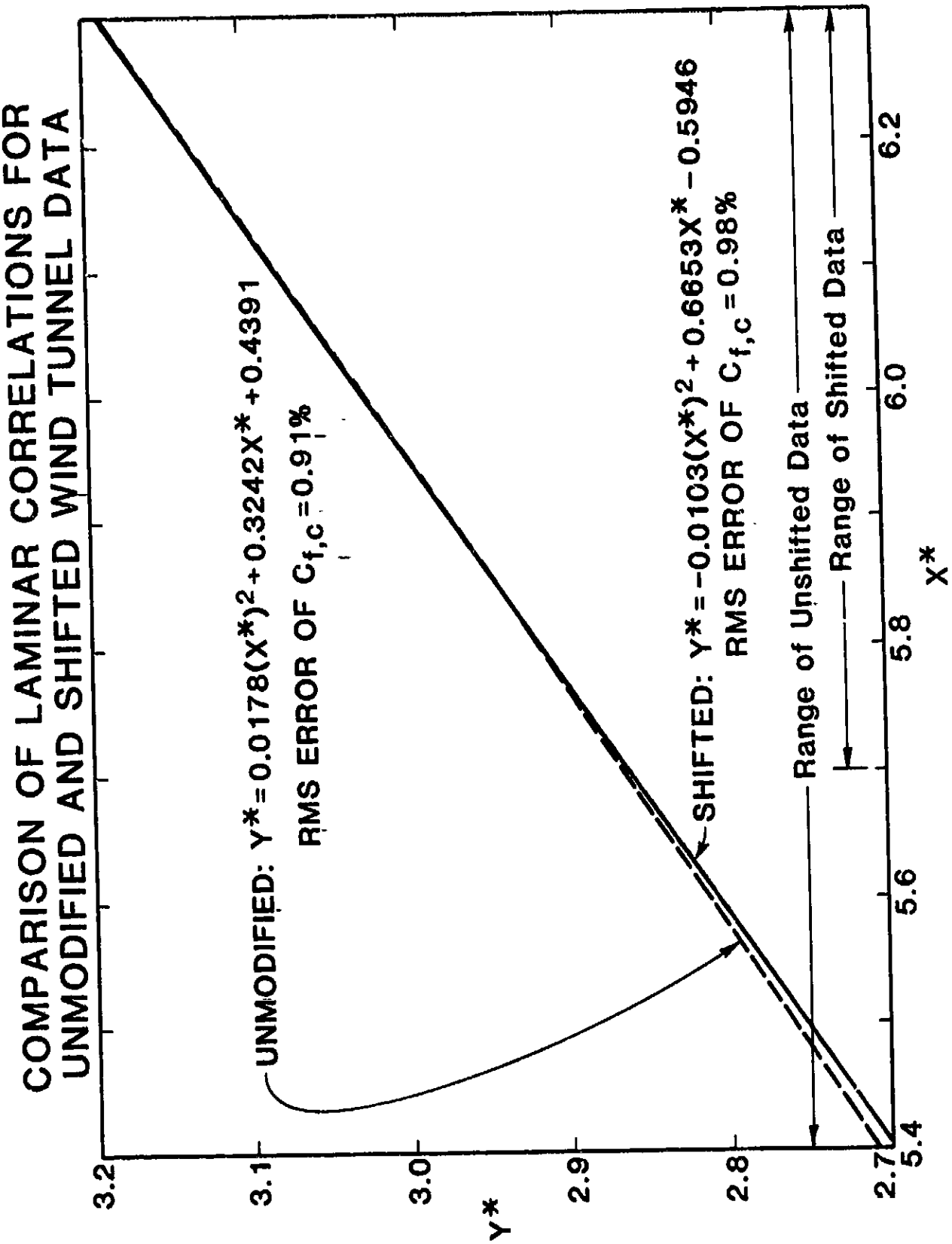

Figure 17

IV. ANALYSIS OF FLIGHT DATA

The AEDC-BLT Cone was mounted on the nose of a McDonnell-Douglas F-15 aircraft for flight tests[8,29] Although the cone apex was over 2m(≈ 7 Ft)ahead of the aircraft nose, it was recognized that the flow field about the aircraft could influence flow about the cone. Hence, it was necessary to obtain measurements of static pressure distribution along the cone by employing a facsimile cone. This cone has the same exterior dimensions as the BLT Cone but was constructed so that interchangeable inserts in the wall permitted measurements of either static pressures or wall temperatures along the surface of the cone. The inserts for static pressure measurements had an orifice with an inside diameter of 0.107 cm (0.042 in.) Table IV lists the locations of these orifices along the surface of the cone.

Most of the flight data were obtained for nonzero pitch and/or yaw. Since we are unable to calculate non-axisymmetric boundary layers with STAN-5, only the cases having negligible α and β were selected for development of a Preston-tube/skin friction correlation. A total of nine cases were identified as having both α and β of the order of 0.1 degree or less. A summary of the selected data is tabulated in Table V. The numbering system used to designate the various flights is as follows:

$$\underbrace{XXX}_{\text{Flight No.}} \cdot \underbrace{YYYY}_{\text{Time of Day}}$$

The listed values of freestream Mach number, unit Reynolds number, dynamic pressure, and pitch and yaw angles are the time-averaged values based on the measured conditions which existed during the time the Preston tube was within the laminar boundary layers.

TABLE IV

PRESSURE INSTRUMENTATION ON FACSIMILE CONE

(a) Surface Distribution of Static Orifices

Orifice	X(in.)	X/L	ϕ(DEG)
1	7	.157	180
2	16	.360	0
3	17	.382	0
4	19	.427	0
5	20	.449	0
6	21	.472	0
7	22	.494	0
8	25	.562	0
9	26	.584	0
10	27	.607	0
11	28	.629	0
12	29	.652	0
13	30	.674	0
14	30	.674	90
15	30	.674	180
16	30	.674	270
17	31	.697	0
18	32	.719	0
19	33	.742	0
20	34	.764	0
21	35	.787	0
22	35	.787	180

(b) Differential Pressures

Orifice	X(in.)	X/L	ϕ
18, 0-180*	18	.404	0 & 180 - pitch plane
18, 90-270	18	.404	90 & 270 - yaw plane

*Note: Leaky Transducer-Unusuable

TABLE V

FLIGHT DATA USED IN DEVELOPMENT OF LAMINAR CORRELATION

[illegible]	M_∞	$Re_{ft} \times 10^{-6}$	q_∞(psf)	T_w(°R)	$\alpha°$	$\beta°$	$(C_p)_{rms}$	X_t(in)	X(in)	P_p (psf)	$K_{eff}(T_w)$
[illegible]	0.86	2.2	304	482.4	-.02	-.04	0.2240		16.0	771.1	2.430
									16.5	766.8	2.410
									17.0	763.9	2.441
									17.5	761.0	2.453
									18.0	759.6	2.470
									18.5	758.1	2.487
									19.0	756.7	2.509
									19.5	755.2	2.532
				$(T_w)_{meas}$ = 494.4				19.9			
[illegible]	0.66	2.4	299	494.9	0.00	-.01	0.1460		16.0	1118.9	1.934
									16.5	1116.0	1.937
									17.0	1113.5	1.941
									17.5	1111.7	1.944
									18.0	1110.2	1.948
									18.5	1107.3	1.953
									19.0	1104.5	1.959
									19.5	1103.0	1.963
									20.0	1101.6	1.969
									20.5	1098.7	1.974
									21.0	1097.2	1.981
									21.5	1095.8	1.989
									22.0	1094.4	1.996
									22.5	1092.9	2.004
									23.0	1092.9	2.013
				$(T_w)_{meas}$ = 496.2				23.6			
329.1028	0.85	2.1	289	478.3	-.06	0.03	0.1224		16.0	744.1	2.468
									16.5	742.7	2.487
									17.0	741.2	2.502
									17.5	739.8	2.522
									18.0	736.9	2.542
									18.5	735.5	2.561
									19.0	734.0	2.578
									19.5	732.6	2.599
									20.0	731.4	2.614
				$(T_w)_{meas}$ = 480.3				20.8			

TABLE V (CONT'D)

FLIGHT DATA USED IN DEVELOPMENT OF LAMINAR CORRELATION

FLT#	M_∞	$Re_{ft} \times 10^{-6}$	q_∞(psf)	T_w(°R)	$\alpha°$	$\beta°$	$(C_p)_{rms}$	X_t(in)	X(in)	P_p (psf)	$K_{eff}(T_w)$
329.1036	0.74	2.2	277	482.4	0.08	0.06	0.0969		16.0	877.8	2.293
									16.5	876.4	2.309
									17.0	875.0	2.325
									17.5	873.5	2.339
									18.0	870.6	2.355
									18.5	869.2	2.368
									19.0	877.8	2.384
									19.5	866.3	2.399
									20.0	864.9	2.414
									20.5	863.4	2.429
									21.0	862.0	2.443
									21.5	860.6	2.457
				$(T_w)_{meas}$ = 484.4				22.2			
329.1042	0.67	2.5	306	490.1	-.12	0.02	0.0954		16.0	1128.5	1.939
									16.5	1127.1	1.946
									17.0	1124.2	1.954
									17.5	1121.3	1.961
									18.0	1119.9	1.970
									18.5	1117.0	1.977
									19.0	1115.6	1.984
									19.5	1114.1	1.992
									20.0	1111.3	2.000
									20.5	1109.8	2.007
									21.0	1108.4	2.015
									21.5	1106.9	2.023
				$(T_w)_{meas}$ = 491.4				22.0			
332.1020	0.93	2.8	451	514.0	-.05	-.01	0.1950		16.0	971.5	1.899
									16.5	967.2	1.902
									17.0	962.9	1.905
									17.5	958.5	1.909
									18.0	954.2	1.915
									18.5	951.3	1.922
				$(T_w)_{meas}$ = 511.1				19.0			
333.1351	0.94	2.8	457	507.1	-.03	-.05	0.0713		16.0	965.4	1.869
									16.5	962.5	1.874
									17.0	958.2	1.879
									17.5	955.3	1.885
									18.0	952.4	1.890
									18.5	949.5	1.896
									19.0	945.2	1.901
									19.5	942.3	1.908
									20.0	938.0	1.913
				$(T_w)_{meas}$ = 477.1				20.7			

TABLE V (CONT'D)

FLIGHT DATA USED IN DEVELOPMENT OF LAMINAR CORRELATION

[illegible]	M_∞	$Re_{ft} \times$ [illegible]	q_∞ (psf)	T_w (°R)	α°	β°	$(C_p)_{rms}$	x_t (in)	x(in)	P_p (psf)	K_{eff} [illegible]
[illegible]	[illegible]	[illegible]	[illegible]	508.9	0.02	-.02	0.1049		16.0	1024.[illegible]	[illegible]
									16.5	1020.[illegible]	[illegible]
				$(T_w)_{meas}$ = 511.1					17.0	[illegible]	[illegible]
									17.5	1012.9	1.85[illegible]
									18.0	1010.[illegible]	1.8[illegible]
									18.5	1005.7	1.865
									19.0	1001.[illegible]	[illegible]
								19.7			
[illegible]	0.75	[illegible]	284	475.5	-.07	0.04	***		16.0	826.7	[illegible]
									16.5	823.8	[illegible]
				$(T_w)_{meas}$ = 477.1					17.0	822.[illegible]	[illegible]
									17.5	820.9	[illegible]
									18.0	819.5	[illegible]
									18.5	818.0	[illegible]
									19.0	816.6	1.735
									19.5	815.2	[illegible]
									20.0	815.2	[illegible]
								20.8			

***Not measured during flight

ORIGINAL PAGE IS OF POOR QUALITY

The first step in calculating the boundary layers for the flight data is to use the measurements of static pressure along the facsimile cone to define the inviscid flow field. Particular data from flight tests of the facsimile cone were selected to match the values of freestream Mach numbers listed in Table V within $\pm$ 0.005. The distributions of $C_p(X)$ were then used with the values of q_∞, listed in Table V, to calculate static pressures along the surface of the BLT Cone.[+] In the flight-test report by Dougherty and Fisher[29], they state that the static pressure is nearly constant along the length of the cone. However, the static pressure data we were given has significant scatter. Figures 18 and 19 show, respectively, a typical favorable and an adverse pressure gradient. In light of this apparently random scatter and the comments of Dougherty and Fisher, a simple straight line was fit to the data for each of the nine flight conditions. The associated rms errors in C_p are listed in Table VI and range from 4 to 6%. Comparisons of the in-flight facsimile cone pressures with the theoretical distributions of Wu and Lock, Fig. 6, indicate that the effect of the airplane is to reduce the favorable pressure gradients which exist on an isolated 10-degree cone.

The effect of orifice-induced errors was estimated using the method of Franklin and Wallace.[30] The increase in measured static pressure, due to flow dipping into the 0.107 cm (0.042 in.) orifices, was estimated for two cases: (1) a laminar boundary layer at X = 17.8 cm and with flow conditions corresponding to Flight #327.0908[++] and (2) a turbulent boundary at X = 48.3 cm with the same freestream conditions. In both cases, the calculated error in static pressure was less than 0.1%. Thus, orifice-induced errors appear to be negligible.

However, the facsimile cone pressures do need to be corrected for differences in pitch and yaw angles. This need arises because when Mach numbers of flight tests of the facsimile cone and the BLT Cone are matched, the values of α and β do not match. A correction for these differences in pitch and yaw angles can be calculated via the Wu and Lock

---

[+]This is consistent with the Wu and Lock theory which states: C_p = fn(M_∞, Cone angle, α, β, X/L).

[++]Within the range of freestream conditions listed in Table V, this corresponds to the lowest Mach number for which static pressures were measured, and thus the thinnest boundary layer exists for this case. However, in retrospect, the flow conditions for Flight No. 333.1351 should have been used because a larger τ_W results, and orifice-induced errors increase with τ_W.

A FAVORABLE SURFACE PRESSURE DISTRIBUTION MEASURED DURING FLIGHT TESTS OF FACSIMILE CONE

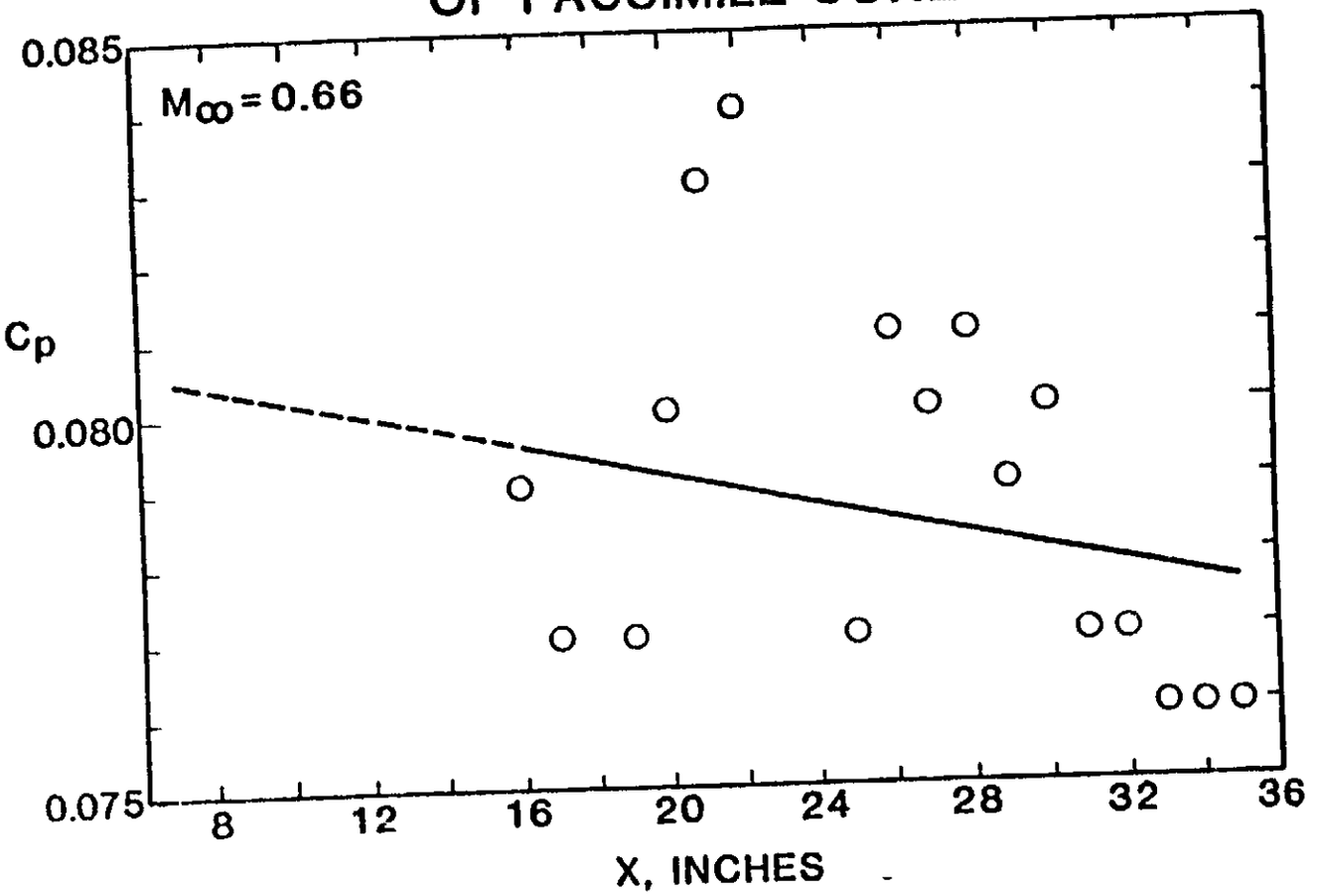

Figure 18

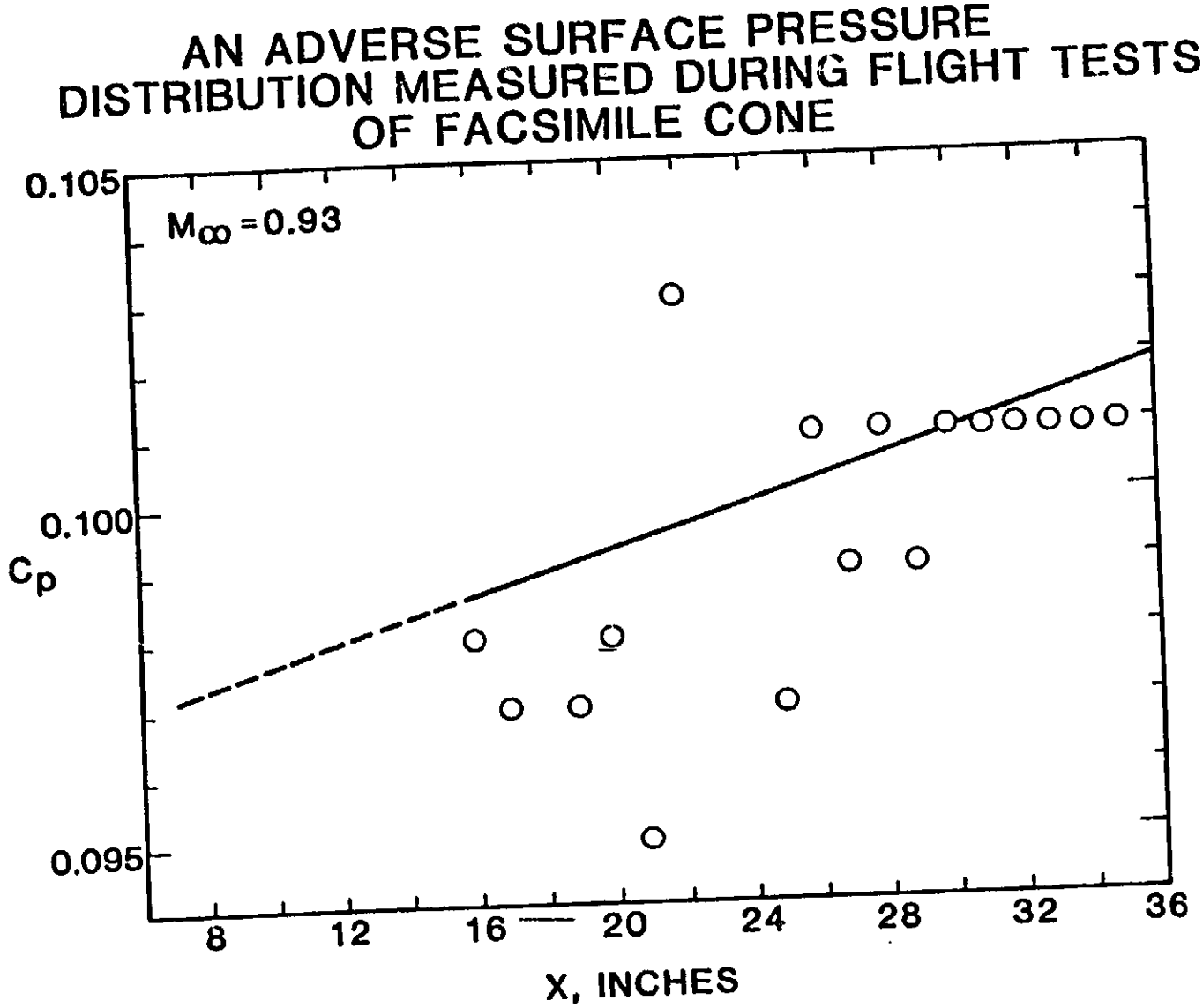

Figure 19

theory. In particular, $C_p(x)$ can be calculated along the location of the Preston-tube traverse (ϕ=0°) for each Γ measured during tests of the facsimile cone and the BLT Cone. In the case of the BLT Cone, the time-averaged value of Γ, during the time the Preston-tube was within the laminar boundary layer, is used for the theoretical calculation of C_p (M_∞, Γ, X/L). The y-intercepts of the straight line curve fits of the facsimile cone pressures are then increased or decreased according to the difference between spatially-averaged (over length of laminar boundary layer) value of C_p for the BLT Cone and the corresponding C_p calculated for the facsimile cone at the same M_∞ but different Γ, i.e.: letting

$(C_p)_{FC} = mx + b$,

then $(C_p)_{FC,Corr} = mx + b + C_p(\Gamma \text{ for BLT Cone}) - C_p(\Gamma \text{ for FC})$. (23)

The resulting equations are tabulated in Table VI. It is relevant to note this procedure assumes the differences in static pressure distribution caused by differences in angles-of-attack are not influenced by the F-15 aircraft.

The measured wall temperatures, tabulated in Table V, were obtained with a single flush-mounted thermocouple at x = 90.2 cm and ϕ = 180 degrees. Since this location is always within the turbulent boundary layer and the subject of this work is laminar boundary layers, it was decided to estimate what thecorresponding wall temperatures should be under the various laminar boundary layers. This can be done by multiplying the measured T_w by the ratio of the laminar over the turbulent adiabatic wall temperature. A turbulent recovery factor of r_t = 0.8825 and a laminar recovery factor of r_l = 0.845 were selected because they are average values based on data from tests of cones, e.g. Rohsenow and Choi[31]. The local edge Mach number at x = 90.2 cm is computed based on the corrected $C_p(X)$ distribution for a given set of flight data, Table VI. A laminar value for M_e is obtained using the spatially-averaged value of C_p over the length of the measured laminar Preston-tube data. The measured wall temperature is then multiplied by the ratio $(T_{aw})_l/(T_{aw})_t$ in order to arrive at the temperatures listed in Table V. As may be seen, the wall temperatures generally decrease by only 2°F.

At this point, sufficient information exists in order to proceed with boundary layer computations for the nine flight conditions. This, of course was done using the STAN-5 Code. The resulting theoretical boundary layer

TABLE VI. Straight-Line Fits of Surface Pressure Distributions Measured on Facsimile Cone (FLT #358)

$\bar{M}_\infty$	Equation	R.M.S. Error (%)	ΔC_p, Correction added to C_p to account for $\overline{\Delta\alpha}$, $\overline{\Delta\beta}$	$\overline{\Delta\alpha}$ (Deg)	$\overline{\Delta\beta}$ (Deg)
0.66	$C_p(X) = 0.0831 - 0.00712\ X/L$	5.35	0.000	-0.04	-.49
0.67	$C_p(X) = 0.0848 - 0.00623\ X/L$	5.77	0.001	-0.07	-.45
0.74	$C_p(X) = 0.0760 + 0.00490\ X/L$	5.79	0.000	-0.11	-.19
0.75	$C_p(X) = 0.0791 + 0.00445\ X/L$	5.90	0.001	-0.24	-.23
0.85	$C_p(X) = 0.0874 + 0.00712\ X/L$	6.07	0.000	0.10	-.27
0.86	$C_p(X) = 0.0894 + 0.00134\ X/L$	5.89	0.000	0.01	-.34
0.88	$C_p(X) = 0.0899 + 0.00312\ X/L$	4.21	0.000	0.06	-.38
0.89	$C_p(X) = 0.0890 + 0.00668\ X/L$	4.38	-0.001	0.17	0.36
0.93	$C_p(X) = 0.0909 + 0.01157\ X/L$	3.95	-0.002	0.39	0.19
0.94	$C_p(X) = 0.0943 + 0.00890\ X/L$	6.05	-0.003	0.47	0.11

profiles can then be used in conjunction with Preston-tube pressures to define effective probe heights. A typical trace of Preston-tube pressure is shown in Fig. 20. The scatter in the laminar portion of the boundary layer can be eliminated by hand fairing a curve through the measured pressures. This has been done for all nine flight conditions.

Using values of the faired Preston-tube pressures, at intervals of 1.27 cm (0.5 in.), a total of 87 values of K_{eff} were calculated. These are listed in Table V and are plotted in Fig. 21 as a function of $U_1 h/\nu_w$. This figure reveals that the semi-empirical values of K_{eff} are mutually inconsistent, and values greater than two are suspected of being erroneous.

However, before attempting any corrections, it is instructive to derive a correlation based on the unmodified data and then to calculate the corresponding effective unit Reynolds numbers for the 11-Ft TWT. Before doing this the distributions of K_{eff}, shown in Fig. 21, were fit with exponential equations to further smooth the data and facilitate the corrections which will be discussed later. These equations are listed in Table VII.

A least-squares curve fit of a quadratic correlation to the laminar flight data, based on the smoothed values of: (1) $C_p(X)$, (2) $P_p(X)$, and (3) K_{eff}, resulted in

$$Y^* = 0.0915(X^*)^2 - 0.5846\ X^* + 3.2259\ , \qquad (24)$$

$$\text{for } 5.8 < X^* < 6.4.$$

A graph of this equation and the associated data are presented in Fig. 22. The corresponding values of C_f are shown in Fig. 23. The rms error in $C_{f,c}$ is 0.56%. This reduced scatter, compared to the wind tunnel data, is not only due to the use of smoothed data but also the fewer number of individual data points and the smaller range of freestream conditions.

This identifies a deficiency of the method for calculating K_{eff} which forces the measured Preston-tube pressures to be consistent with the theoretical solutions of the conservation equations for the boundary layer. This procedure results in values of X* and Y* for the high values of P_p to agree with and correlate with the rest of the data. Only the plot of K_{eff} points to a possible problem with some of the measured flight data.

The correlation for the unmodified flight data, Eq. (24), is compared with the correlation for the shifted wind-tunnel data, Eq. (22), in Fig. 24. The two correlations cross near X* = 5.77, which is outside

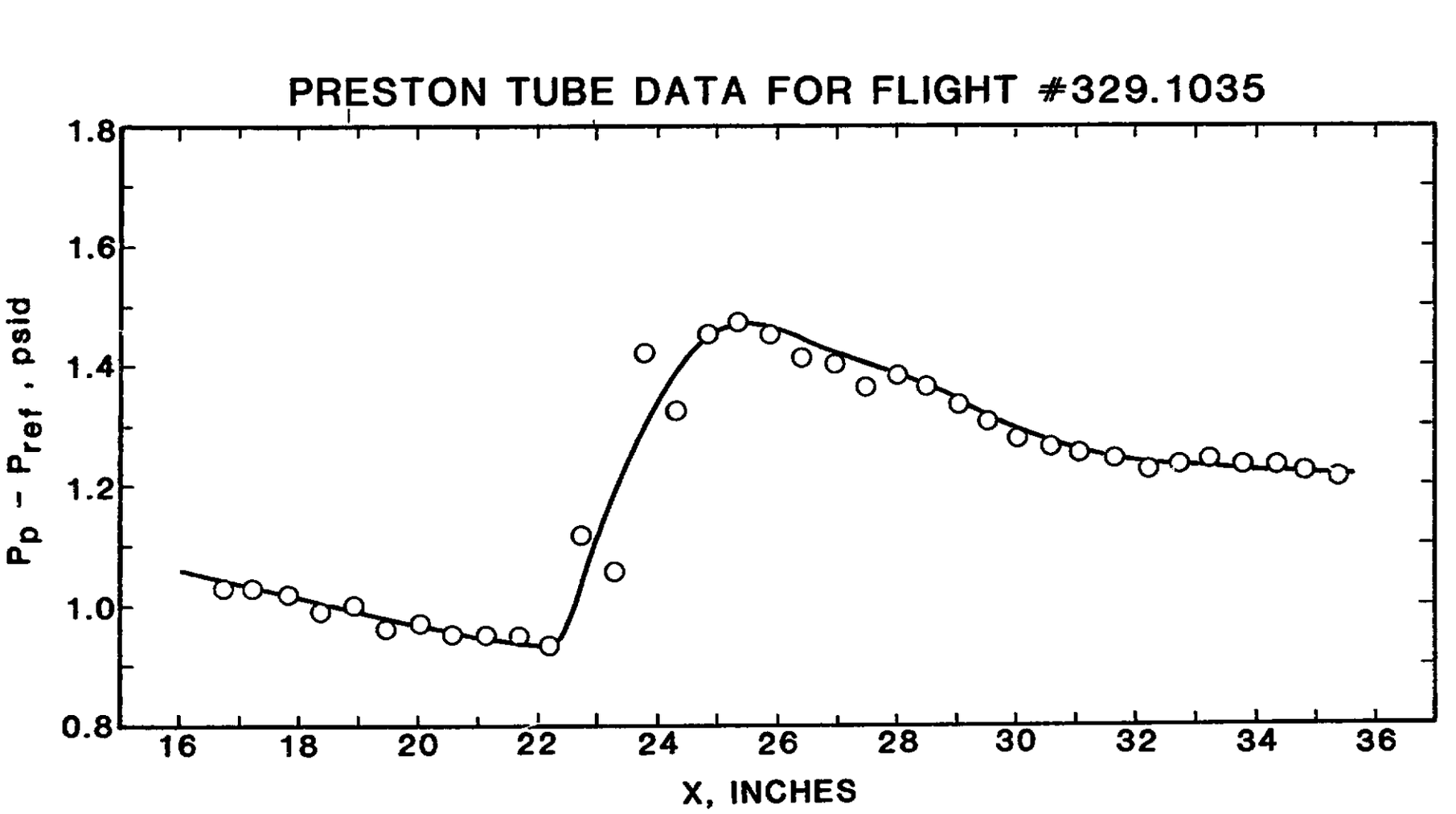
PRESTON TUBE DATA FOR FLIGHT #329.1035
1.8
1.6
1.4
1.2
1.0
0.8
$P_p - P_{ref}$, psid
16
18
20
22
24
26
28
30
32
34
36
X, INCHES

Figure 20

DISTRIBUTIONS OF EFFECTIVE PROBE HEIGHT FOR FLIGHT DATA

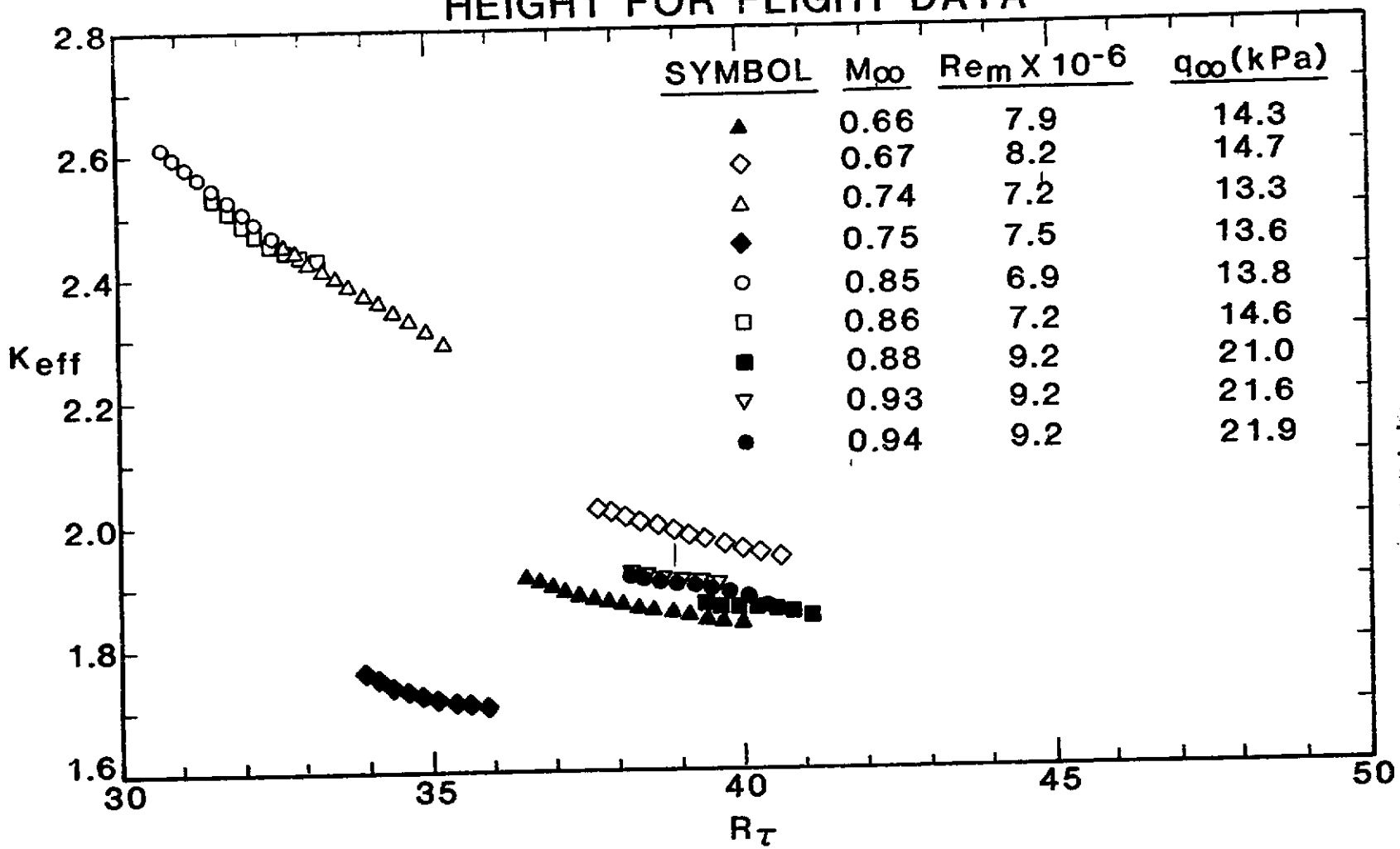

Figure 21

TABLE VII

RESULTS OF LEAST-SQUARES CURVE FITS OF
EXPONENTIALS TO EFFECTIVE PROBE HEIGHTS FOR FLIGHT DATA

Flt#	M_∞	Equation for K_{eff}
329.0918	0.66	$0.0510\ EXP\ [-0.4452\ (R_\tau^{\dagger} - 38.0321)] + 1.8133$
329.1042	0.67	$0.2287\ EXP\ [-0.1298\ (R_\tau - 38.9423)] + 1.7539$
329.1036	0.74	$0.5689\ EXP\ [-0.1154\ (R_\tau - 33.8301)] + 1.8118$
349.1400	0.75	$0.0387\ EXP\ [-0.8187\ (R_\tau - 34.6364)] + 1.6866$
329.1027	0.85	$0.4787\ EXP\ [-0.1809\ (R_\tau - 31.4714)] + 2.0779$
327.0907	0.86	$0.0887\ EXP\ [-0.8263\ (R_\tau - 32.3159)] + 2.3808$
333.1353	0.88	$0.0437\ EXP\ [-0.2315\ (R_\tau - 40.0836)] + 1.8146$
332.1020	0.93	$0.0194\ EXP\ [-1.0018\ (R_\tau - 38.6302)] + 1.8922$
333.1350	0.94	$0.1090\ EXP\ [-0.1914\ (R_\tau - 39.1318)] + 1.7825$

†Here $R_\tau \equiv U_\tau h/\nu_w$

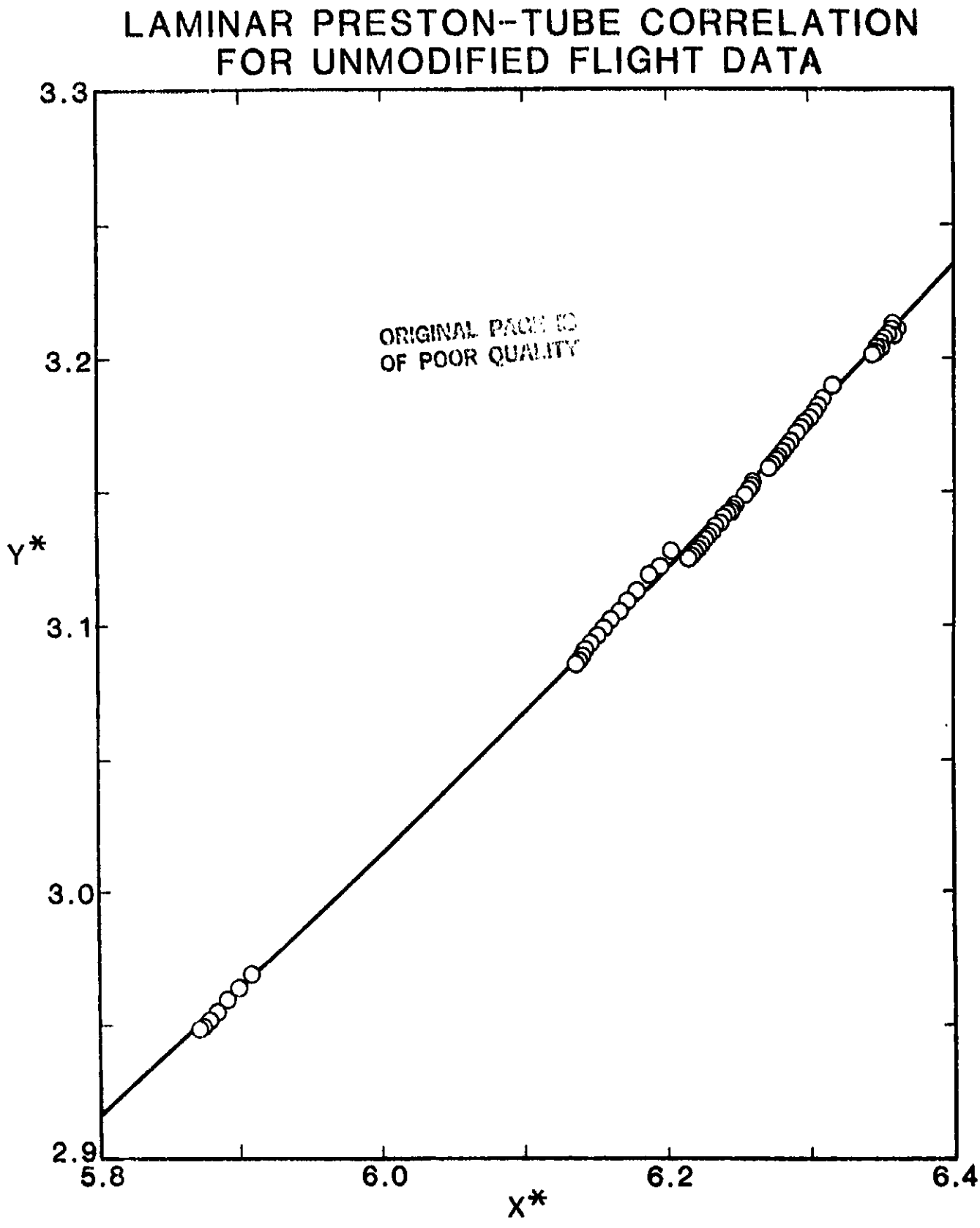

Figure 22

SCATTER OF THEORETICAL LAMINAR SKIN FRICTION ABOUT CORRELATION FOR UNMODIFIED FLIGHT DATA

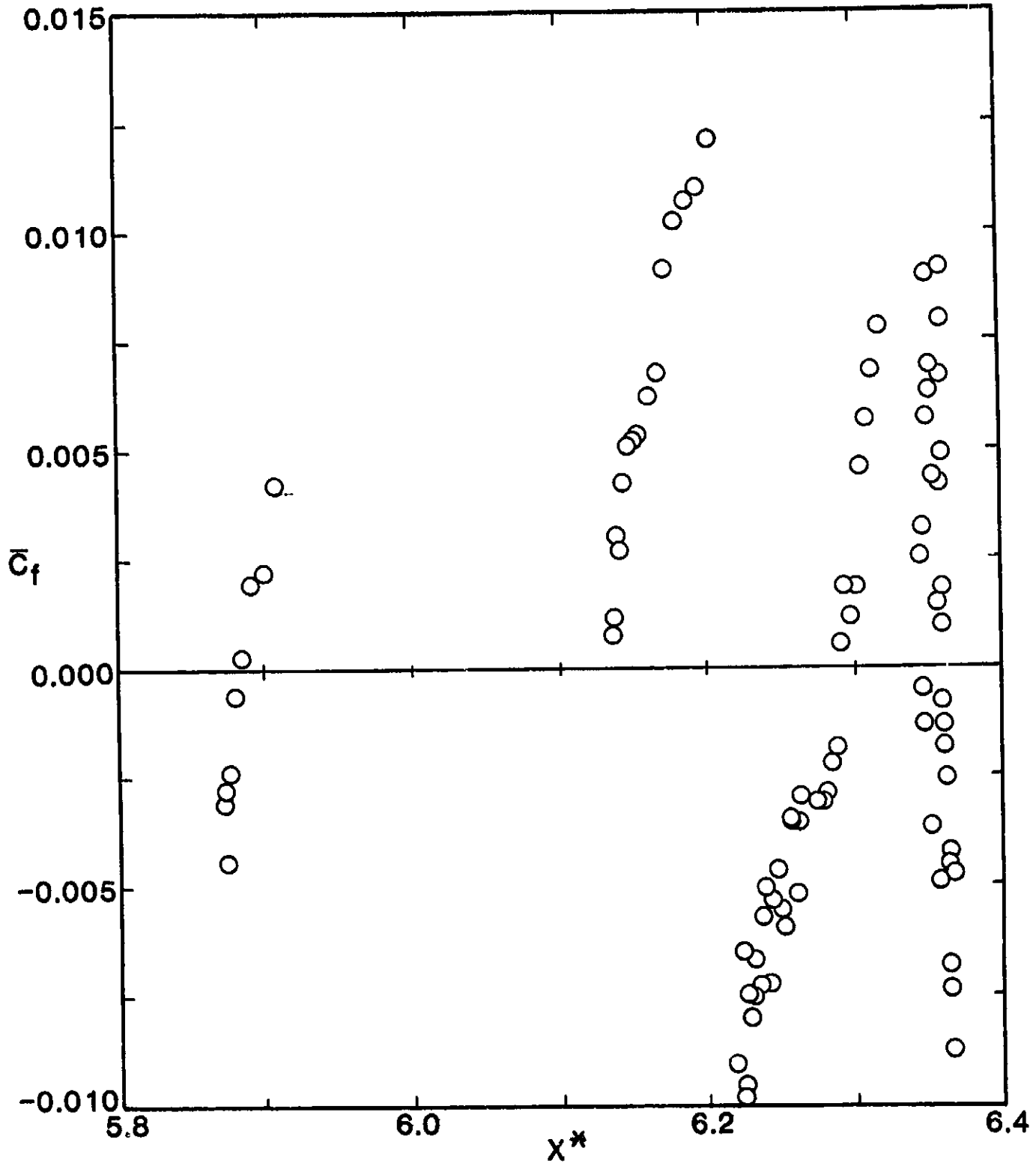

Figure 23

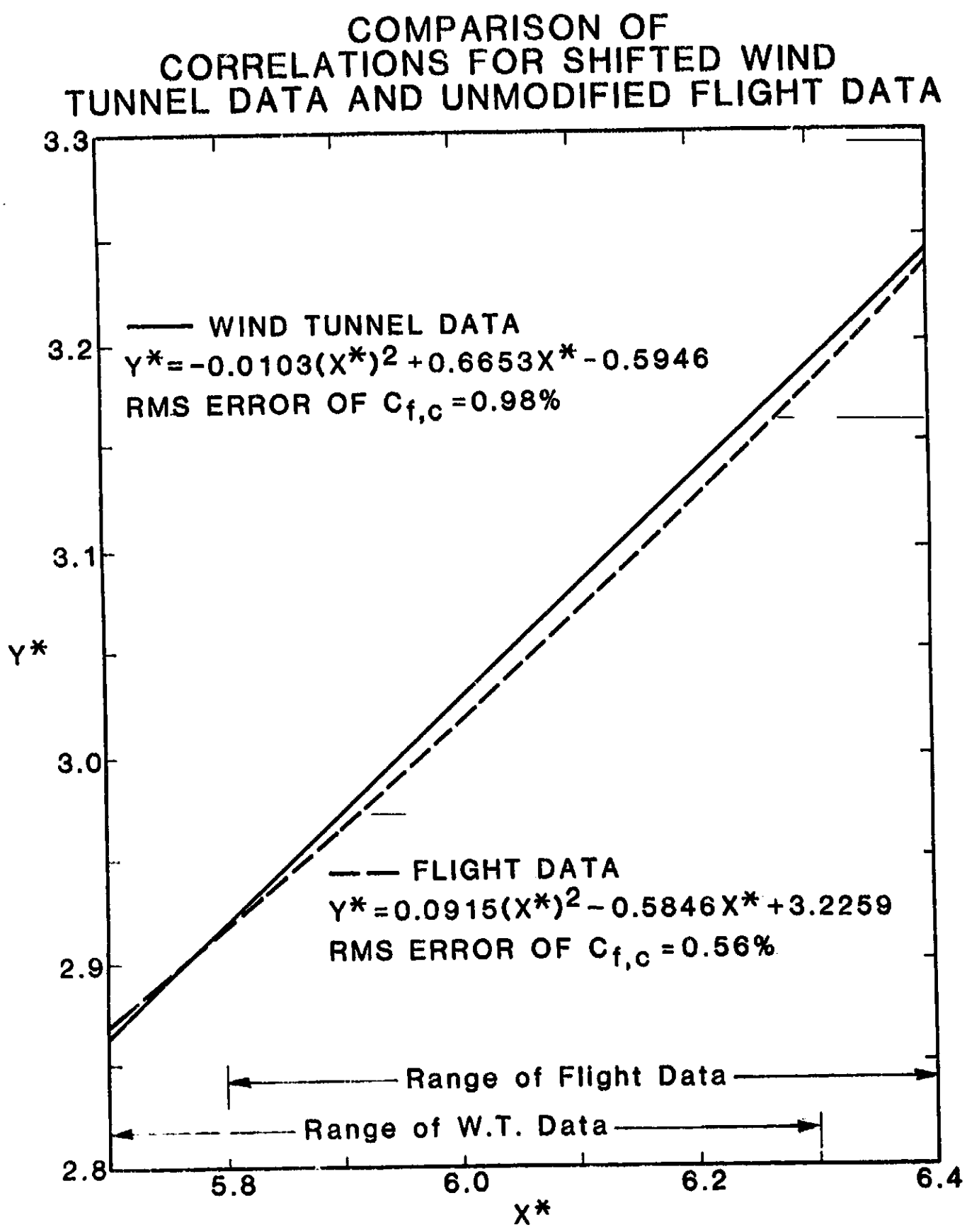

Figure 24

the range of the flight data, and a maximum difference occurs near $X^* = 6.05$. The wind-tunnel correlation is above the flight data correlation over the range of the flight data. This is consistent with the fact that larger disturbances are present within a transonic wind tunnel. The difference between the two correlations can be used to define an effective freestream unit Reynolds number. A description of this procedure is given in the following section.

V. COMPARISON OF CORRELATIONS AND CALCULATION OF AN EFFECTIVE FREESTREAM UNIT REYNOLDS NUMBER

A. Unmodified Flight Data

In analogy to the classical definition of effective freestream Reynolds number based on equal values of drag coefficients of a sphere, one can use Eqs. (22) and (24) to accomplish the same objective by equating values of skin friction coefficient. This procedure requires the following set of conditions be specified at a point on the cone.

1. Freestream conditions: M_∞, q_∞, Re_m
2. Inviscid pressure
3. Preston-tube pressure
4. Y_{eff}
5. Wall temperature

These conditions permit calculation of numbers for all the variables which appear in X* and Y*, except C_f. If these values are used in the correlation for flight data, Eq. (24), a supposedly interference-free value of laminar skin friction coefficient is obtained. Now when this value of C_f and all the other specified variables, except Re_m, are substituted into the wind-tunnel correlation, Eq. (22), an "effective" freestream unit Reynolds number can be calculated. For given freestream conditions, the effective Reynolds number should be independent of X. The only restriction is that the appropriate values of P_p, P_e, Y_{eff} and T_w be used for a given X. However, small variations are found to occur with X simply due to inaccuracies in the data and the correlation procedure. These small variations within a given traverse were eliminated by averaging over X. This has been done for all of the 19 wind-tunnel cases, and the results are presented in Fig. 25.

Surprisingly, the calculated effective unit Reynolds numbers are only about 7.5% larger than the values calculated by traditional methods. These results are surprising because they are much smaller than those suggested by Reynolds numbers based on the distance to the end of transition. For example, data for the 11-Ft TWT is presented in Fig. 26 which suggests the effective Reynolds number at $M_\infty = 0.80$ should be of the order of 35% larger than the normal unit Reynolds number. Also, since $(C_p)_{rms}$ peaks at $M_\infty \approx 0.70$ in the 11-Ft TWT, as shown in Fig. 27, and Re_T is approximately proportional to $(C_p)_{rms}^{-2.5}$ (see Appendix A), it appears reasonable to expect $(Re_m)_{eff}$ to also peak near $M_\infty = 0.70$. This type of behavior was anticipated because any differences between the wind tunnel and flight data are assumed to be due to wind-tunnel-environment effects which were <u>not</u> included or modelled in the

EFFECTIVE UNIT REYNOLDS NUMBER BASED ON SHIFTED WIND TUNNEL DATA AND UNMODIFIED FLIGHT DATA

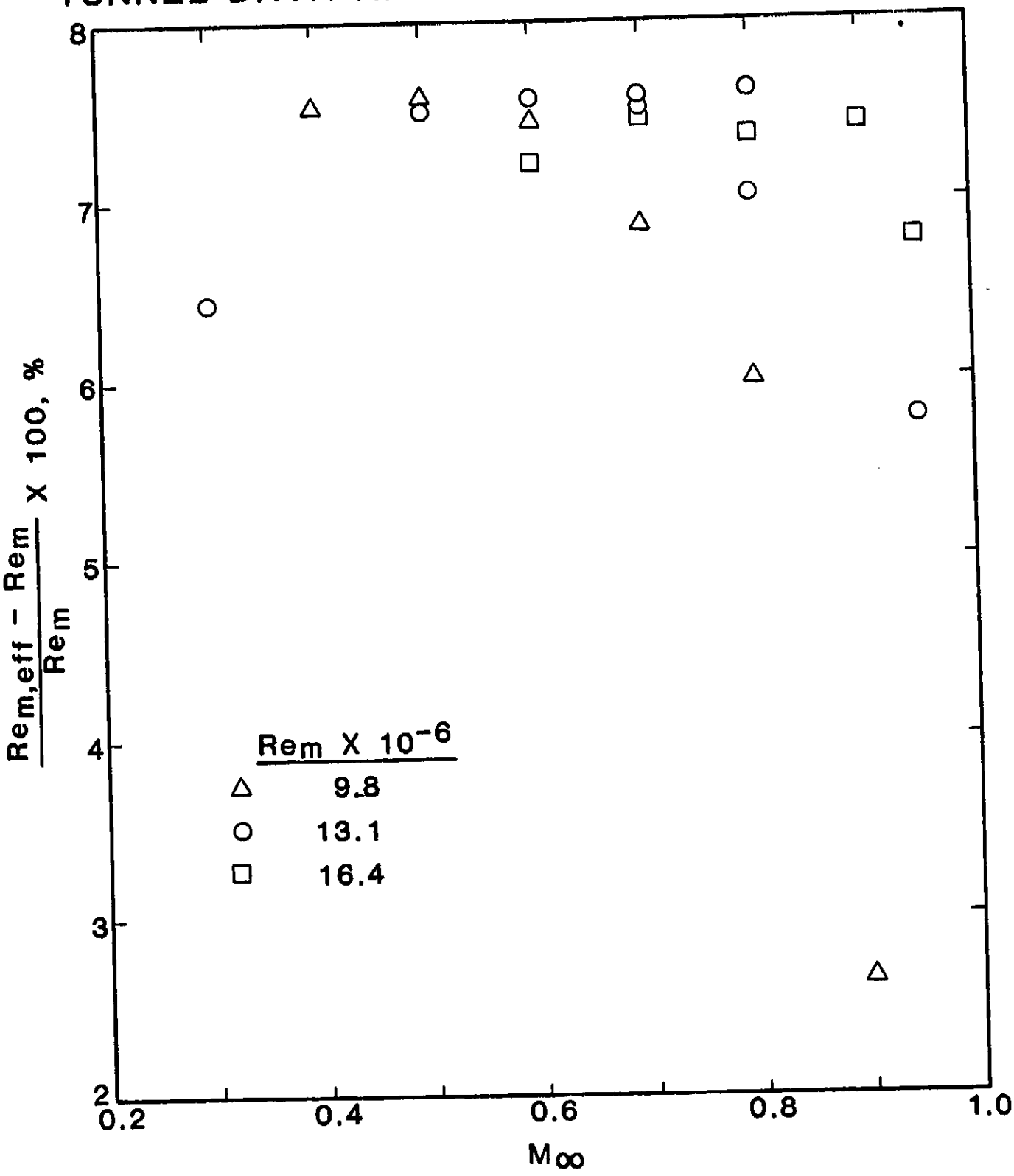

Figure 25

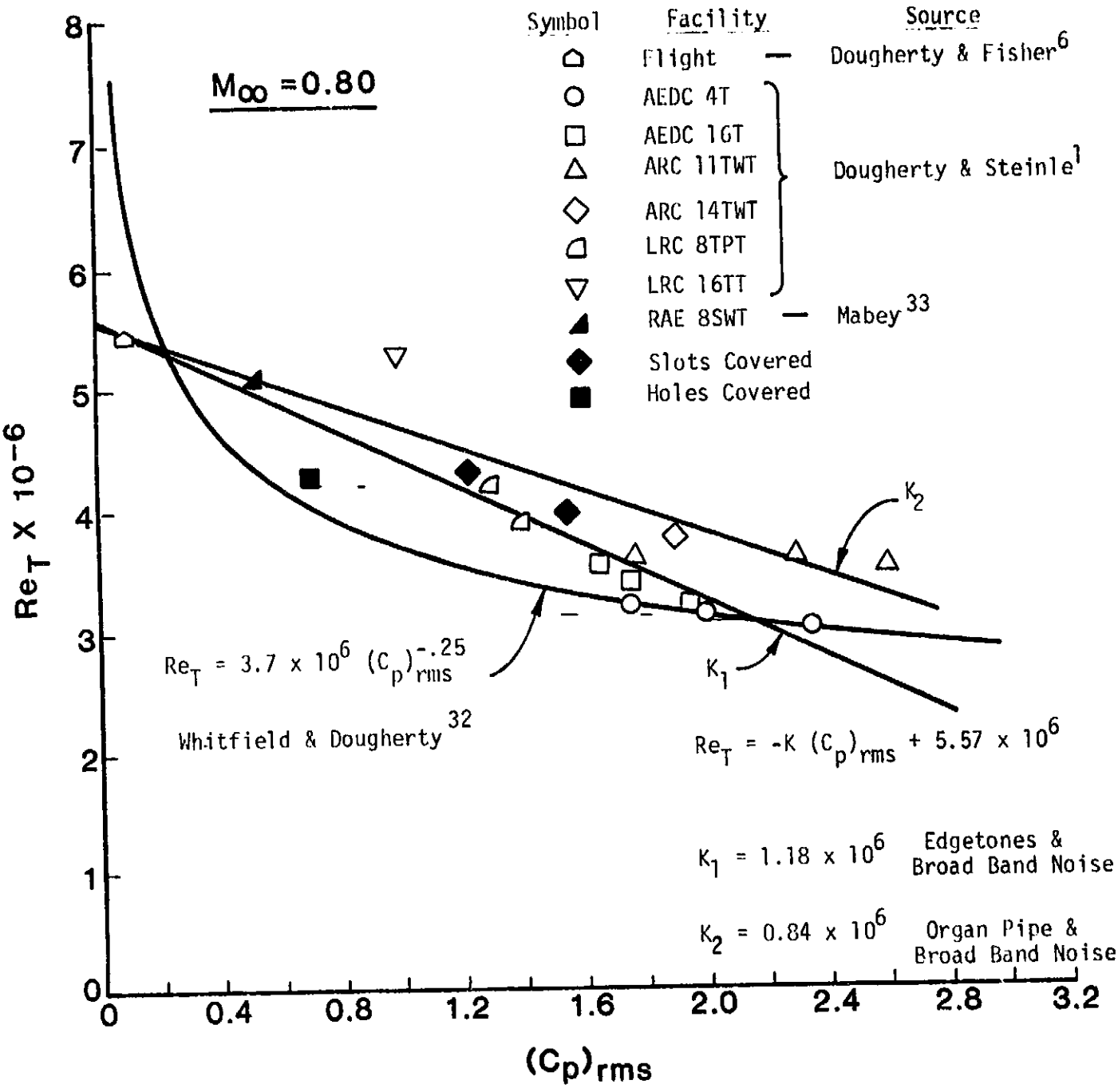

EFFECT OF NOISE ON BOUNDARY LAYER TRANSITION

Figure 26

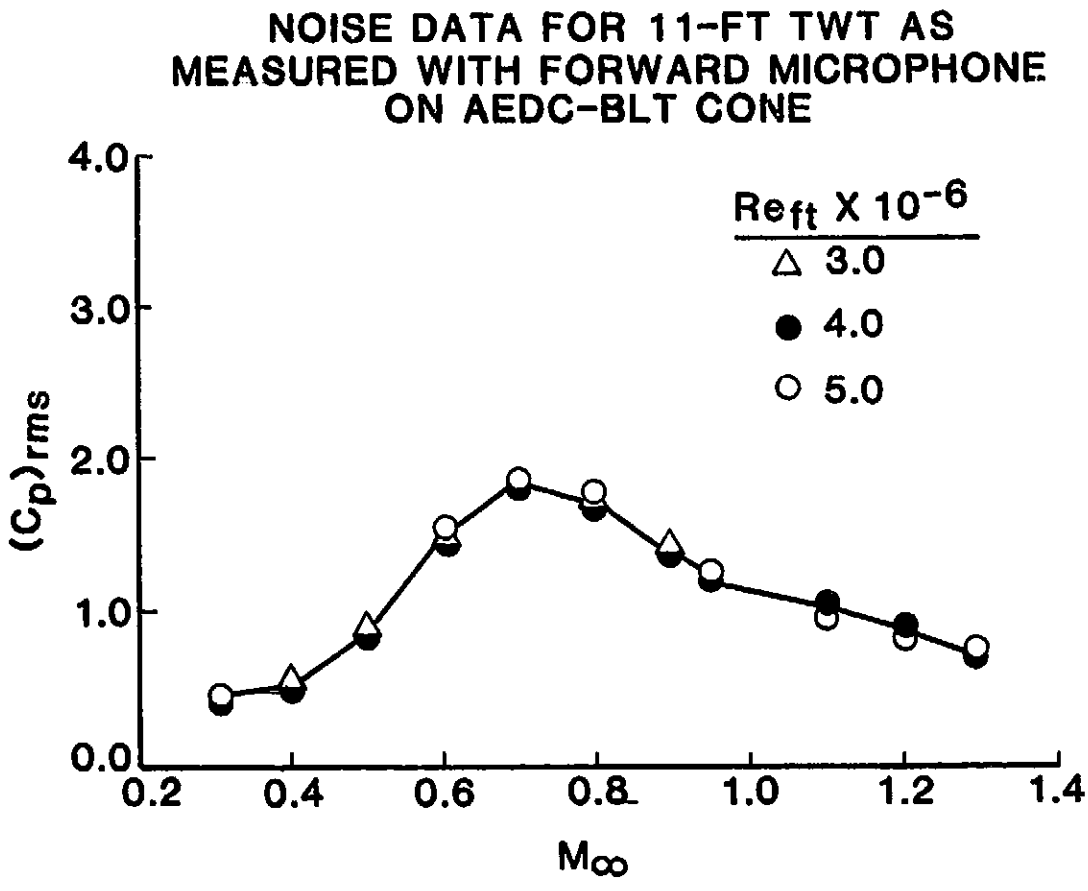

Figure 27

data analysis, viz., noise and freestream turbulence. All of this suggests that wind-tunnel noise alters the average laminar skin friction significantly less than it does transition.

However, before accepting this conclusion, we must resolve the question whether the semi-empirical flight values for K_{eff} (Fig. 21), which clearly point to erroneous data, have any significant effect on this conclusion. Thus, the question arises: Is there a rational procedure which can be employed to correct the Preston-tube pressures measured during the flight tests and thereby permit the calculation of more correct effective unit Reynolds numbers? The following section discusses our search for such a procedure.

B. Search For A Procedure to Correct Flight Data

If we assume K_{eff} should be less than two, the conclusions from Fig. 21 is that the data for M_∞ = 0.85, 0.86, 0.74 are too high. The source of these errors is unknown. The level of P_p for M_∞ = 0.85 and 0.86 would need to be reduced by approximately 2.54 kPa (53 psf) in order to reduce the largest value of K_{eff} to 2. In the case of M_∞ = 0.74, P_p would have to be reduced by 2.39 kPa (50 psf) in order to match the pressure measured for the case M_∞ = 0.75.

In addition to level of pressure, there are at least three other variables which must be considered. Firstly, the data is expected to follow the wind-tunnel pattern of decreasing K_{eff} data with increasing M_∞, and secondly, orderly spacing between individual cases is expected. Thirdly, in any attempt to correct the K_{eff} data, one must decide if the measured differences in P_p for a given traverse are valid or not. If the errors in P_p are caused by zero shifts in the transducer read-out equipment, it would normally be correct to assume zero drift was negligible during a given traverse which required less than a minute. However, even the differences in P_p for the various traverses do not agree, see Fig. 21. For example, the total difference in P_p between 40.6 cm $\leq X \leq$ 50.8 cm of Flight No. 329.1036 (M_∞ = 0.74) is 0.618 kPa (12.9 psf); whereas, the corresponding difference for Flight No. 349.1400 (M_∞ = 0.75) is 0.551 kPa (11.5 psf). As shown on Fig. 21 and in Table V, there are no significant differences in unit Reynolds number or freestream dynamic pressure. In summary, there does not appear to be a concensus on either level or distribution of Preston-tube pressures!

The first attempt to correct the values of P_p, measured during flight

tests, is based on the idea that the flight data and the wind-tunnel data have a common asymptotic value of K_{eff} as $R_\tau \to \infty$, and the Preston tube moves to the tip of the cone and out of the boundary layer. This requirement can be imposed by using the exponential equation developed from a least-squares curve fit of the wind-tunnel values of K_{eff} between M_∞ = 0.6 - 0.95 (see Fig. 14) and the equations of Table VII. The wind-tunnel equation defines the asymptotic values of K_{eff} to be given by $0.655\ (1-M_\infty^2)^{0.173}$ when $U_\tau h/\nu_w \to \infty$. This equation is then used to define new values for the additive constants, which appear in Table VII, by inserting a given flight Mach number. The resulting modified values of K_{eff} are plotted in Fig. 28. Now the K_{eff} are much lower but the order of the curves with respect to M_∞ is still incorrect. The correlation which results from use of these values of K_{eff} is

$$Y^* = -0.00016\ (X^*)^2 + 0.5054X^* - 0.0194\ . \qquad (25)$$

This equation is plotted in Fig. 29 and is compared with the shifted wind-tunnel correlation, Eq. (22). The associated rms error in $C_{f,c}$ is now 0.15%. This extremely low error in C_f is caused by the close proximity to the wall. In this region, total pressure within the laminar boundary layers is relatively insensitive to changes in K_{eff}, see Fig. 13, and the corrected values of P_p are approximately equal to P_w. This results in nearly constant values of P_p and is considered to be invalid. However, the corresponding effective Reynolds numbers vary nearly monotonically from a maximum of 18% above the normal Reynolds number for M_∞ = 0.30, $Re_m = 13.1 \times 10^6$ down to a minimum of 4% at M_∞ = 0.90, $Re_m = 9.8 \times 10^6$. A graph of these Reynolds numbers is presented in Fig. 30.

In light of the above inconclusive results, a second correction procedure was investigated. This second procedure is based on the assumption that the effects of freestream turbulence and noise on the measured laminar Preston-tube pressures are a minimum at the beginning of boundary layer transition. This, in effect, assumes the flight and wind tunnel values of K_{eff} are equal at X_t for a given R_τ and M_∞. This then leads to use of the asymptotic curve fit of the shifted wind-tunnel data, Fig. 14, to calculate $K_{eff}(X_t)$. The theoretical values of $R_\tau \equiv U_\tau h/\nu_w$ at X_t are substituted into

$$K_{eff} = 2.865e^{-0.0273 R_\tau} + 0.655\ (1-M_\infty^2)^{0.173} \qquad (26)$$

for the nine different flights. The differences between these new values of $K_{eff}\ (X_t)$ and the original flight values defines an increment which was added (or subtracted) from the complete set of K_{eff}'s for a given flight. The

DISTRIBUTIONS OF EFFECTIVE PROBE HEIGHT FOR FLIGHT DATA BASED ON ASYMPTOTES DEFINED BY CURVE FIT OF SHIFTED WIND TUNNEL DATA

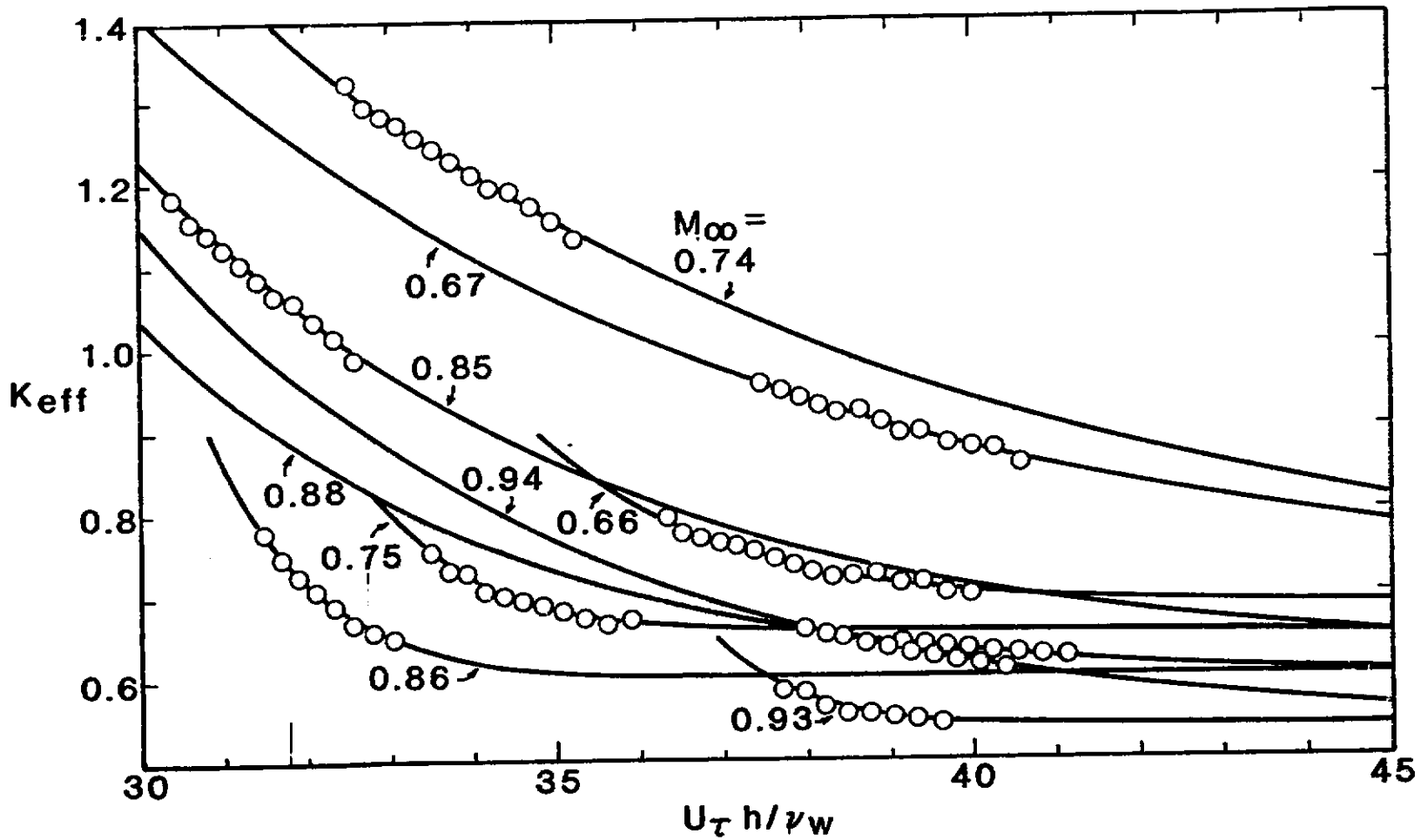

Figure 28

COMPARISON OF CORRELATIONS FOR SHIFTED WIND TUNNEL AND FLIGHT DATA SHIFTED ACCORDING TO WIND TUNNEL ASYMPTOTES

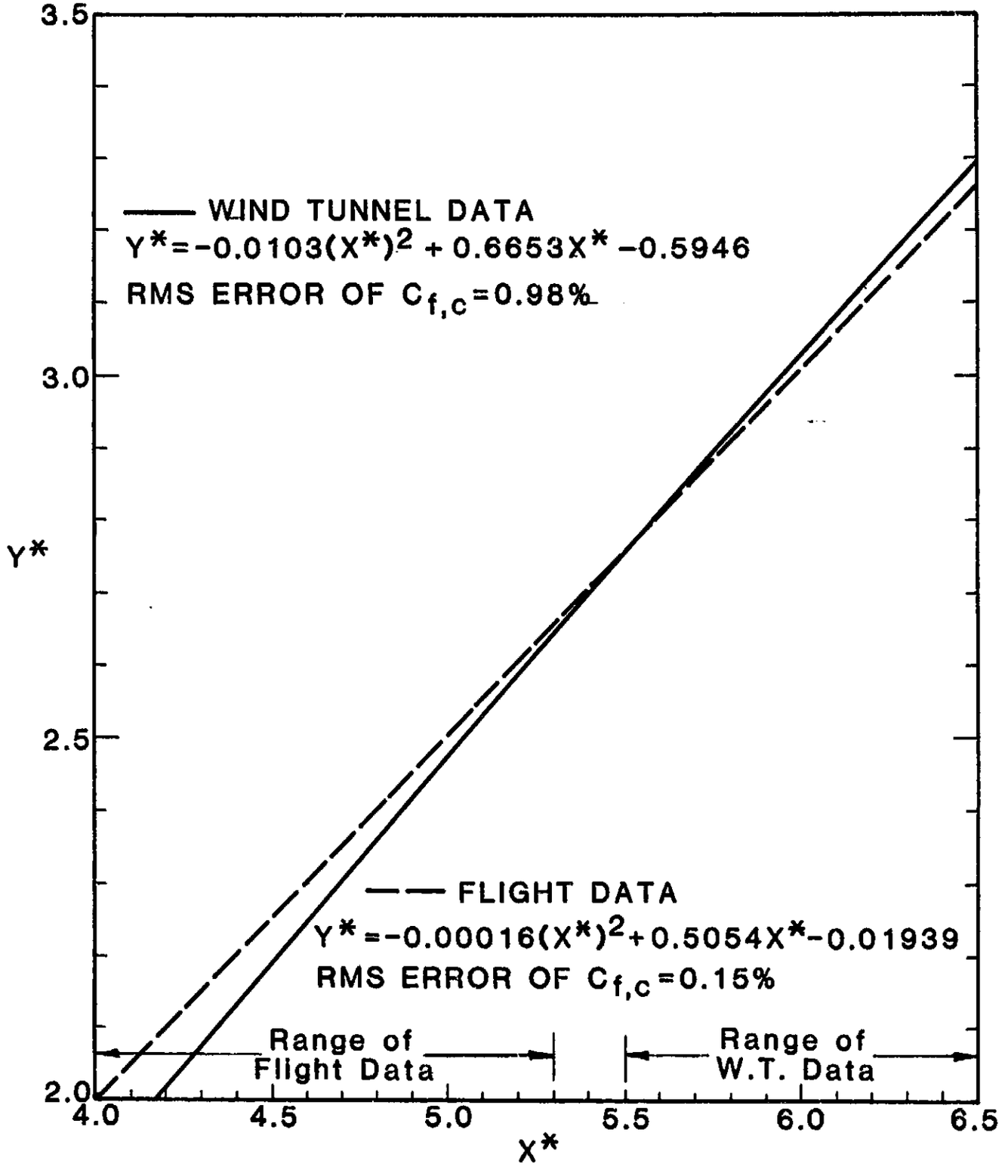

Figure 29

VARIATION OF EFFECTIVE UNIT REYNOLDS NUMBER BASED ON SHIFTS OF FLIGHT VALUES OF K_{eff} TO ASYMPTOTES DEFINED BY CURVE FIT OF SHIFTED WIND TUNNEL DATA

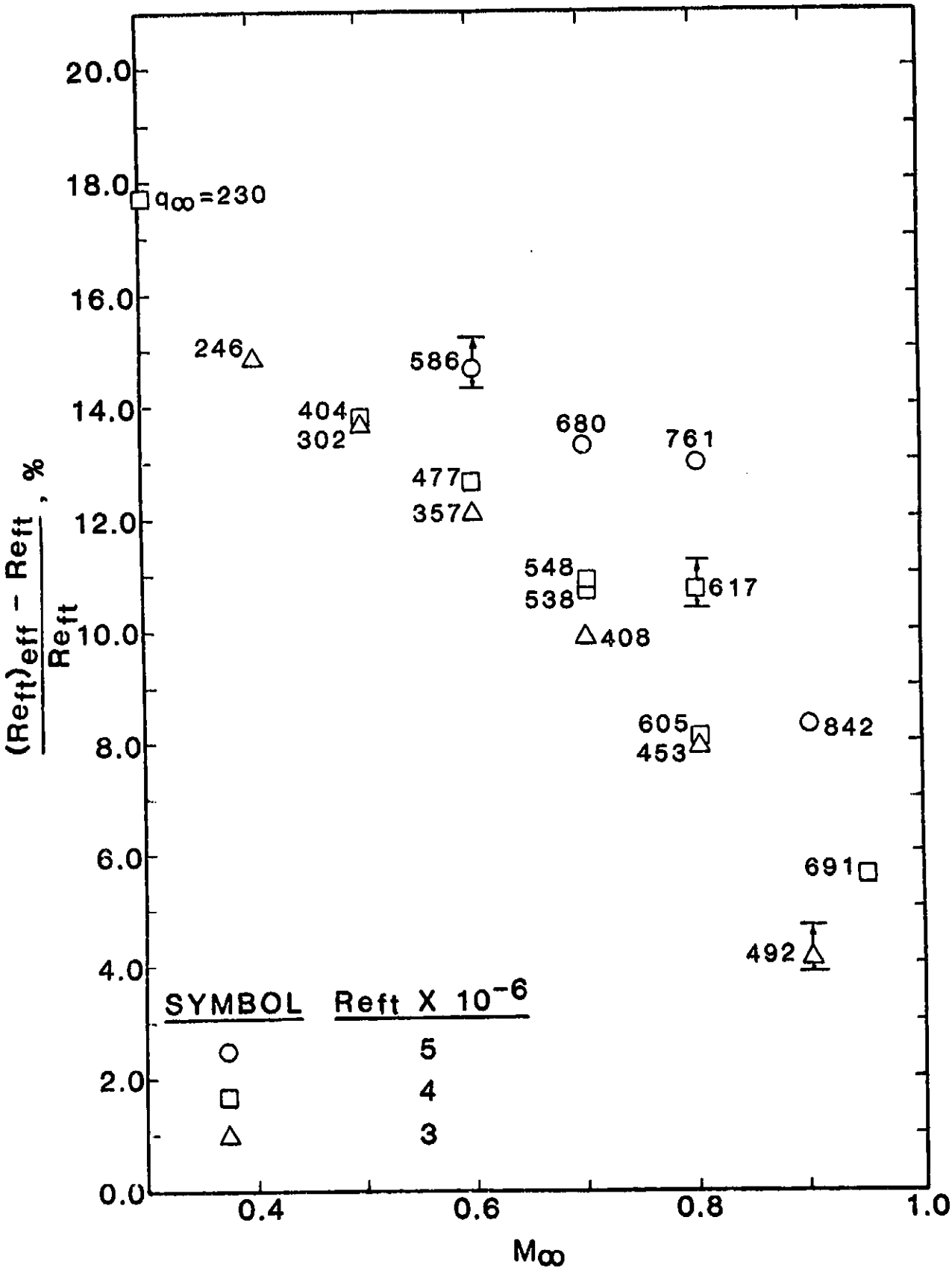

Figure 30

resulting correlation is

$$Y^* = 0.1247(X^*)^2 - 0.9210\ X^* + 4.0548, \quad \text{for } 5.6 < X^* < 6.0. \tag{27}$$

This equation is compared in Fig. 31 with the preferred wind-tunnel correlation, Eq. (22). Unfortunately, the two correlations cross. This results in effective Reynolds numbers varying between 6% above and 6% below the normal Reynolds number. Thus, this procedure is not helpful.

A third correction procedure focuses on using the unmodified values of K_{eff} for Flight No. 349.1400 ($M_\infty = 0.75$) as a reference for the rest of the flight data. This case is attractive because it appears to have the most realistic values of K_{eff}, i.e., $1.7 < K_{eff} < 1.8$. In order to apply this assumption, it is necessary to determine how the rest of the K_{eff} data should be distributed about this reference case. This can also be done using the curve fit of the shifted wind-tunnel data, Eq. (26). Corrections for the three cases in the upper left of Fig. 21 were calculated by using the exponential curve fits for each case (Table VII) to define a corrected K_{eff} at a value of R_τ corresponding to the midpoint of the reference case, $M_\infty = 0.75$. The corrections for the five cases on the right of Fig. 21 were calculated by using the exponential curve fit of the reference case to extrapolate K_{eff} to an R_τ defined by the midpoint of each of the five cases. The reference Mach number, 0.75, and the five different values of R_τ were used in Eq. (26) to calculate reference values of K_{eff}. The five different values of R_τ and M_∞ were then used in Eq. (26) to define "correct" differences between these data and the reference case. Each of the calculated differences in K_{eff} were then used to shift the center of the K_{eff} data for the corresponding eight flights. This procedure provides a more realistic spacing of the eight flights about the selected reference case. In addition, this time it was assumed the measured differences in P_p for a given traverse are valid and should be maintained. This requirement leads to a particular distribution of K_{eff} about the shifted midpoints. The results are illustrated in Fig. 32. The rather weird distributions of K_{eff} are caused by the fact that P_t is a function of both x and y and the derivative dP_t/dx changes with shifts in distance from the wall, y. The associated correlation is

$$Y^* = 0.0598(X^*)^2 - 0.1777\ X^* + 1.928, \quad \text{for } 5.64 < X^* < 6.09\ . \tag{28}$$

COMPARISON OF CORRELATIONS FOR SHIFTED WIND TUNNEL DATA AND FLIGHT DATA SHIFTED TO HAVE THE VALUE OF $K_{eff}(X_t)$ PRESCRIBED BY CURVE FIT OF WIND TUNNEL DATA IN THE RANGE $0.60 \leq M_\infty \leq 0.95$

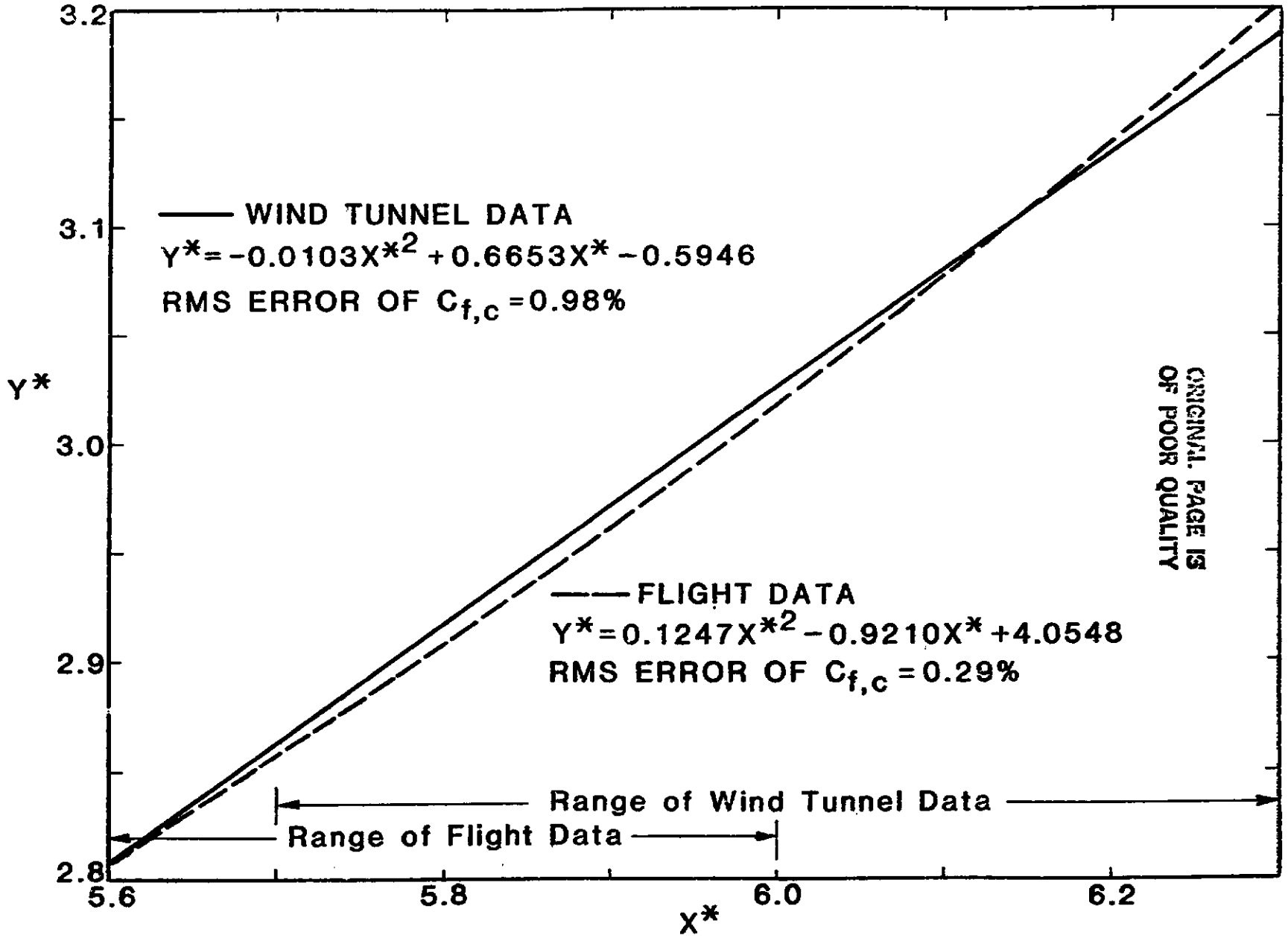

Figure 31

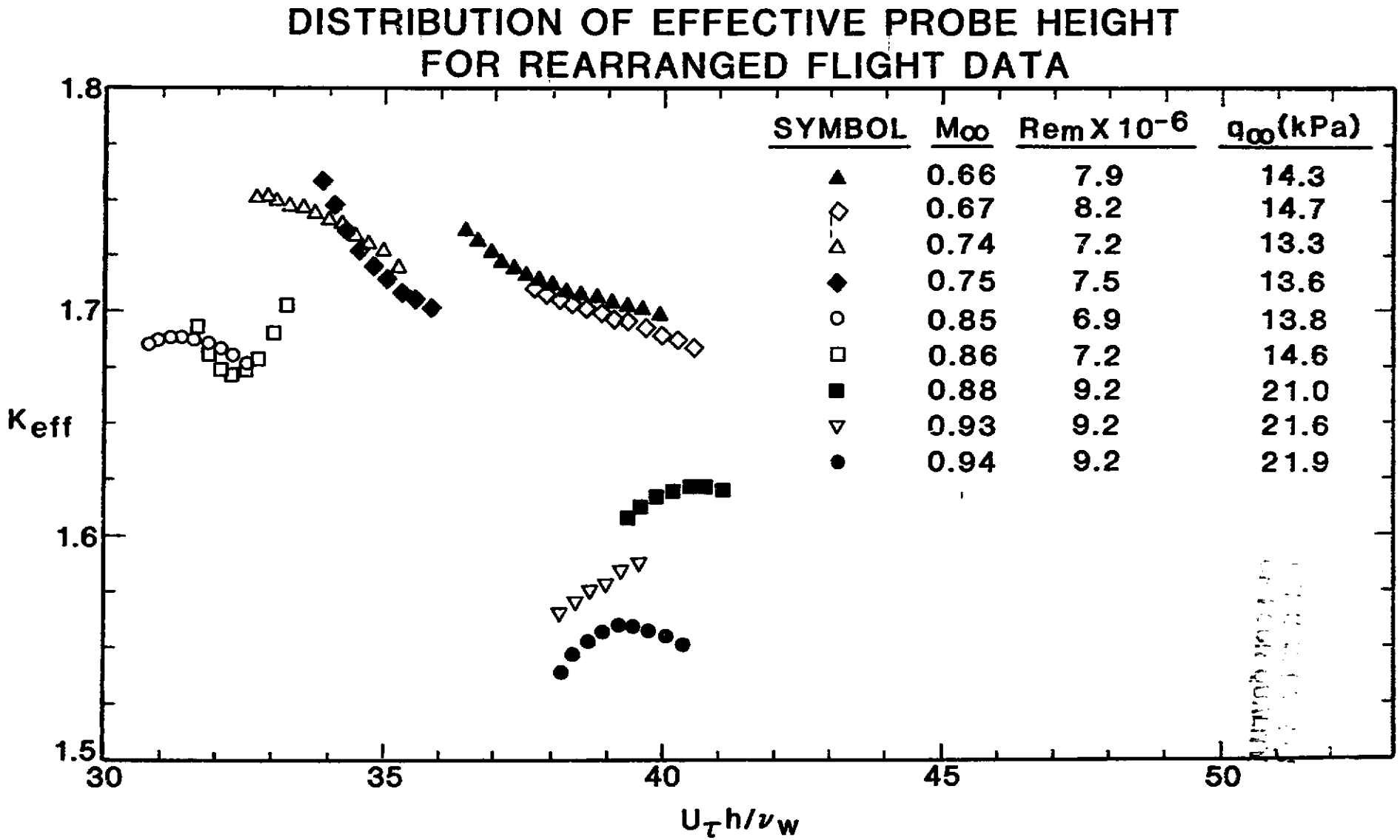
DISTRIBUTION OF EFFECTIVE PROBE HEIGHT
FOR REARRANGED FLIGHT DATA
SYMBOL
M∞
Rem X 10⁻⁶
q∞(kPa)
0.66 7.9 14.3
0.67 8.2 14.7
0.74 7.2 13.3
0.75 7.5 13.6
0.85 6.9 13.8
0.86 7.2 14.6
0.88 9.2 21.0
0.93 9.2 21.6
0.94 9.2 21.9
Keff
1.8
1.7
1.6
1.5
30
35
40
45
50
Uτh/νw

Figure 32

This equation is shown in Fig. 33 along with the individual data points. A comparison between Eq. (28) and the preferred wind-tunnel correlation is made in Fig. 34.

The small scatter of theoretical skin friction coefficient about values computed from Eq. (28) is presented in Fig. 35. The rms error in skin friction coefficient is 0.37% which is less than the 0.97% scatter found for the shifted wind-tunnel data, Fig. 16. It is revelant to here note that the scatter in C_f generally decreases as Y_{eff} decreases. This is illustrated by comparing the values of K_{eff} shown in Fig. 28 with the higher values of Fig. 32 and noting the lower rms error in $C_{f,c}$ of 0.15% as indicated on Fig. 29. Thus, one can legitimately question whether the flight data have been shifted down too much toward the wall.

Before addressing this question, we need to first present the values of effective unit Reynolds numbers which result from using the two correlations shown in Fig. 34. Values for the nineteen wind-tunnel conditions are shown in Fig. 36. The maximum effective Reynolds numbers are approximately 6.5% larger than the corresponding standard wind-tunnel values. These are about 1% less than those obtained for the unmodified flight data, Fig. 25. The distribution has only a vague resemblance to the measured noise curve shown in Fig. 27. The two lowest values of effective Reynolds number ($\simeq 1.04\ Re_m$) occur for $M_\infty = 0.3$, $Re_m = 13.1 \times 10^6$ and $M_\infty = 0.9$, $Re_m = 9.8 \times 10^6$. Data for both of these two cases depart from the majority of the data shown in Fig. 14. The low Mach number case appears to be too high and has values of K_{eff} shifted toward the flight data. The corresponding values of X* lie between 6.26 - 6.28. As indicated in Fig. 34, the difference between the two correlations is less in this range of X* and this results in a smaller value of effective Reynolds number. The high Mach number case appears to have a slope dK_{eff}/dR_τ that is conspicuously large. However, the primary reason $Re_{m,eff}$ is small for this case is that X* lies in the range 5.73 - 5.80. This corresponds to the far left of Fig. 34 where a smaller difference between the two correlations also exists. Finally, we face the questions what happens to the effective Reynolds numbers if the flight values of K_{eff} are shifted either up or down. This was investigated by shifting the K_{eff} data of Fig. 32 according to the following procedure. The average R_τ and the corresponding K_{eff} was calculated for the reference case ($M_\infty = 0.75$) and likewise for the other flight conditions. The data were then shifted by arbitrarily adding a constant increment to each of the average K_{eff}'s. These new distances from the wall were then used tolocate a new value of P_p within the corresponding STAN-5 boundary layer at that streamwise station. The increment in Preston-

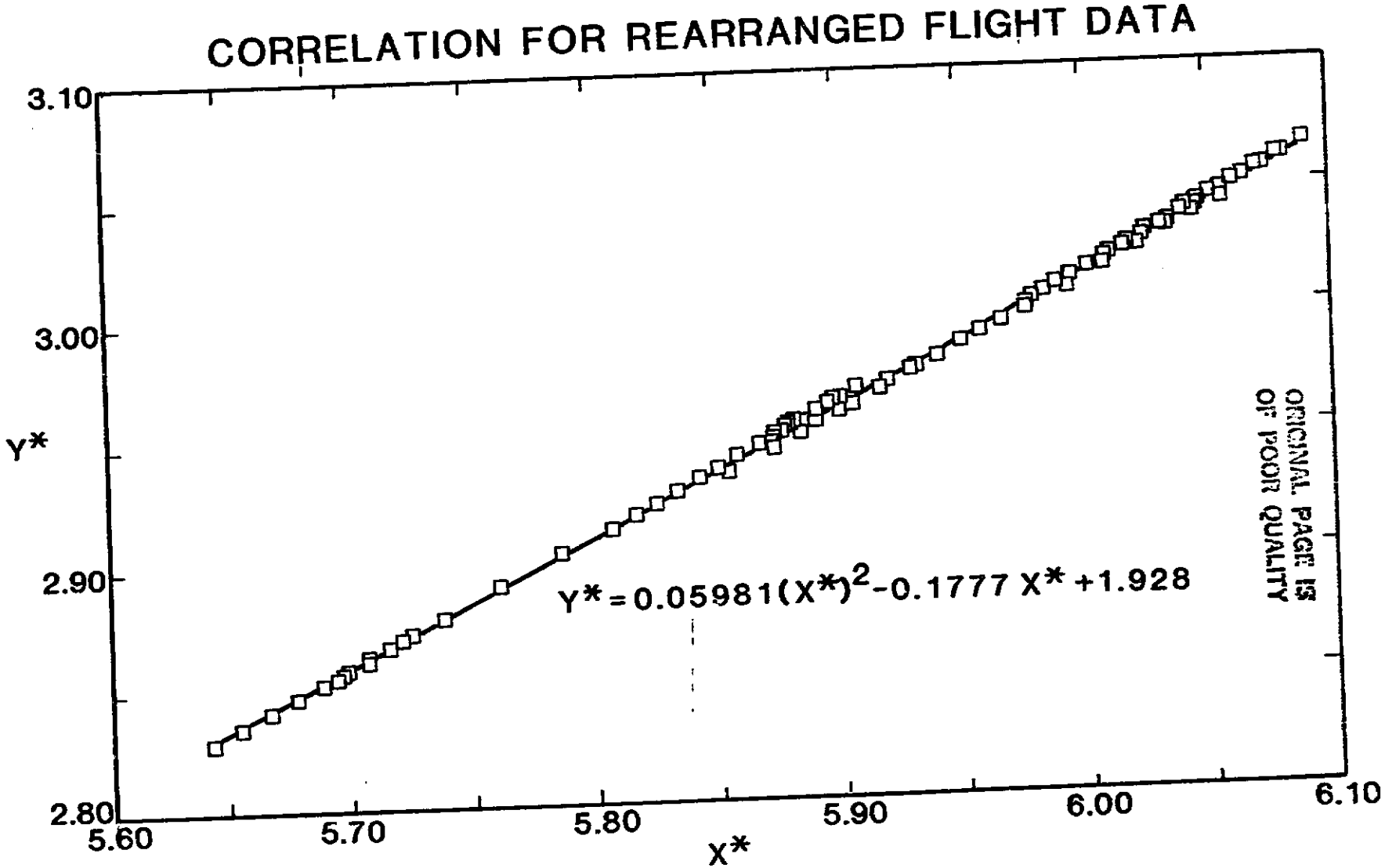
CORRELATION FOR REARRANGED FLIGHT DATA
3.10
3.00
2.90
2.80
Y*
5.60
5.70
5.80
5.90
6.00
6.10
X*
Y* = 0.05981(X*)2 - 0.1777 X* + 1.928
ORIGINAL PAGE IS
OF POOR QUALITY

Figure 33

COMPARISON OF CORRELATIONS FOR SHIFTED WIND TUNNEL DATA AND THE REARRANGED FLIGHT DATA

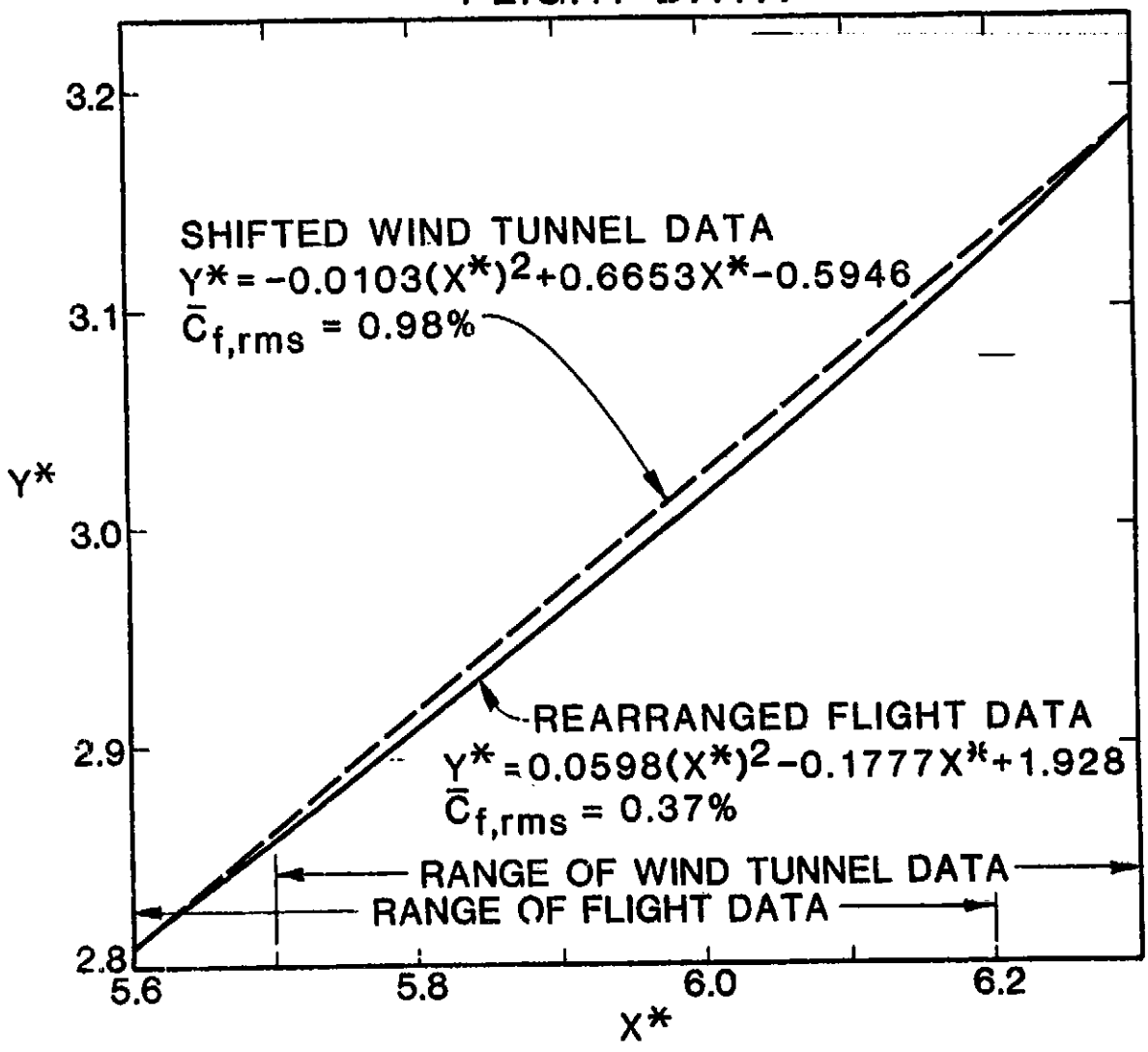

Figure 34

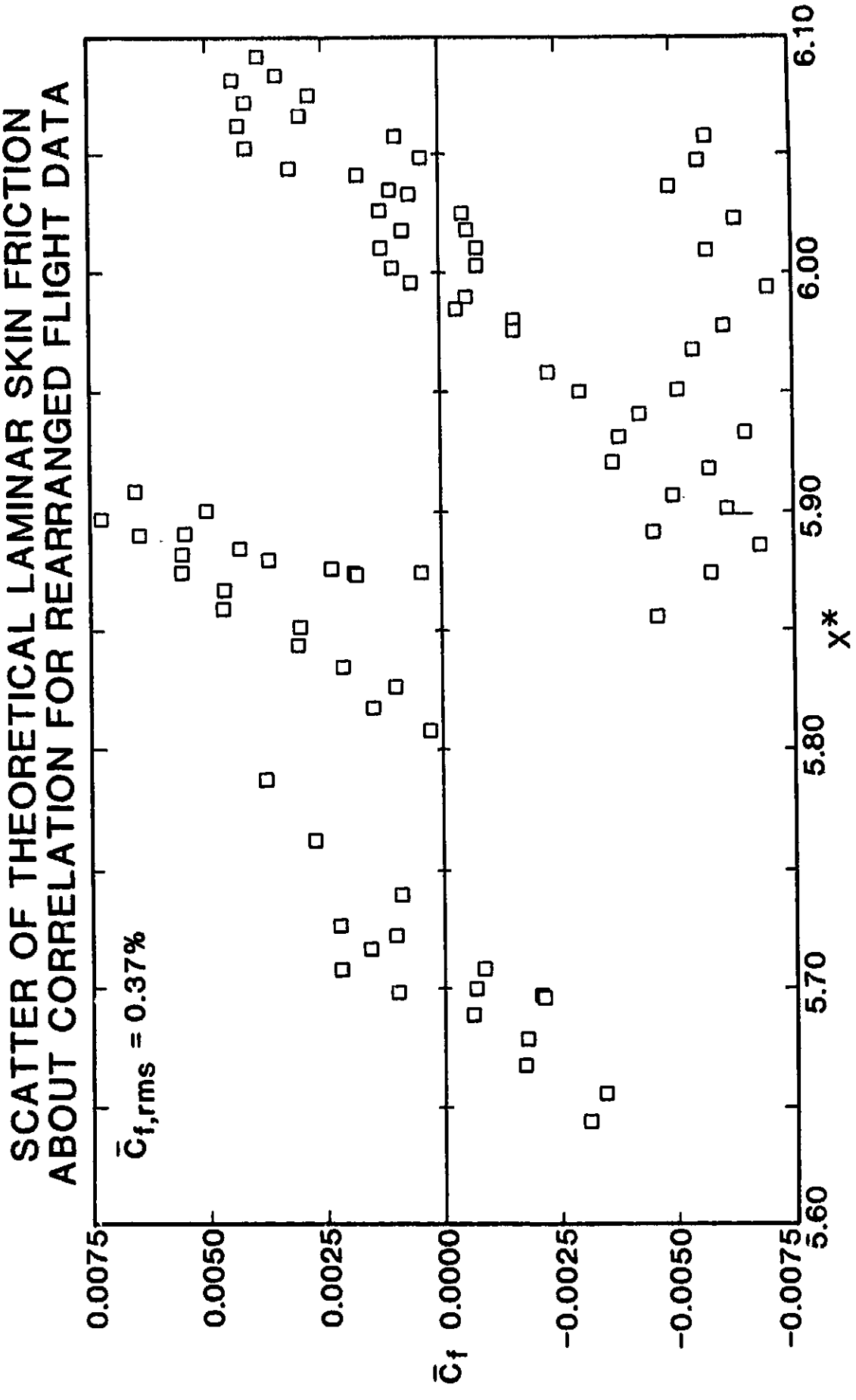

Figure 35

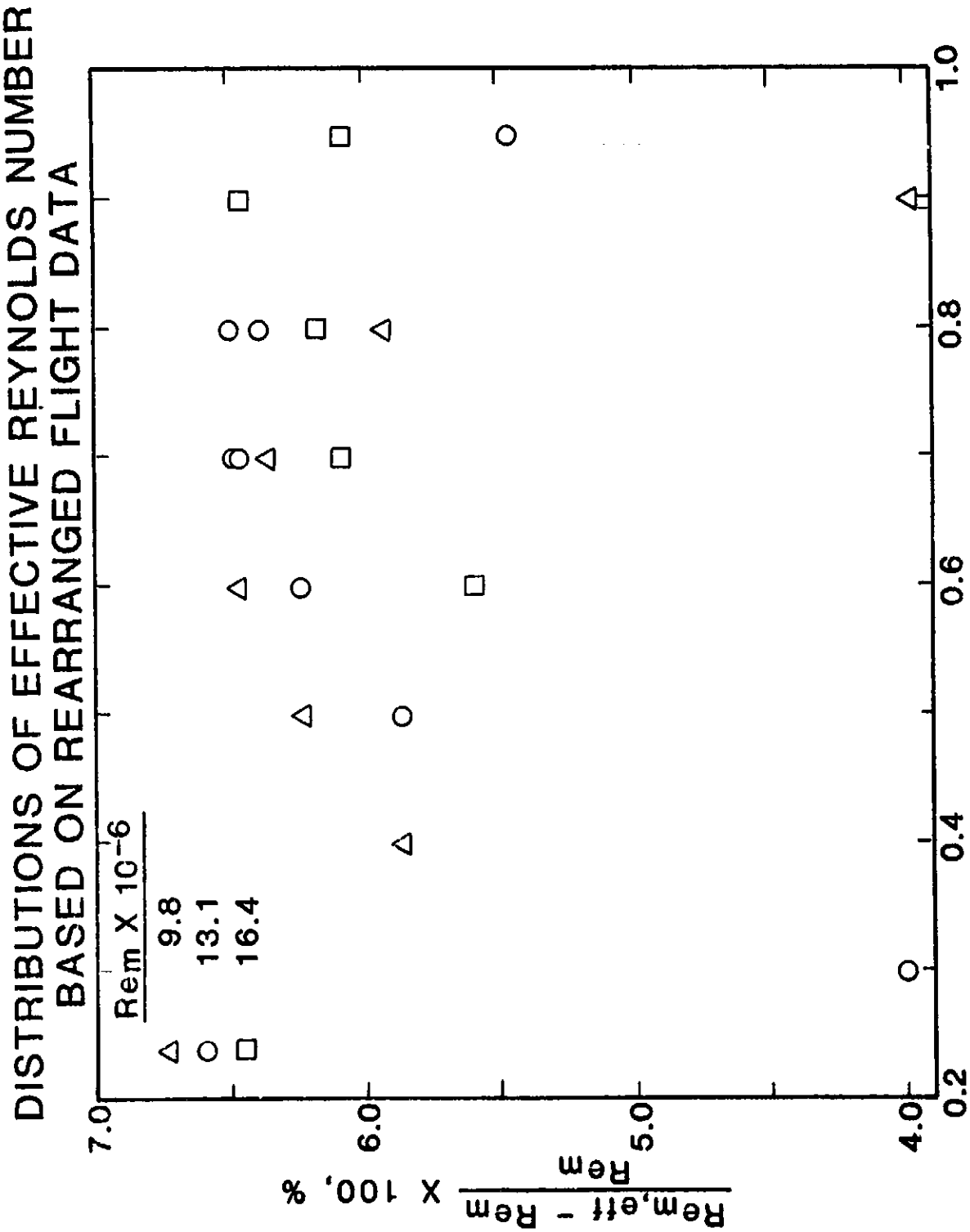

Figure 36

tube pressure, for a given flight condition, was then added or subtracted from all of the P_p for that traverse. These new values of P_p were then used in conjunction with the theoretical profiles to define new distributions of K_{eff} and the associated values of X^* and Y^*. A new least-squares curve fit of these data provides a
new correlation equation which can then be used with the wind-tunnel correlation to define a new set of effective unit Reynolds numbers.

The reference value of $K_{eff} \simeq 1.72$ was increased up to 2.12 and was decreased down to 1.42. The resulting distribution of $Re_{m,eff}$ is presented in Fig. 37 for $M_\infty = 0.80$. This clearly shows that the calculated effective Reynolds number have a maximum of approximately 1.065 Re_m. Thus, we may conclude that the procedure selected for correcting the flight values of K_{eff} reduces the maximum values of $Re_{m,eff}$ by about 1% of Re_m.

CHANGES IN EFFECTIVE REYNOLDS NUMBER PRODUCED BY CHANGES IN THE REFERENCE VALUE OF K_{eff} FOR THE REARRANGED FLIGHT DATA

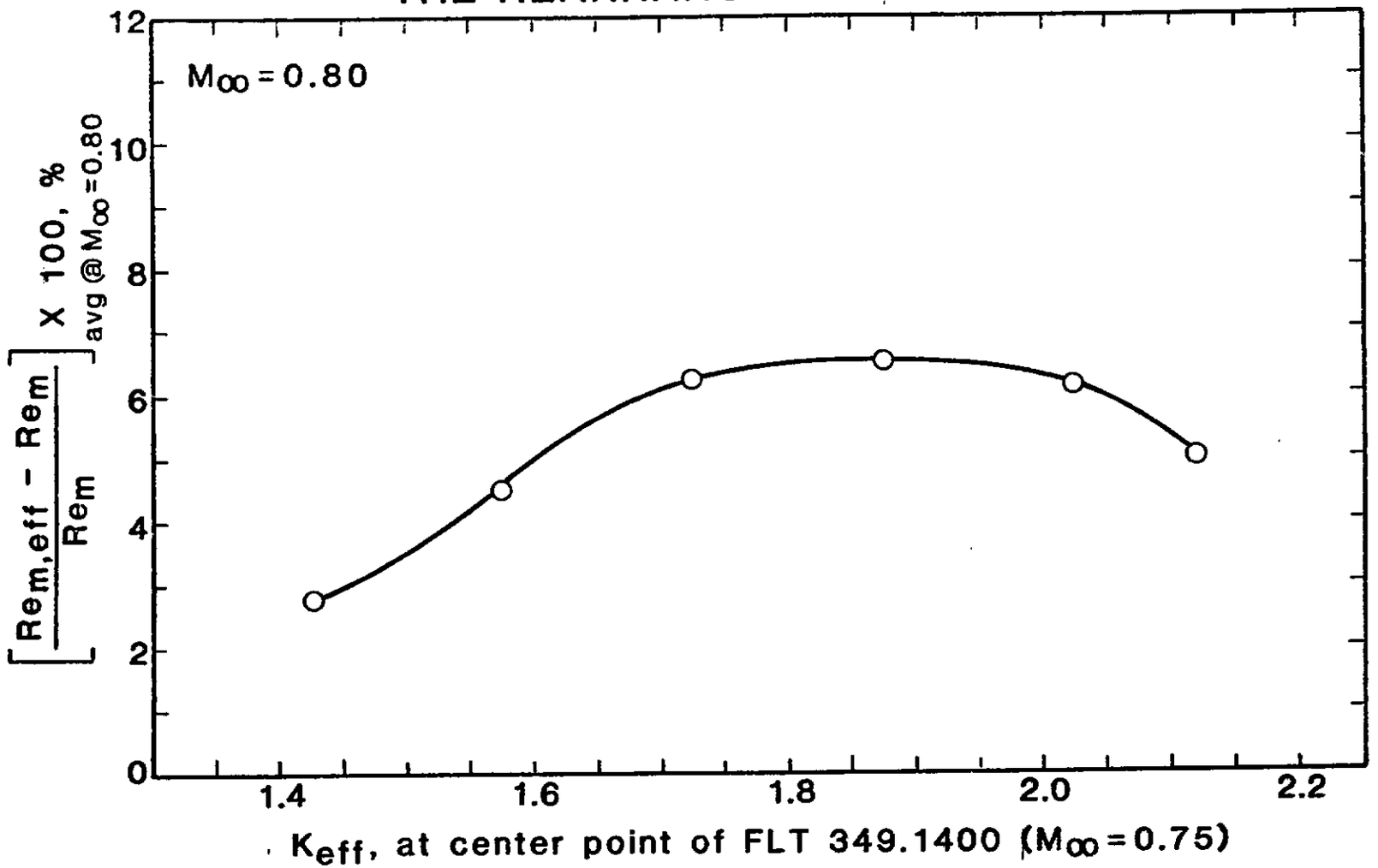

Figure 37

CONCLUSIONS AND RECOMMENDATIONS

Analyses of Preston-tube data, obtained with the AEDC Transition Cone in both the 11-ft TWT and flight tests, have revealed that these data have errors. The errors in the 11-ft TWT data are relatively minor and are comparatively easy to correct. A satisfactory correlation between the corrected wind-tunnel Preston-tube pressures and theoretical laminar skin friction has been developed. The standard deviation between the correlated skin friction coefficients and the corresponding theoretical values is 0.98%.

The errors in the flight data were found to be more severe and a great deal of effort was expended in the search for a rational correction procedure. Three distinct correction procedures were investigated, and correlations have been developed based on each of these modified sets of flight data. The preferred correction procedure forces the flight data to exhibit some of the orderly characteristics of the wind-tunnel data. The corresponding preferred Preston-tube/skin friction correlation exhibits an rms error in skin friction of only 0.37%.

The wind-tunnel and flight correlations have been successfully used to define "effective" freestream unit Reynolds numbers for the 11-ft TWT. Based on the preferred rearrangement of the flight data, the maximum effective values of Re_m are approximately 6.5% higher than the normal tunnel values. This compares with 7.5% which results when using the unmodified flight data. The maximum effective Reynolds numbers occur for Mach numbers between 0.60 and 0.80 and for normal tunnel unit Reynolds numbers of 9.8, 13.1, and 16.4 million per meter.

The distribution of $(Re_m)_{eff}$ with Mach number only vaguely resembles the distribution of total noise intensity as measured in the 11-ft TWT with microphones on the AEDC Cone. Also, the values of $(Re_m)_{eff}$ are low for a given noise intensity when compared to the noise/boundary-layer-transition correlation of Doughterty and Fisher[8]. Thus, we are led to conclude that wind-tunnel noise effects the <u>average</u> laminar skin friction much less than it effects boundary layer transition.

It is recommended that the analyses used herein to develop Preston-tube/skin-friction correlations be applied next to the analysis of turbulent boundary layers and finally to the transition region which is known from

the work of Dougherty, et al.[7,8,27] to be sensitive to tunnel noise. These new correlations can be used to define additional values of $(Re_m)_{eff}$ which can be compared to values reported here.

Boundary Layer Transition Data

Data for the onset, extent, and end of boundary layer transition are summarized and presented in a systematic form in Appendix A. Boundary-layer-transition data for the 11-ft TWT appear to be correlated by the product $Re_T(C_p)^{0.25}_{rms}$. In the range $0.60 < M_\infty < 0.95$, this product is near 4 and decreases rapidly as Mach number decreases below 0.60.

Effects of Nose Radius

The effects of variations in nose radius on the transonic flow about a cone are discussed in Appendix B. The radius of a hemispherical nose has been found to have an important and dominant effect on boundary-layer transition and flow separation at supercritical speeds. Increasing nose radius allows the growth of a thicker boundary layer prior to encountering the transonic shock near the juncture of the nose with the cone. This promotes both earlier transition and laminar flow separation. An analytical procedure has been developed to model this phenomena, and a comparative study of the effects of nose radius, Mach number, Reynolds number, and heat transfer can now be performed.

VII. REFERENCES

1. Pope, A. and Harper, J. J.: Low-Speed Wind Tunnel Testing, Wiley, 1966.

2. Lu, P-C.: Fluid Mechanics, An Introductory Course, Iowa State University Press, 1979.

3. Loehrke, R. I. and Nagib, H. M.: "Experiments on Management of Free-Stream Turbulence," AGARD-R-598, Sept. 1972.

4. Eckert, W. T.; Mort, K. W.; and Piazza, J. E.: "An Experimental Investigation of End Treatments for Nonreturn Wind Tunnels," NASA TM X-3402.

5. Reed, T. D.; Pope, T. C.; and Cooksey, J. M.: "Calibration of Transonic and Supersonic Wind Tunnels," NASA CR-2920, Nov. 1977.

6. Treon, S. L., et. al.: "Further Correlation of Data from Investigations of a High-Subsonic-Speed Transport Aircraft Model in Three Major Transonic Wind Tunnels," AIAA Paper No. 71-291, March 1971.

7. Dougherty, N. S., Jr. and Steinle, F. W., Jr.: "Transition Reynolds Number Comparisons in Several Major Transonic Tunnels," AIAA Paper No. 74-627, July 1974.

8. Dougherty, N. S., Jr. and Fisher, D. F.: "Boundary Layer Transition on a 10-Degree Cone: Wind Tunnel/Flight Data Correlation," AIAA Paper No. 80-0154, Jan. 1980.

9. Jones, B. Melvill: "Flight Experiments on the Boundary Layer," First Wright Brothers' Lecture, December 17, 1937, reprinted in Aero. & Astro, Feb. 1981.

10. Preston, J. H.: "The Determination of Turbulent Skin Friction by Means of Pitot Tubes," Journal of Royal Aero. Soc., Vol. 58, pp. 109-121, 1954.

11. Stephens, A. V. and Haslam, J. A. G.: "Flight Experiments on Boundary Layer Transition in Relation to Profile Drag," R.& M.1800, Aug. 1938.

12. Reed, T. D., Moretti, P. M., and Abu-Mostafa, A.: "Study of Boundary-Layer Transition Using Transonic-Cone Preston-Tube Data," Semiannual Progress Report, Jan.-June 1980, p. 28.

13. Young, A. D. and Maas, J. N.: "The Behavior of a Pitot-tube in a Transverse Total-Pressure Gradient," R.& M., No.1770, 1937.

14. Chue, S. H.: "Pressure Probes for Fluid Measurement," Prog. Aerospace Science, Vol. 16, No. 2, pp. 147-221, Pergamon Press, 1975.

15. MacMillan, F. A.: "Experiments on Pitot-Tubes in Shear Flow," R. & M. No. 3028, 1957.

16. Patel, V. C.: "Calibration of the Preston-Tube and Limitations on Its Use in Pressure Gradients," Jour. Fluid Mech., Vol 23, pp. 185-208, 1965.

17. Quarmby, A. and Das, H. K.: "Measurement of Skin Friction Using a Rectangular Mouthed Preston Tube," Aero. Jour. Roy. Aero. Soc., Vol. 73, March 1969.

18. Allen, J. M.: "Reevaluation of Compressible-Flow Preston Tube Calibrations," NASA TM X-3488, 1977.

19. Sommer, S. C. and Short, B. J.: "Free-Flight Measurements of Turbulent-Boundary-Layer Skin Friction in the Presence of Severe Aerodynamic Heating at Mach Numbers from 2.8 to 7.0," NACA TN 3391, 1955.

20. Allen, J. M.: "Evaluation of Compressible-Flow Preston Tube Calibrations," NASA TN D-7190, 1973.

21. Allen, J. M.: "Experimental Study of Error Sources in Skin-Friction Balance Measurements," ASME Journal Fluids Engr., March 1977, and NASA TN D-8291, October 1976.

22. Allen, J. M.: "An Improved Sensing Element for Skin-Friction Balance Measurements," AIAA Journal, Vol. 18, No. 11, November 1980.

23. Prozorov, A. G.: "Determination of the Skin Friction in the Boundary Layer with a Small Pitot Probe," Fluid Mech. - Soviet Research, Vol. 5, No. 6, Nov.-Dec. 1976.

24. Wu, J-M and Lock, R. C.: "A Theory for Subsonic and Transonic Flow Over a Cone - With and Without Small Yaw Angle," U.S. Army Missile Command, Redstone Arsenal, Alabama, Tech. Report RD-74-2, Dec. 1973.

25. Crawford, M. E. and Kays, W. M.: "STAN5 - A Program for Numerical Computation of Two-Dimensional Internal/External Boundary Layer Flows," Report No. HMT-23, Department of Mechanical Engineering, Stanford University, December 1975.

26. Quarmby, A. and Das, H. K.: "Displacement Effects on Pitot Tubes with Rectangular Mouths," Aero. Quarterly, May 1969.

27. Bradshaw, P. and Unsworth, K.: "Comment on "Evaluation of Preston Tube Calibration Equations in Supersonic Flow"," AIAA Journal, Vol. 12, No. 9, Sept. 1974.

28. Allen, J. M.: "Evaluation of Preston Tube Calibration Equations in Supersonic Flow," AIAA Journal, Vol. 11, No. 11, Nov. 1973.

29. Fisher, D. F. and Dougherty, N. S., Jr.: "In-Flight Transition Measurement on a 10° Cone at Mach Numbers From 0.5 to 2.0," NASA Tech. Paper 1971, June 1982.

30. Franklin, R. E. and Wallace, J. M.: "Errors in Measurements of Static-Hole Error Using Flush Transducers," Journal of Fluid Mechanics, Vol. 42, Pt. 1, June, 1970.

31. Rohsenow, T. S. and Choi, S. W.: Heat, Mass and Momentum Transfer, Prentice-Hall, 1961, p. 268.

32. Whitfield, J. D. and Dougherty, N. S., Jr.: "A Survey of Transition Research at AEDC," Paper No. 25, AGARD-CP-224, Oct., 1977.

33. Mabey, D. G.: "Boundary Layer Transition Measurements on the AEDC 10° Cone in Three RAE Wind Tunnels and Their Implications," Aeronautical Research Council, R&M No. 3821, June, 1976.

34. Hsieh, T.: "Hemisphere-Cylinder in Transonic Flow, M_∞ = 0.7 ~ 1.0," AIAA Journal, October 1975.

35. Nietubicz, C. J., Pulliam, T. H., and Steger, J. L.: "Numerical Solution of the Azimuthal-Invariant Thin-Layer Navier-Stokes Equations," AIAA Journal, Vol. 18, No. 12, Dec. 1980 and AIAA Paper No. 79-0010, Jan. 1979.

36. Wazzan, A. R., Gazley, C. and Smith, A. M. O.: "The H-R_X Method for Predicting Transition," Rand Tech. Paper P-6581, the Rand Corp., Santa Monica, CA, Jan. 1981.

37. Jaffe, N. A., Okamura, T. T., and Smith, A. M. O.: "Determination of Spatial Amplification Factors and Their Application to Predicting Transition," AIAA Journal, Vol. 8, No. 2, Feb. 1970.

APPENDIX A

SUMMARY OF SUBSONIC BOUNDARY LAYER TRANSITION DATA

Wind Tunnel Data

The surface distances from the nose of the cone to the onset (X_t) and end-of-transtion (X_T) are tabulated in Table A-1 for twenty one different subsonic, wind-tunnel conditions. The test conditions include Mach numbers from 0.3 to 0.95 and free-stream unit Reynolds numbers of 3, 4 and 5 million per foot. The extent of the transition zone (ΔX), the related ratio X_T/X_t, and the root-mean-square of the fluctuating pressure coefficient [$(C_p)_{rms}$] are also included in Table A-1. $(C_p)_{rms}$ is based on microphone data taken with a 1/4 in. diameter microphone mounted flush with the cone surface at a distance of 18 in. aft of the nose. Data over the frequency spectrum between 0.2 and 30 kHz were used to define $(C_p)_{rms}$. Transition Reynolds numbers, based on the product of free-stream unit Reynolds number and the distance to the end-of-transition, are included because this parameter was initially used by Dougherty[7] to correlate with $(C_p)_{rms}$.

Whitfield and Dougherty[29] have stated that a wide variety of previous test data indicate the ratio of X_T/X_t is approximately 2 and is nearly independent of flow conditions. However, the values of this parameter in Table A-1 range from 1.10 to 1.23. There appears to be a slight tendency for X_T/X_t to increase with Mach number. As is shown later in Table A-2, the flight values of X_T/X_t also fall within this same range. Thus, the value of two is not characteristic of these tests.

The effects of M_∞ and free-stream unit Reynolds number on X_t and X_T are shown, respectively, in Figs. A-1 and A-2. The primary results to note are that the distances to onset and end-of-transition (1) increase with decreasing Re_{ft}, but vary only slightly with M_∞ and (2) are smaller, i.e., occur closer to the nose, when $M_\infty = 0.70$. This corresponds to the Mach number at which $(C_p)_{rms}$ reaches a maximum in the Ames 11-ft TWT, e.g., see Dougherty and Fisher.[8] In Ref. 29, Dougherty presented a correlation of wind-tunnel data which indicated $Re_T = 3.7 \times 10^6 (C_p)_{rms}^{-.25}$ within $\pm$ 20%. Thus, $Re_T(C_p)_{rms}^{.25}$ is plotted in Fig. A-3 as a function of M_∞ in order to

TABLE A-1

SUBSONIC BOUNDARY LAYER TRANSITION DATA FROM 11-FT TWT

Plotting Symbols	Run No.	$Re_{ft} \times 10^{-6}$	M_∞	q_∞(PSF)	X_t(in)	X_T(in)	ΔX(in)	X_T/X_t	$Re_T \times 10^{-6}$	$(C_p)_{rms}$
	61.636	3.0	.4	246	11.6	14.0	2.4	1.21	3.50	0.534
	60.635	3.0	.5	302	11.7	14.1	2.4	1.21	3.525	0.862
O	59.634	3.0	.6	357	11.8	14.3	2.5	1.21	3.575	1.468
	58.633	3.0	.7	408	11.1	13.4	2.3	1.21	3.35	1.866
	57.632	3.0	.8	453	11.4	14.0	2.6	1.23	3.50	1.745
	56.631	3.0	.9	492	12.1	14.5	2.4	1.20	3.625	1.488
	29.440	4.0	.3	230	9.5	10.8	1.3	1.14	3.60	0.400
	27.411	4.0	.4	322	9.0	10.9	1.9	1.21	3.63	NA
	25.376	4.0	.5	404	9.3	11.0	1.7	1.18	3.67	0.793
	23.346	4.0	.6	477	9.3	11.0	1.7	1.18	3.67	1.395
◇	21.318	4.0	.7	548	8.6	10.3	1.7	1.20	3.43	1.807
	70.726	4.0	.7	538	8.9	10.7	1.8	1.20	3.57	1.918
	19.289	4.0	.8	617	8.6	10.4	1.8	1.21	3.47	1.706
	72.748	4.0	.8	605	9.1	11.0	1.9	1.21	3.67	1.788
	15.231	4.0	.95	693	9.2	11.1	1.9	1.21	3.70	1.397
	39.545	5.0	.4	396	7.7	8.5	.8	1.10	3.54	NA
	40.547	5.0	.6	586	7.8	9.0	1.2	1.15	3.75	1.583
△	41.548	5.0	.7	680	6.9	8.1	1.2	1.17	3.375	1.970
	42.549	5.0	.8	761	7.2	8.4	1.2	1.17	3.50	1.793
	43.550	5.0	.9	842	7.3	8.6	1.3	1.18	3.58	1.512
	44.551	5.0	.95	873	7.4	8.9	1.5	1.20	3.71	1.391

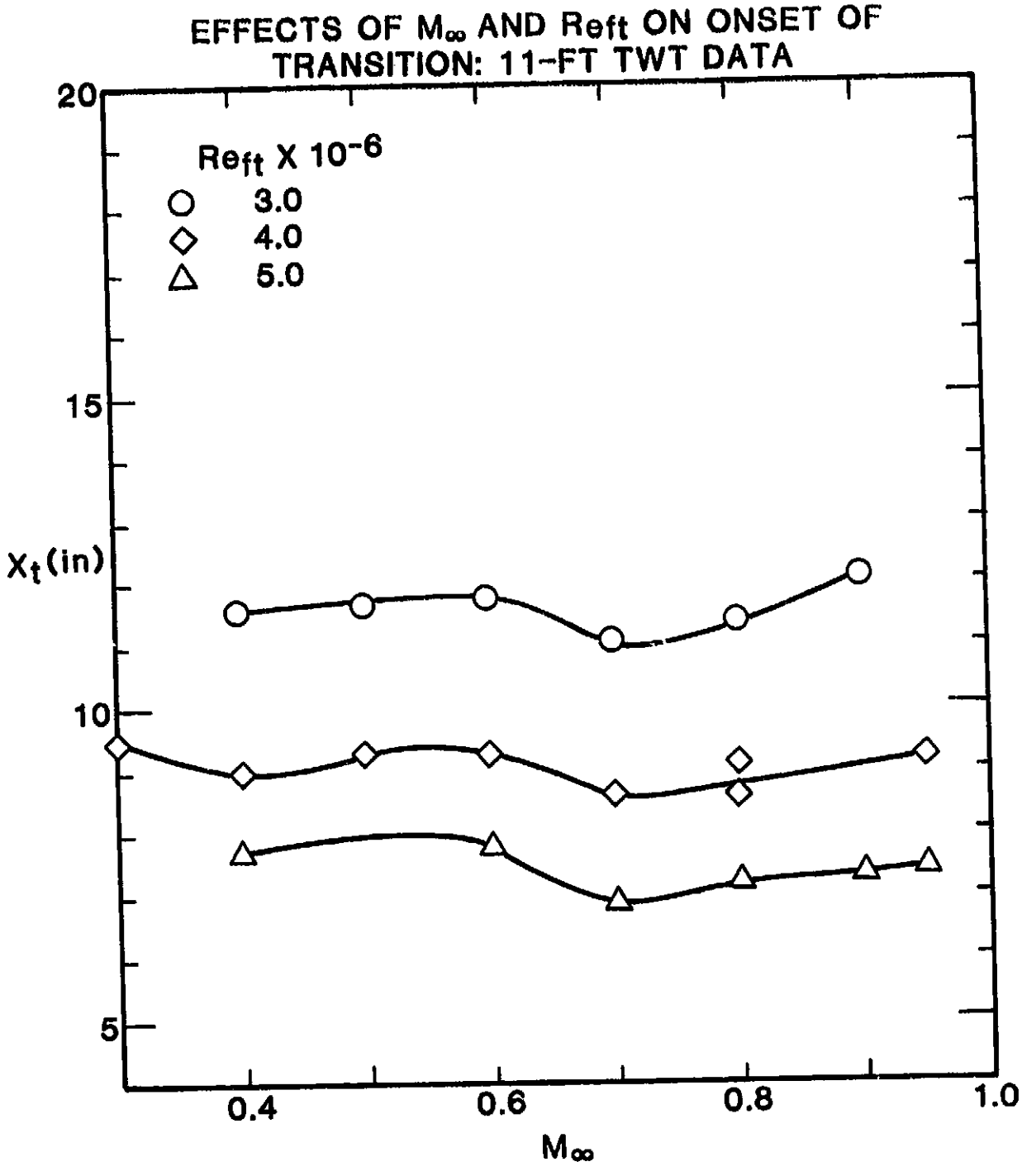

Figure A-1

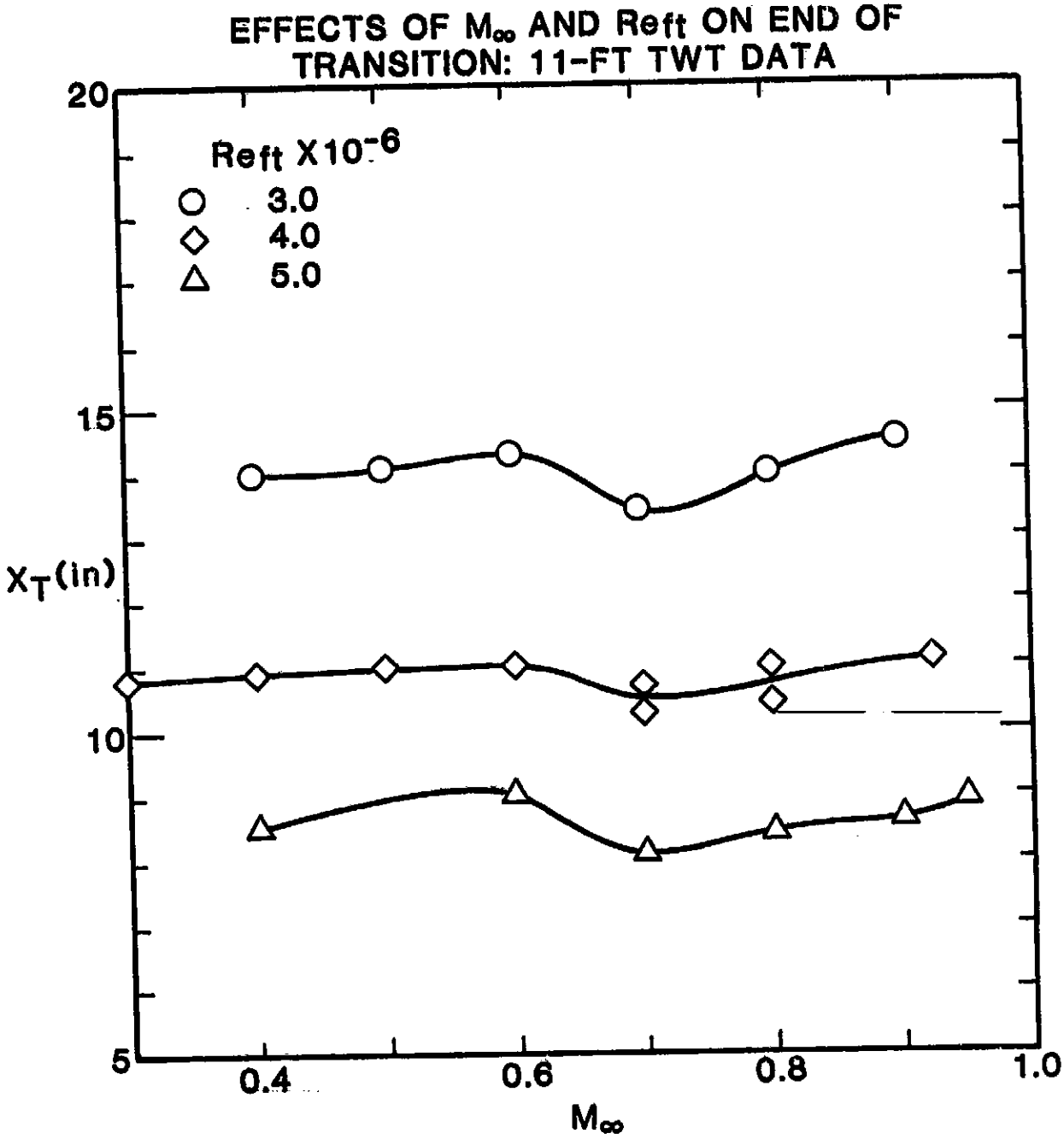

Figure A-2

C-2

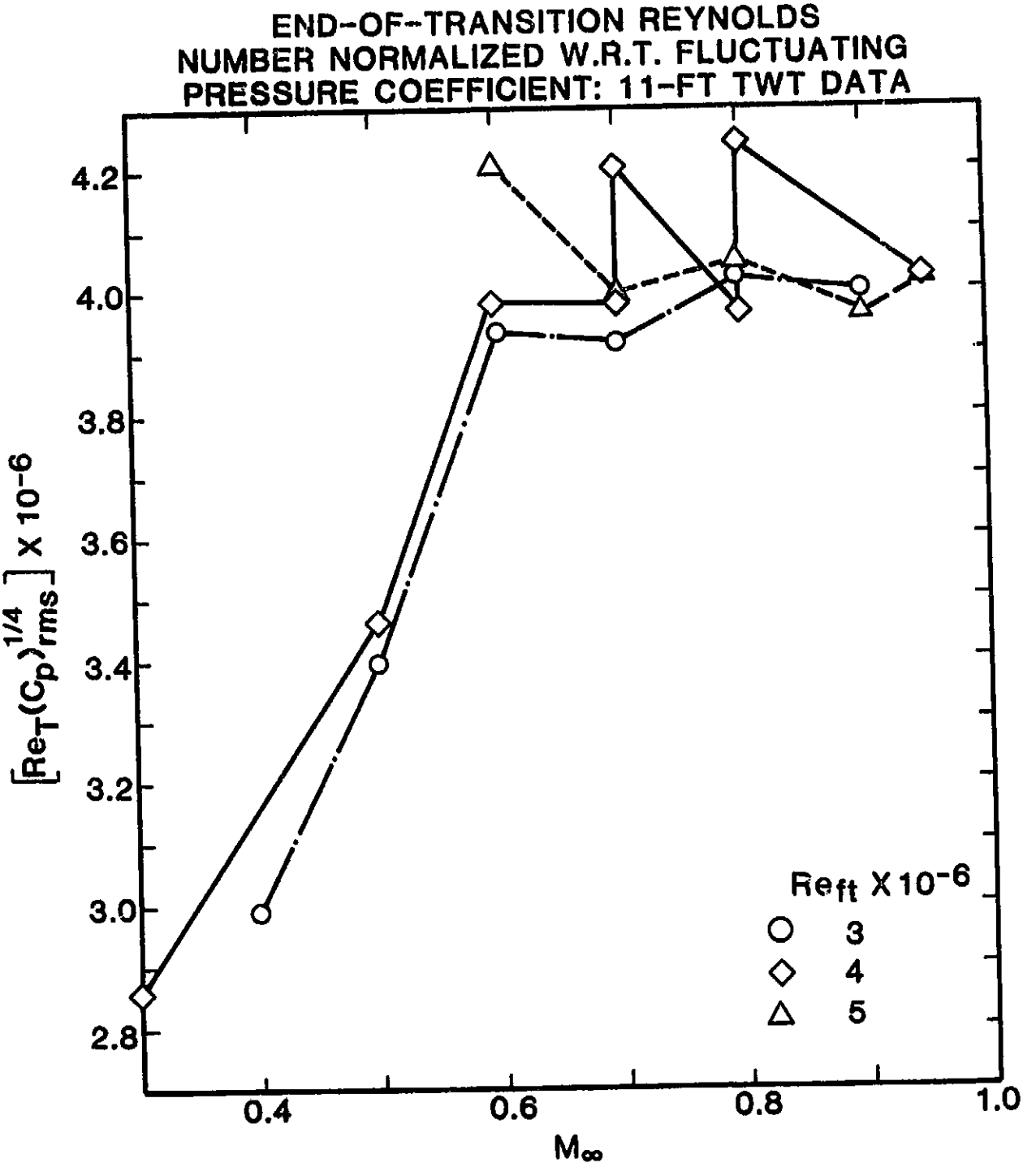

Figure A-3

ascertain if this parameter is indeed independent of Mach number. For M_∞ between 0.60 and 0.95, an average value of approximately 4×10^6 appears to be a good correlation. In this Mach number range tunnel-generated noise reaches the highest intensity levels. As M_∞ decreases below 0.6, the noise level also decreases rapidly. This rapid decay in noise is reflected in the decreasing values of $Re_T(C_p)^{.25}_{rms}$ as Mach number decreases. The data suggests that this parameter is a unique function of M_∞ for the AEDC Transition Cone in the 11-FT TWT. However, there is insufficient data to support a definite conclusion.

The effects of M_∞ and Re_{ft} on the length of the transition zone are presented in Fig. A-4. The extent-of-transition appears to have a local minimum near $M_\infty = 0.70$ only for the case $Re_{ft} = 3 \times 10^6$. The significance of this observation in unknown at this time.

Before proceeding to discuss the subsonic flight data, it is relevant to note that wind-tunnel data were used to estimate corrections of X_t and X_T for flight cases which had nonzero pitch and/or yaw angles. Figures A-5 and A-6 present the data for ΔX as a function of Γ, the total angle-of-attack; the corresponding vaues of X_t and X_T were used to correct the subsonic flight data. Figure A-5 expresses the data as a nondimensional ratio $\Delta X_\Gamma / \Delta X_{\Gamma = 0}$ vs. Γ, and Figure A-6 recast the data in terms of $(\Delta X_\Gamma - \Delta X_{\Gamma = 0})/L$. The wind-tunnel data were obtained from tests of the 10-deg cone in four different tunnels. In all cases, the pitch angle (α) was varied with yaw angle (β) equal to zero, and then β was varied with $\alpha = 0$.

The flight values of α and β are known from measurements with the calibrated flow angularity probe (yawmeter). The following equations were used to calculate values of Γ and ϕ (azimuthal angle of the Preston tube, measured positively in the clockwise direction from the windward element of the cone, looking forward along the axis).

$$\Gamma = (\alpha^2 + \beta^2)^{\frac{1}{2}}$$

$$\phi = \tan^{-1} \frac{\beta}{\alpha} - \Pi$$

These values were then used to interpolate wind-tunnel values of $X_t/(X_t)_{\Gamma = 0}$ and $X_T/(X_T)_{\Gamma = 0}$ as a function of Γ and ϕ. The measured flight values of X_t and X_T were corrected for nonzero Γ by dividing by the ratios which corresponded to an M_∞ nearest to the flight Mach number.

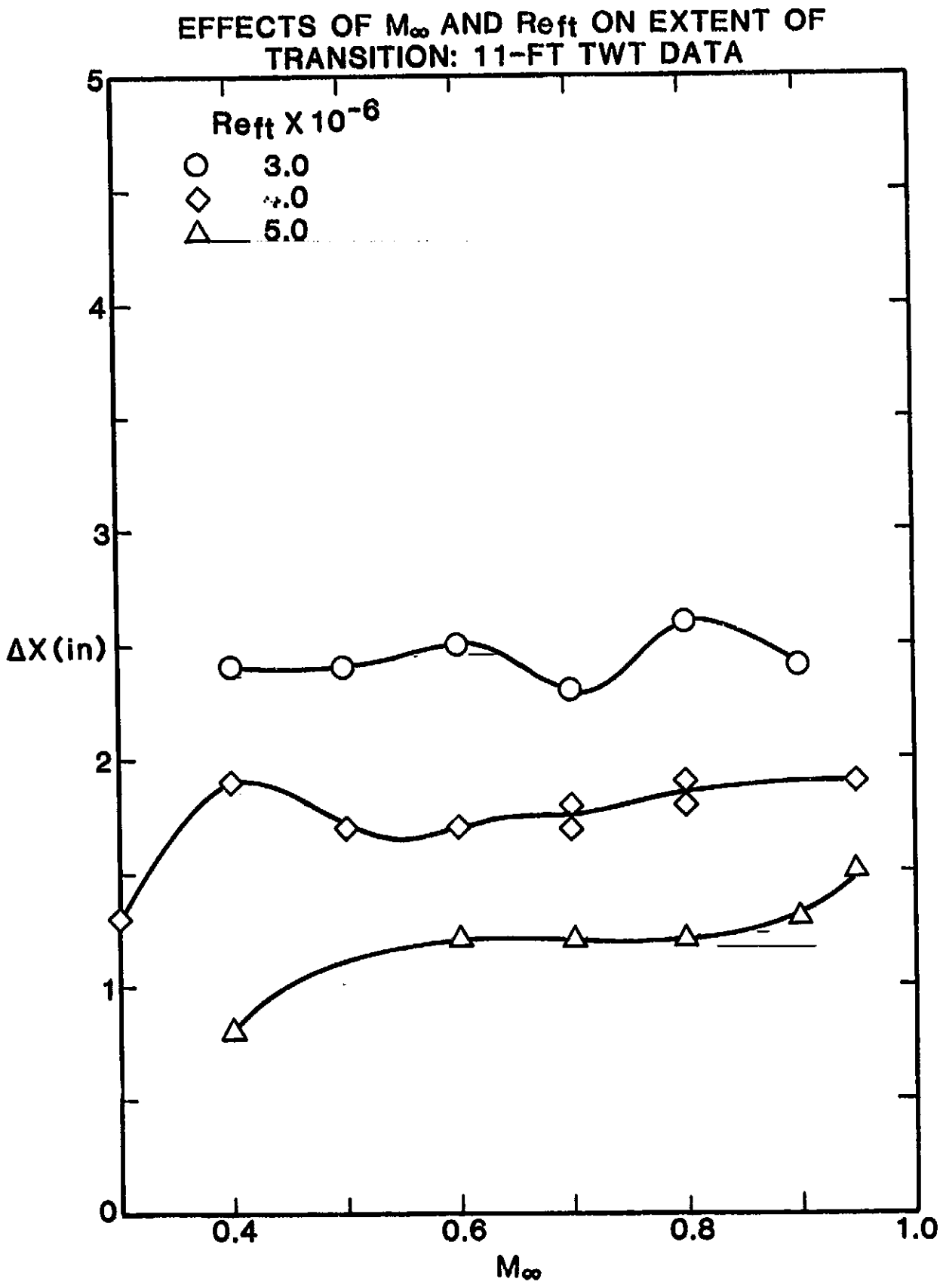

Figure A-4

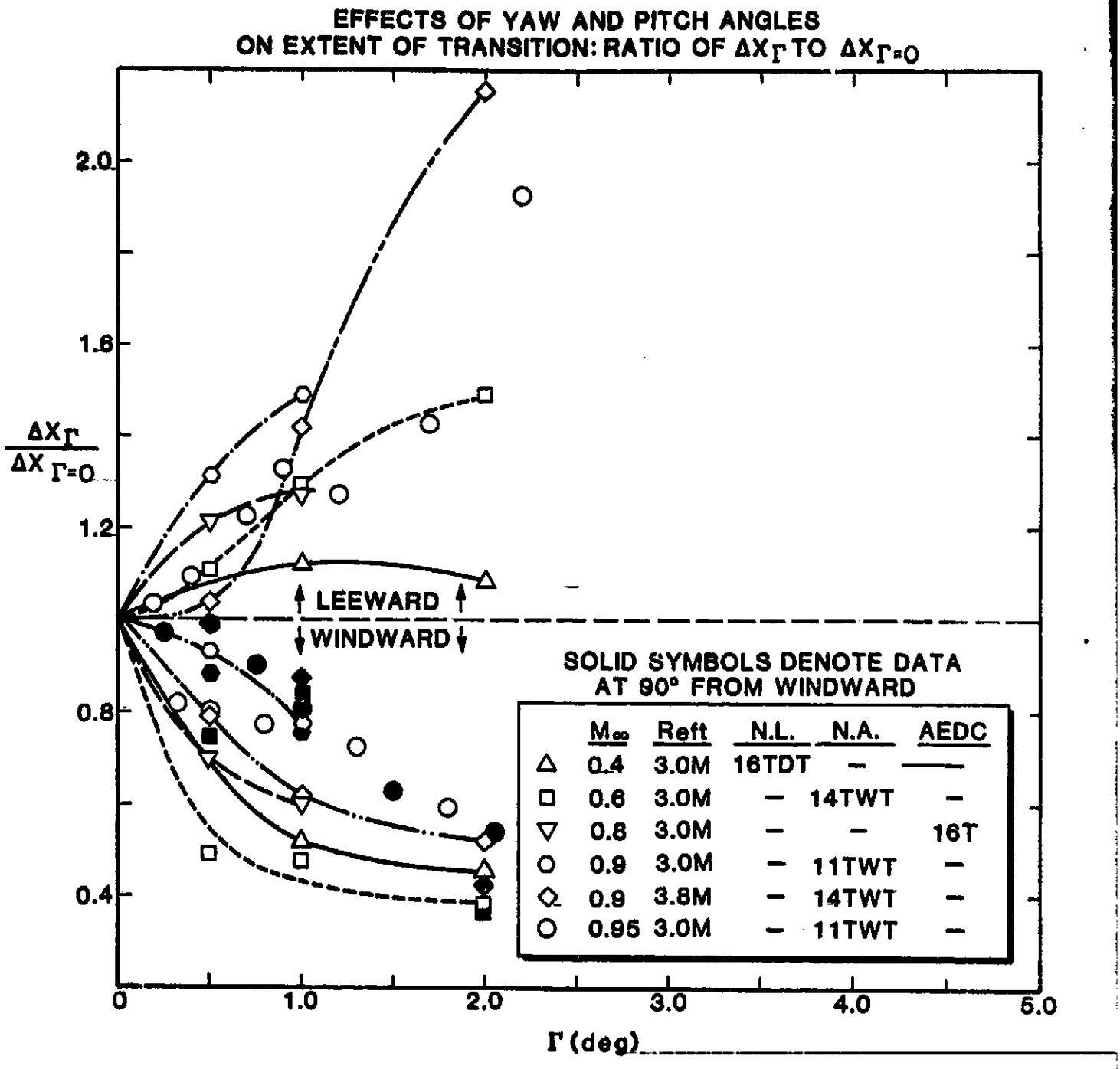

Figure A-5

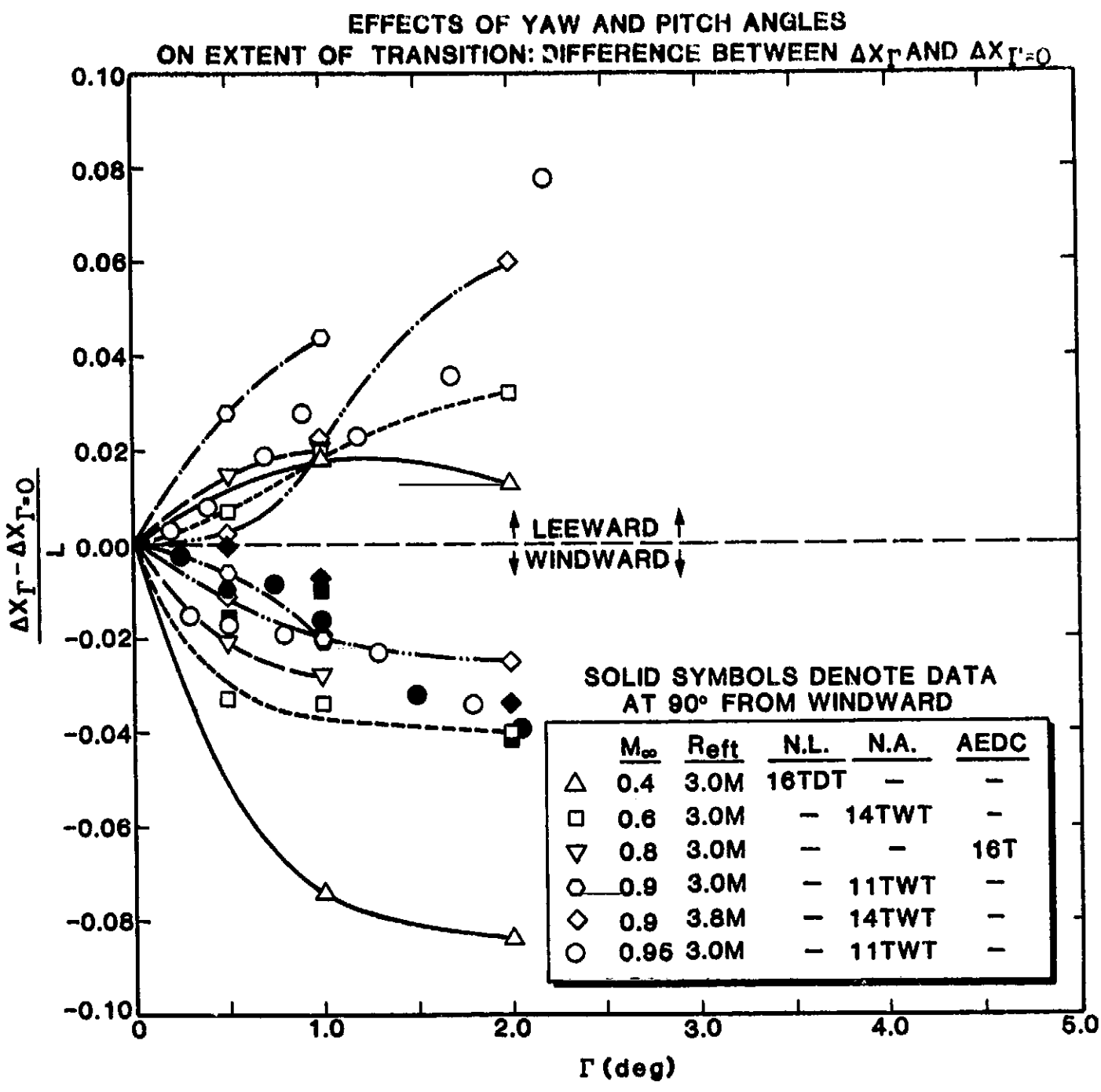

Figure A-6

The inconsistency of the data shown in Figs. A-5 and A-6 suggests this procedure becomes progressively more inaccurate as Γ increases and as the difference between flight and wind-tunnel Mach number increases. Fortunately, the subsonic values of Γ were of the order 1/2 deg or less, see Table A-2. Only the data from the Ames 11-Ft and 14-Ft tunnels at $M_\infty = 0.90$ are comparable. When $\Gamma = 0.5$ deg, Fig. A-5 shows a difference in ΔX on the leeward side of $0.28\ (\Delta X)_{\Gamma = 0}$ or a 28% discrepancy; whereas on the windward side, the difference is 14%. An estimate of the errors for other Mach numbers is not possible. Because of this uncertainty in the procedure for correcting flight transition data for nonzero Γ and the inability of the STAN5 program to model asymmetric boundary layers, only flight cases for which $|\Gamma| < 0.11$ deg were used in the development of the Preston-tube/skin-friction correlation.

Flight Data

The subsonic flight data are summarized in Table A-2. As discussed previously, the last four digits in the flight number designate time of day during which the data were taken. For example, 349.1347 denotes flight number 349, and the data were obtained at 13:47 hours. In addition to nonzero values of Γ, the "corrected" data for X_t, X_T and ΔX have also been modified to account for non-adiabatic wall temperatures via the following equation.

$$\frac{(X_t)_{T \neq T_{aw}}}{(X_t)_{aw}} = \frac{(X_T)_{T \neq T_{aw}}}{(X_T)_{aw}} = \left[\frac{T}{T_{aw}}\right]^{-7}$$

This is an empirical equation which is based on a curve fit of flight data, see Ref. 8.

Figures A-7 and A-8 present the distance to transition onset for the uncorrected and corrected data as a function of M_∞ and Re_{ft}. Figures A-9 and A-10 present similar plots of distance to end-of-transition for the uncorrected and corrected data. In both cases, the corrected values of X_t and X_T show a considerable improvement in defining a discernible dependence on M_∞ and Re_{ft}. The general trend for both X_t and X_T is that transition occurs earlier (i.e., X's decrease) with increasing Re_{ft} and decreasing M_∞.

In Fig. A-11 transition Reynolds numbers Re_T, based on the product of Re_{ft} and X_T, are shown as a function of M_∞. It is relevant to here note that the difference between U_∞/ν_∞ and U_e/ν_e for the subsonic flight conditions is less than 1%. Since the data is not collasped into a single curve, it

TABLE A-2

SUBSONIC BOUNDARY LAYER TRANSITION DATA FROM FLIGHT TESTS

Plotting Symbols	Flight No.	$Re_{ft} \times 10^{-6}$	M_∞	q_∞(PSF)	X_t (uncorrected, in)	X_T (uncorrected, in)	ΔX (uncorrected, in)	$\Gamma°$	$\phi°$	T_w/T_{aw}	X_t (corrected, in)	X_T (corrected, in)	ΔX (corrected, in)	X_T/X_t	$Re_T \times 10^{-6}$	$(C_p)_{rms}$
△	353.1417	1.38	.82	170	29.2	33.1	3.9	.732	122.2	0.986	28.1	33.9	5.83	1.21	3.90	*****
	351.0914	1.41	.92	189	27.0	31.0	4.0	.591	118.3	1.021	32.8	38.3	5.33	1.17	4.50	.0838
	350.1357	1.56	.88	198	26.6	29.8	3.2	.136	107.1	1.024	31.6	35.4	3.77	1.12	4.60	*****
	350.1359	1.59	.86	201	24.8	29.5	4.7	.194	124.5	1.022	29.2	34.6	5.36	1.185	4.59	*****
	352.1456	1.63	.71	175	21.7	24.4	2.7	.251	151.2	0.991	20.4	23.1	2.72	1.13	3.14	*****
▽	350.1403	1.63	.90	216	24.5	30.0	5.5	.550	182.1	1.004	24.4	31.1	6.70	1.13	4.23	*****
	352.1446	1.65	.71	176	22.2	25.4	3.2	.547	108.1	1.005	24.0	27.5	3.49	1.15	3.78	*****
	352.1454	1.66	.71	177	24.6	27.5	2.9	.314	120.6	0.997	24.5	27.5	3.04	1.12	3.81	*****
	353.1355	1.94	.87	192	21.0	23.4	2.4	.655	108.7	0.983	19.7	22.4	2.66	1.14	3.62	.1149
◇	350.1344	1.99	.66	216	19.6	22.9	3.3	.535	249.2	1.014	22.5	26.0	3.50	1.16	4.31	*****
	352.1351	2.02	.60	209	18.6	22.2	3.6	.570	91.0	1.001	19.6	23.4	3.80	1.19	3.94	*****
	329.1031	2.12	.85	288	21.5	24.3	2.8	.110	185.2	1.005	22.0	25.1	3.11	1.14	4.43	.1098
	349.1332	2.12	.87	285	20.3	22.4	2.1	.480	90.1	1.009	22.9	25.1	2.21	1.10	4.44	*****
	329.1028	2.15	.86	294	20.8	23.2	2.4	.036	123.7	1.005	20.7	24.0	3.07	1.16	4.30	.1224
	349.1333	2.15	.88	293	19.4	22.2	2.8	.453	90.0	1.003	21.3	24.1	2.85	1.13	4.25	*****
	349.1339	2.20	.85	296	19.5	22.6	3.1	.576	98.0	0.994	19.9	23.3	3.44	1.17	4.28	*****
○	327.0907	2.21	.86	304	19.9	22.2	2.3	.045	243.6	1.014	21.9	24.4	2.50	1.11	4.50	.1240
	329.1036	2.23	.75	284	22.2	25.3	3.1	.113	225.0	0.988	20.4	23.2	2.85	1.14	4.31	.0969
	349.1354	2.24	.75	282	20.4	24.1	3.7	.250	106.3	0.990	19.5	22.9	3.43	1.17	4.28	*****
	349.1400	2.27	.75	287	20.8	23.0	2.2	.110	174.8	0.992	19.5	22.0	2.48	1.13	4.16	*****
	349.1347	2.27	.75	287	19.8	23.0	3.2	.567	99.1	0.985	18.9	22.1	3.22	1.17	4.19	*****

Table A-2 (continued)

Plotting Symbols	Flight No.	$Re_{ft} \times 10^{-6}$	M_∞	q_∞(PSF)	X_t	X_T	ΔX	$\Gamma°$	$\phi°$	T_w/T_{aw}	X_t	X_T	ΔX	X_T/X_t	$Re_T \times 10^{-6}$	$(C_p)_{rms}$
	353.1327	2.29	.49	212	17.4	20.1	2.7	.158	161.7	0.992	16.4	18.9	2.46	1.15	3.61	.2650
	353.1427	2.30	.70	169	20.5	24.3	3.8	.555	113.4	1.008	22.6	26.9	4.33	1.19	5.16	.1074
	349.1409	2.40	.62	294	19.9	22.5	2.6	.493	264.2	0.972	17.0	19.2	2.20	1.13	3.84	*****
□	349.1411	2.45	.63	286	19.2	22.0	2.8	.291	116.5	0.978	16.7	19.1	2.40	1.14	3.90	*****
	327.0918	2.45	.66	303	23.6	27.8	4.2	.014	135.0	0.969	18.8	22.2	3.37	1.18	4.54	.1460
	329.1042	2.46	.68	299	22.0	26.6	4.6	.100	185.7	0.967	17.3	21.0	3.66	1.21	4.31	.0954
	333.1351	2.83	.93	450	20.7	24.0	3.3	.072	236.3	0.996	20.2	23.4	3.22	1.16	5.51	.0713
○	332.1020	2.86	.93	455	19.0	22.5	3.5	.070	180.0	1.008	20.0	23.7	3.69	1.185	5.65	.1950
	333.1354	2.88	.89	448	19.7	22.4	2.7	.100	95.7	0.993	18.8	21.4	2.58	1.14	5.13	.1049
	330.0952	2.90	.89	449	17.2	19.7	2.5	.051	258.7	0.995	16.6	19.0	2.40	1.14	4.59	.7010*
●	333.1358	3.08	.79	454	18.6	21.6	3.0	.114	217.9	0.980	16.1	18.7	2.61	1.16	4.81	.1455

***** Not measured during flight

* Indicates unusually high free-stream turbulence; boundary layer transition did occur closer to nose than comparable cases.

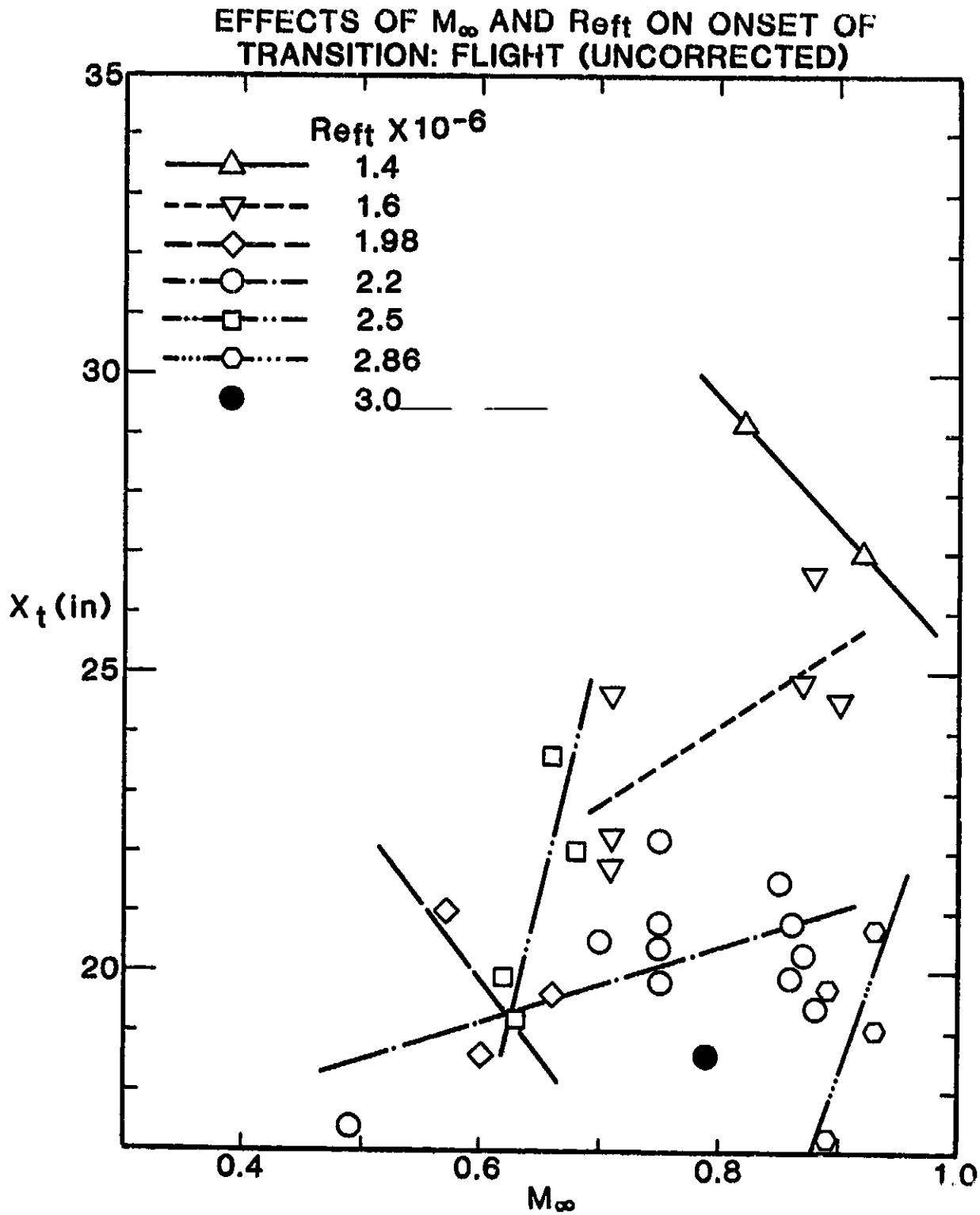

Figure A-7

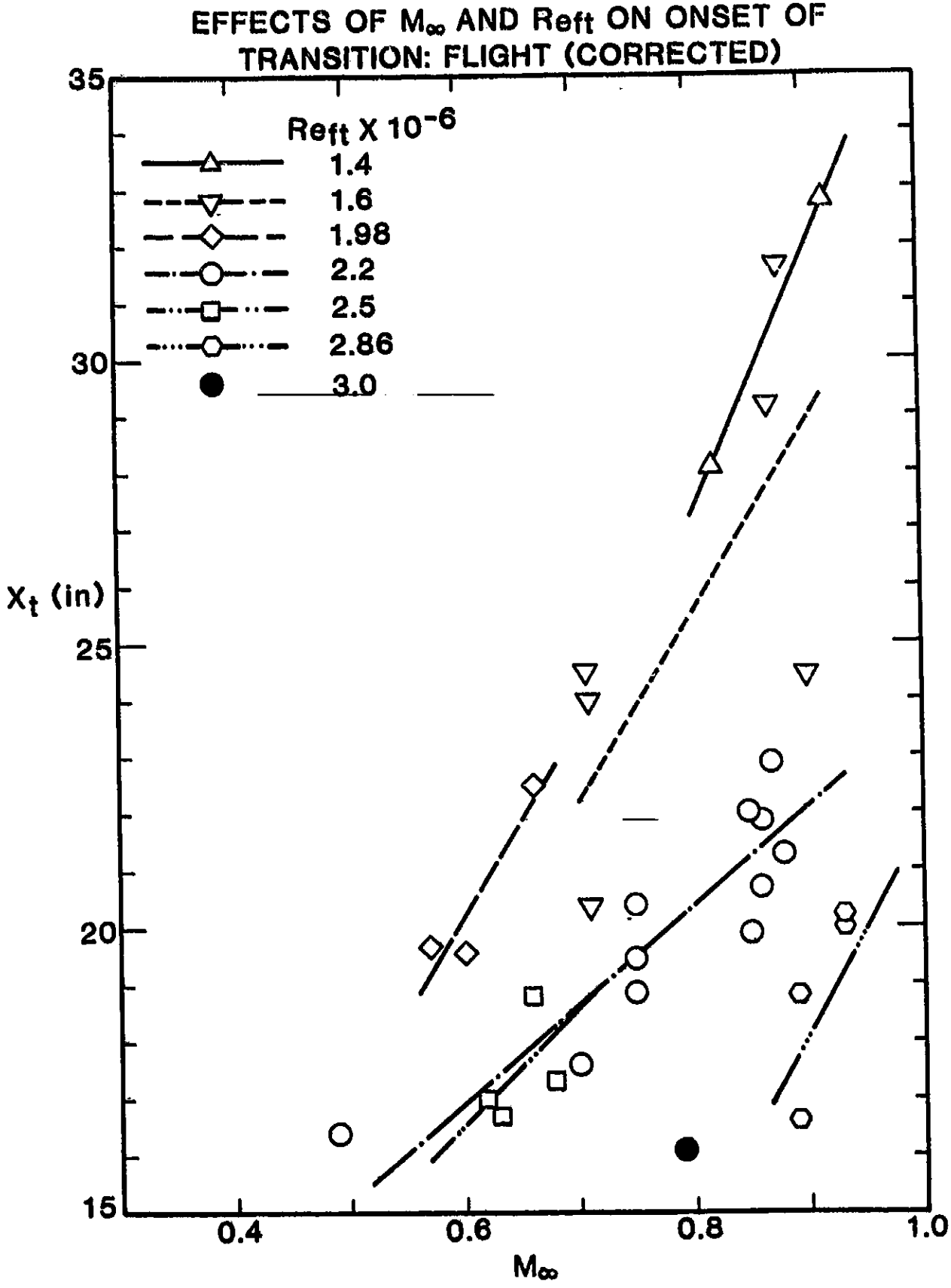

Figure A-8.

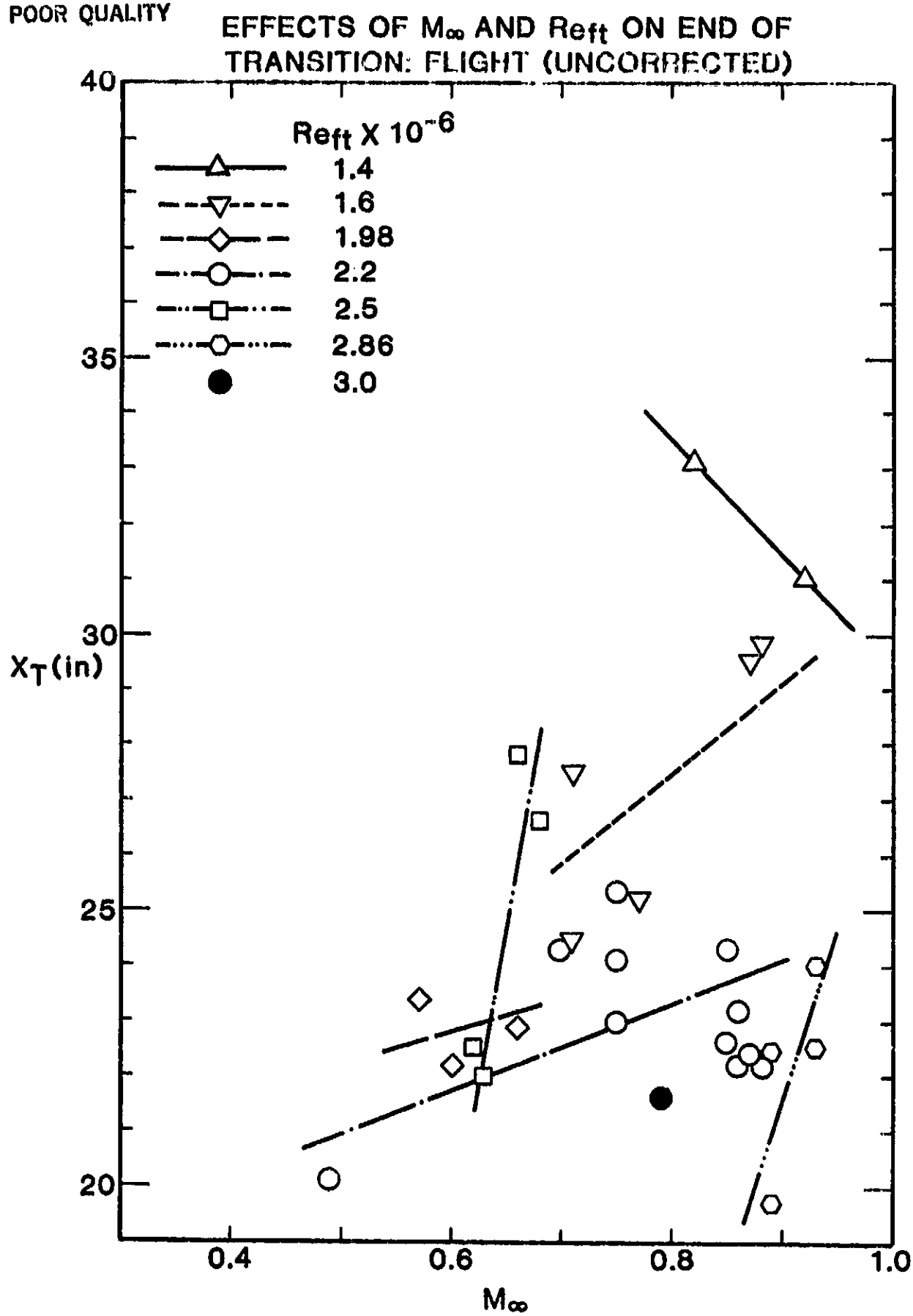

Figure A-9

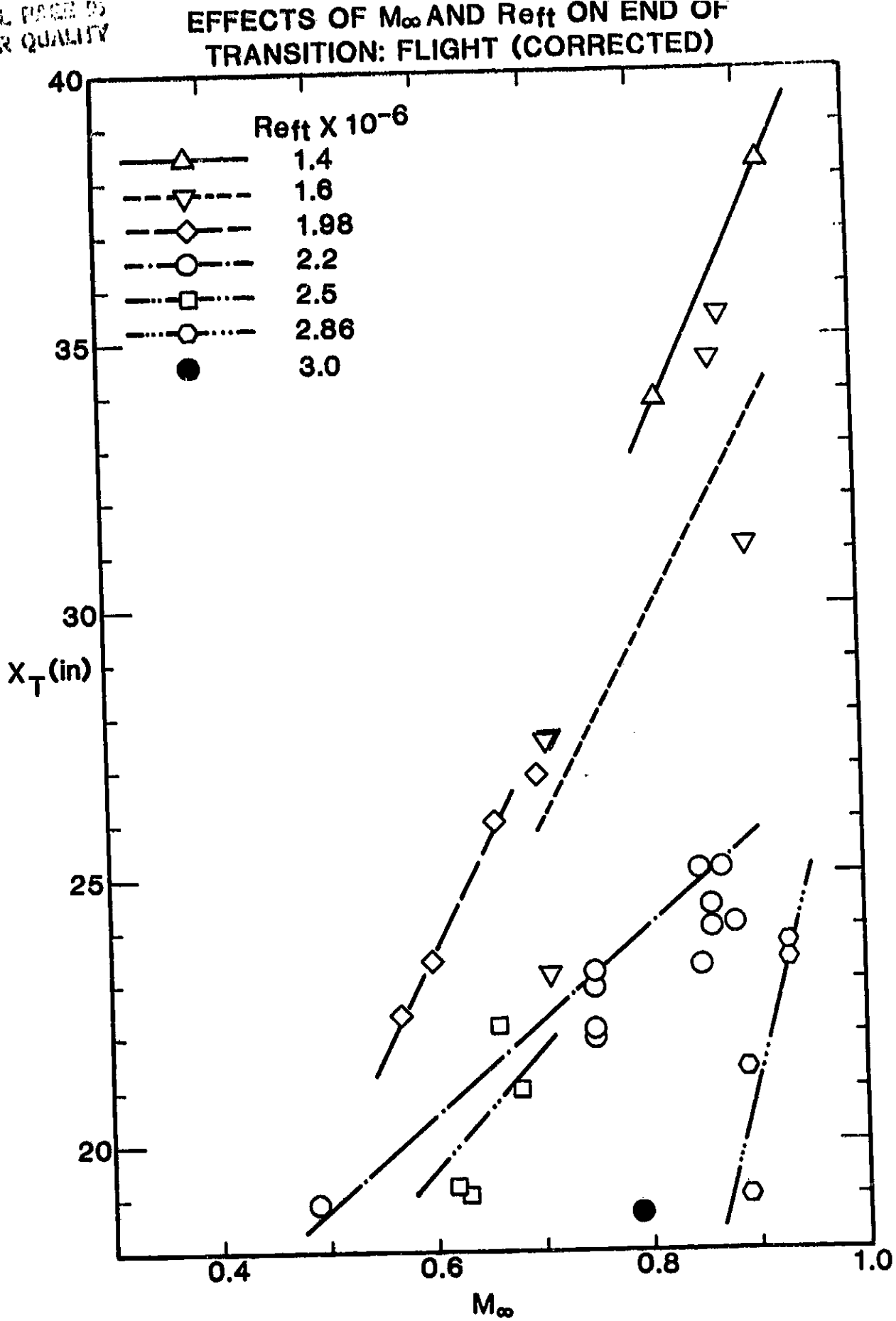

Figure A-10

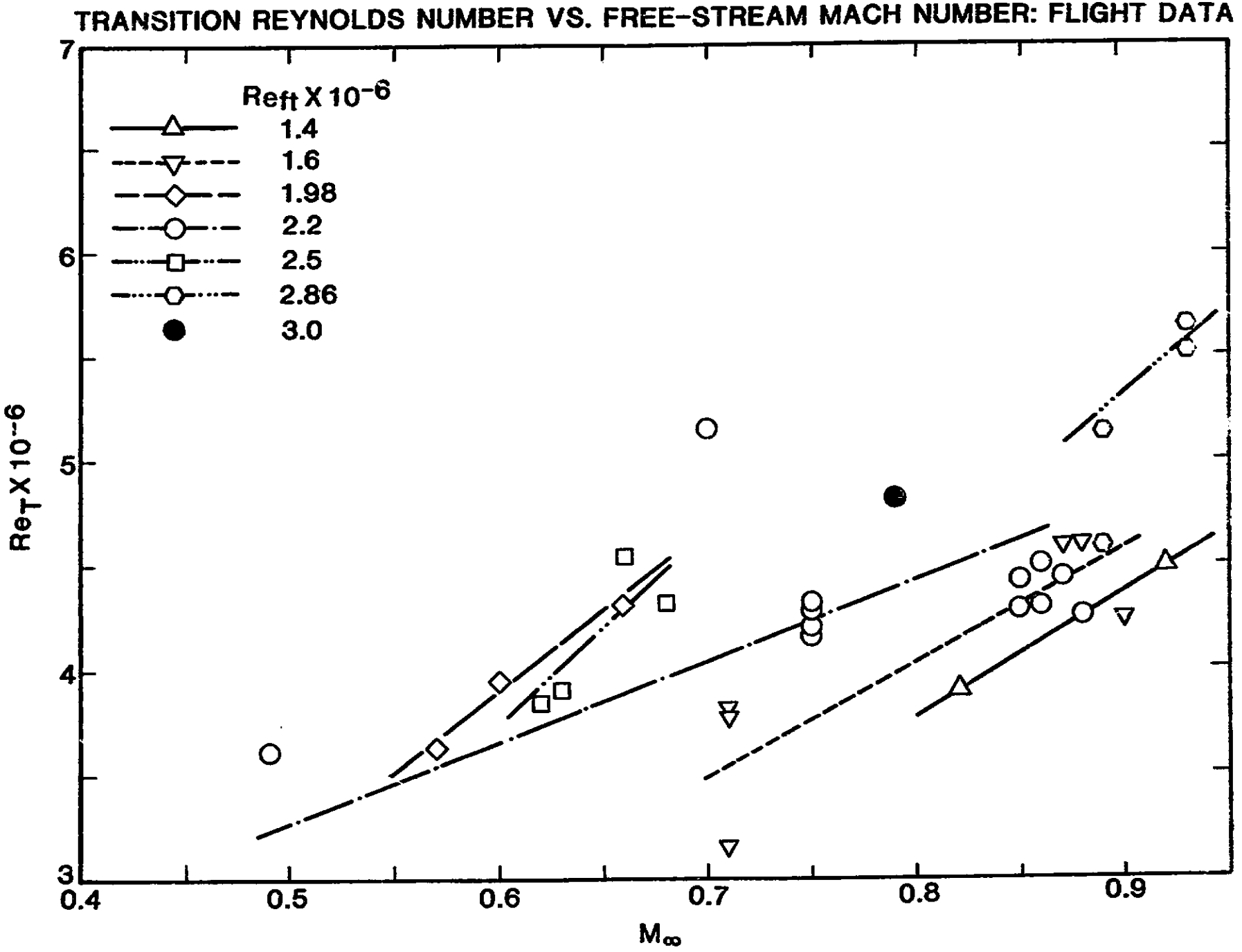
TRANSITION REYNOLDS NUMBER VS. FREE-STREAM MACH NUMBER: FLIGHT DATA
Reft X 10⁻⁶
1.4
1.6
1.98
2.2
2.5
2.86
3.0
Re_T X 10⁻⁶
7
6
5
4
3
0.4
0.5
0.6
0.7
0.8
0.9
M∞

Figure A-11

appears that other variables, such as $(C_p)_{rms}$, are involved. Unfortunately, $(C_p)_{rms}$ was not recorded during the majority of the subsonic flights.

The extent of the transition zone is plotted in Figs. A-12 and A-13. In this case, the corrected values in Fig. A-13 show no discernible reduction in scatter,and the correlation remains unsatisfactory.

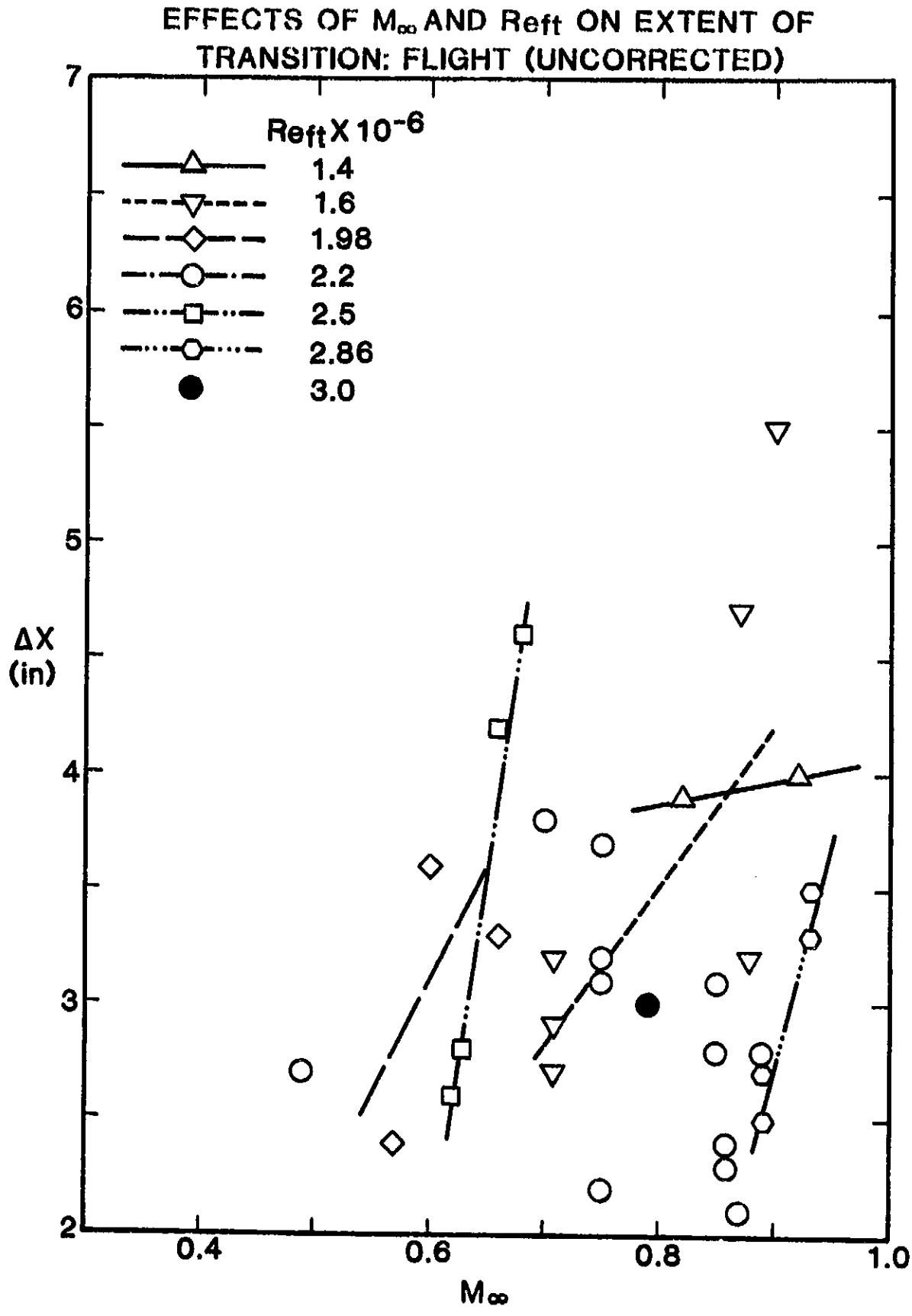

Figure A-12

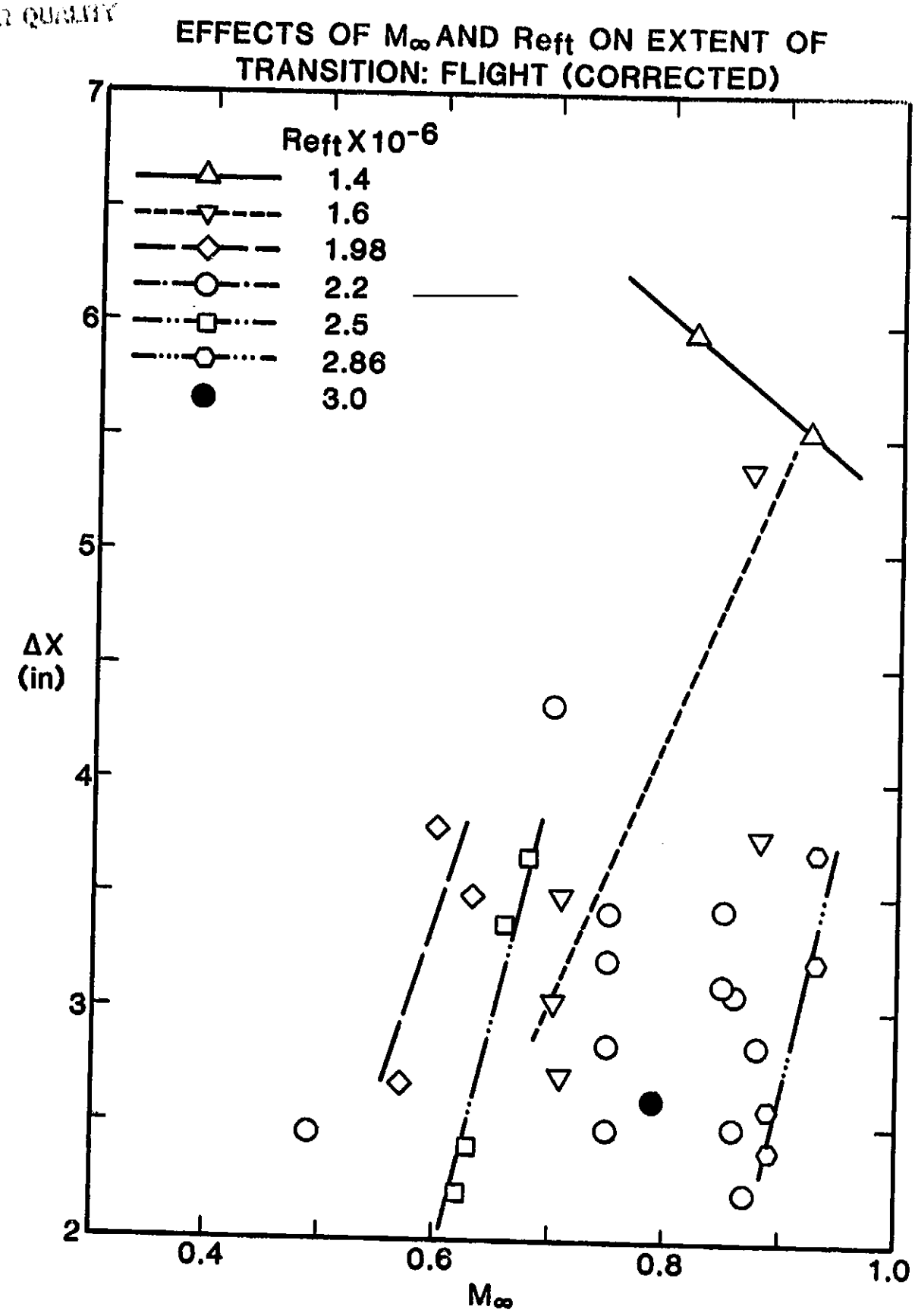

Figure A-13

APPENDIX B

EFFECTS OF SPHERICAL NOSE BLUNTNESS ON BOUNDARY-LAYER TRANSITION AT SUPERCRITICAL SPEEDS

In Ref. 8, Dougherty and Fisher declare that the AEDC-BLT Cone has an apex with an "equivalent" diameter of 0.004-in. (The word equivalent is apparently used to denote the fact that the nose-tip is not exactly spherical.) Since it is known that hemisphere-cylinders generate rather strong shock waves at high subsonic Mach numbers, e.g., Hsieh[30], a natural question is: how does nose bluntness affect boundary-layer transition with in the transonic regime?

In order to answer this question via analysis, it is necessary to have at least two computational tools. One is a computer code which will calculate both the inviscid flow with shock waves and the associated profiles of the boundary layer. The second required tool is a procedure to estimate when and where boundary layer transition occurs. The computer code developed by Nietubicz, et al.[31] was identified as a state-of-the-art method for solving the Navier-Stokes Equations about axisymmetric bodies and at transonic speeds. The second needed tool was located by contacting Paul Granville at NSRDC. He was contacted because he had previously published papers dealing with boundary-layer transition on axisymmetric bodies. Although none of his work was directly applicable to the transonic cone question, he did supply us with a copy of a very recent paper by Wazzan, et al.[32]

The important results of this paper is the following equation for estimating the onset of boundary-layer transition.

$$\log_{10} [R_s(e^9)] = -40.4557 + 64.8066H - 26.7538H^2 + 3.3819H^3 , \qquad (B\text{-}1)$$

for $2.1 < H < 2.8$. The authors claim that this equation correlates the well-known "e^9 method", see Ref. 33. Thus, the use of Eq. (B-1) avoids the need for lengthy stability calculations. The authors state that the method is applicable to incompressible flows which:

1. do not vary too much from local similarity,
2. have small surface roughness and/or vibration,
3. low freestream turbulence, and
4. small heating rates, i.e., $T_w - T_\infty < 23°C$.

For the purpose of conducting a comparative study of the effect of nose-bluntness on boundary-layer transition on the cone, it was decided to apply Eq. (B-1) to the compressible boundary layer by evaluating the kinematic viscosity that appears in R_s at the reference temperature of Sommer and Short, Eq. (11).

Next, Dr. Nietubicz was approached about using his program for this type of analysis. He agreed that this was a problem that no one has studied and thought his code should be able to do the job. Unfortunately, his Navier-Stokes solver did not print out the conventional, boundary-layer parameters. He stated that he didn't have the time to add a subroutine to accomplish this and suggested the first author visit BRL to perform this task. A three-day trip was made and with some additional debugging via the mail, this subroutine was successfully added to the BRL program.

The original agreement with Nietubicz was that one or two cases would be run in order to check for satisfactory execution, and at that point, Dr. Pulliam at NASA Ames would run the code for a set of freestream conditions and different nose radii. An initial case was run during the check-out process for a spherical nose radius of 0.05 in. and with $M_\infty = 0.95$, $Re_{ft} = 3 \times 10^6$, $T_\infty = 450°R$, and $T_w = 530°R$. The results are summarized in Figures B-1 thru B-3. Figure B-1 shows a portion of the 40 x 80 set of grid points that were used in the finite difference solution of the equations. Figures B-2 shows the distribution of pressure coefficient about the nose. Here, the axial distance X is normalized with respect to a diameter of 1.4 in., and in order to focus on the nose region, only the first 8 in. of the cone was modelled. Figure B-3 presents the corresponding Mach number contours. The central interior Mach contour encloses the region with local Mach numbers ≥ 1.10, and Mach number decreases 0.01 with each larger contour out to a Mach number of 0.95. The pressure distribution and the Mach contours indicate a rather smooth recompression as the flow passes from the nose cap onto the cone, and furthermore, the flow remains attached. As freestream Mach number is increased, it is anticipated that a shock wave would form and the boundary layer would thicken and possibly separate as M_∞ approaches one. However, the above calculation assumes a laminar boundary layer. If transition to a turbulent boundary layer occurs, separation would be either delayed or, possibly, would not occur at all. The boundary-layer subroutine was not ready at the time this case was computed; thus, no information is presently available concerning transition.

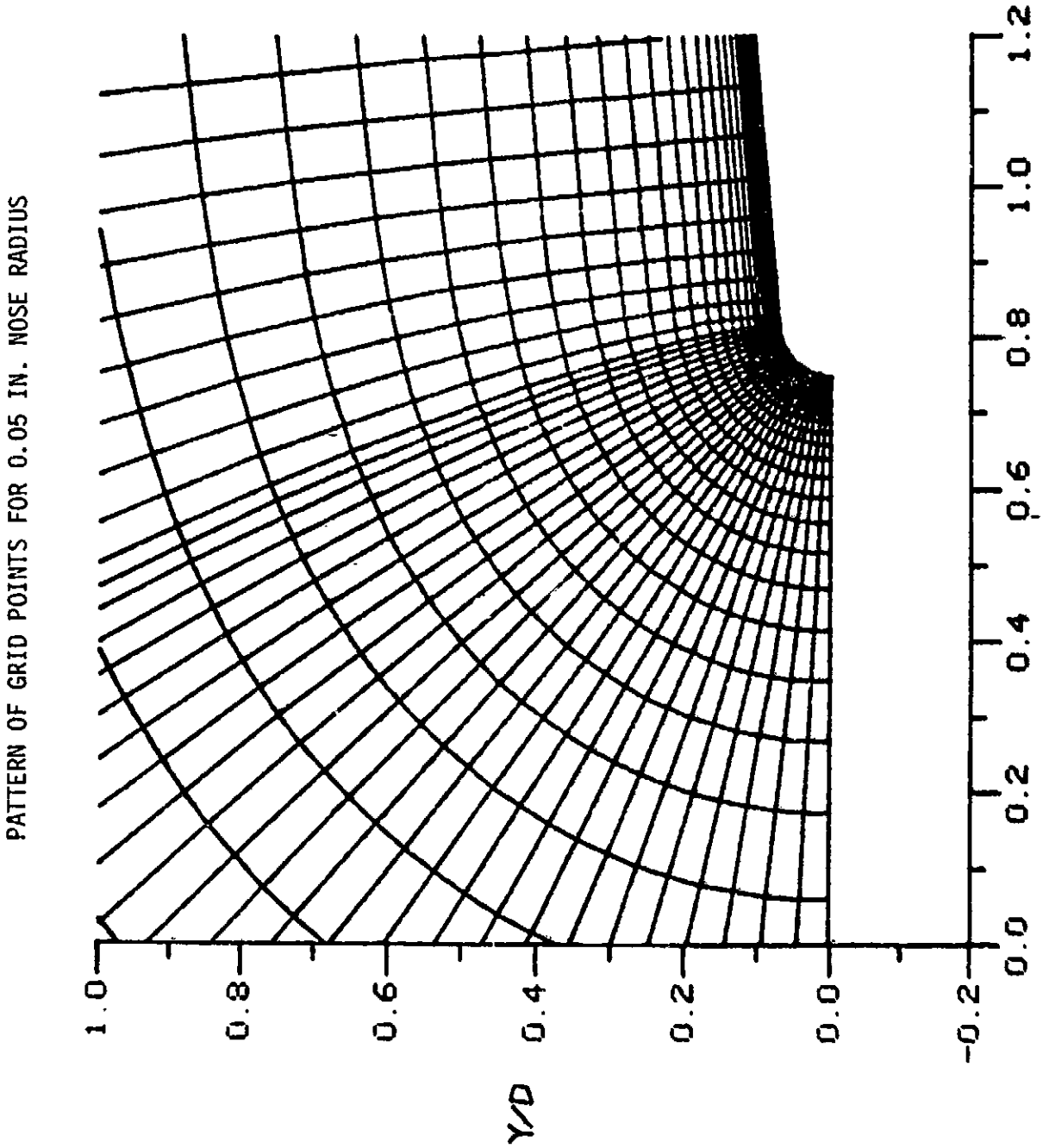

Figure B-1.

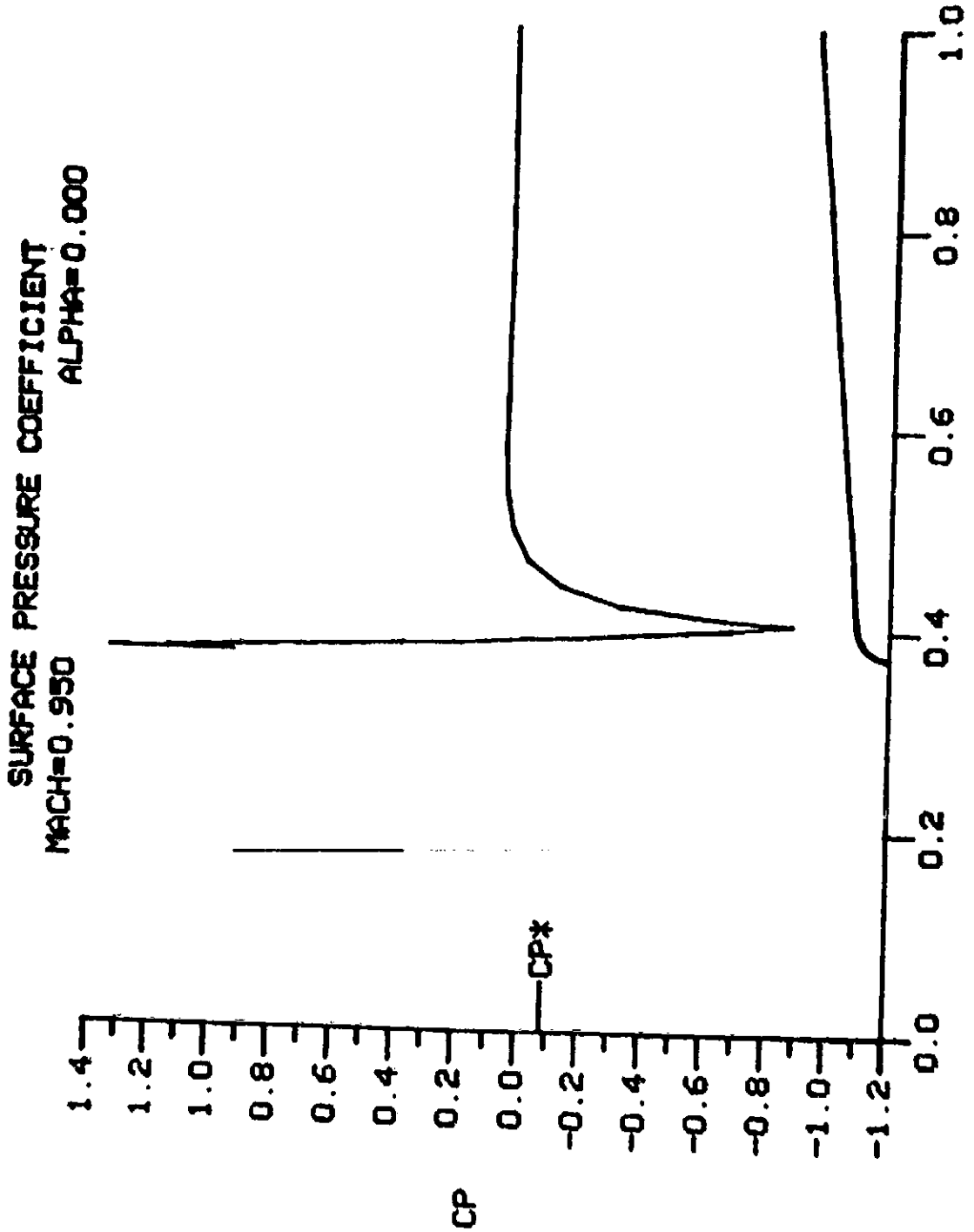

Figure B-2.

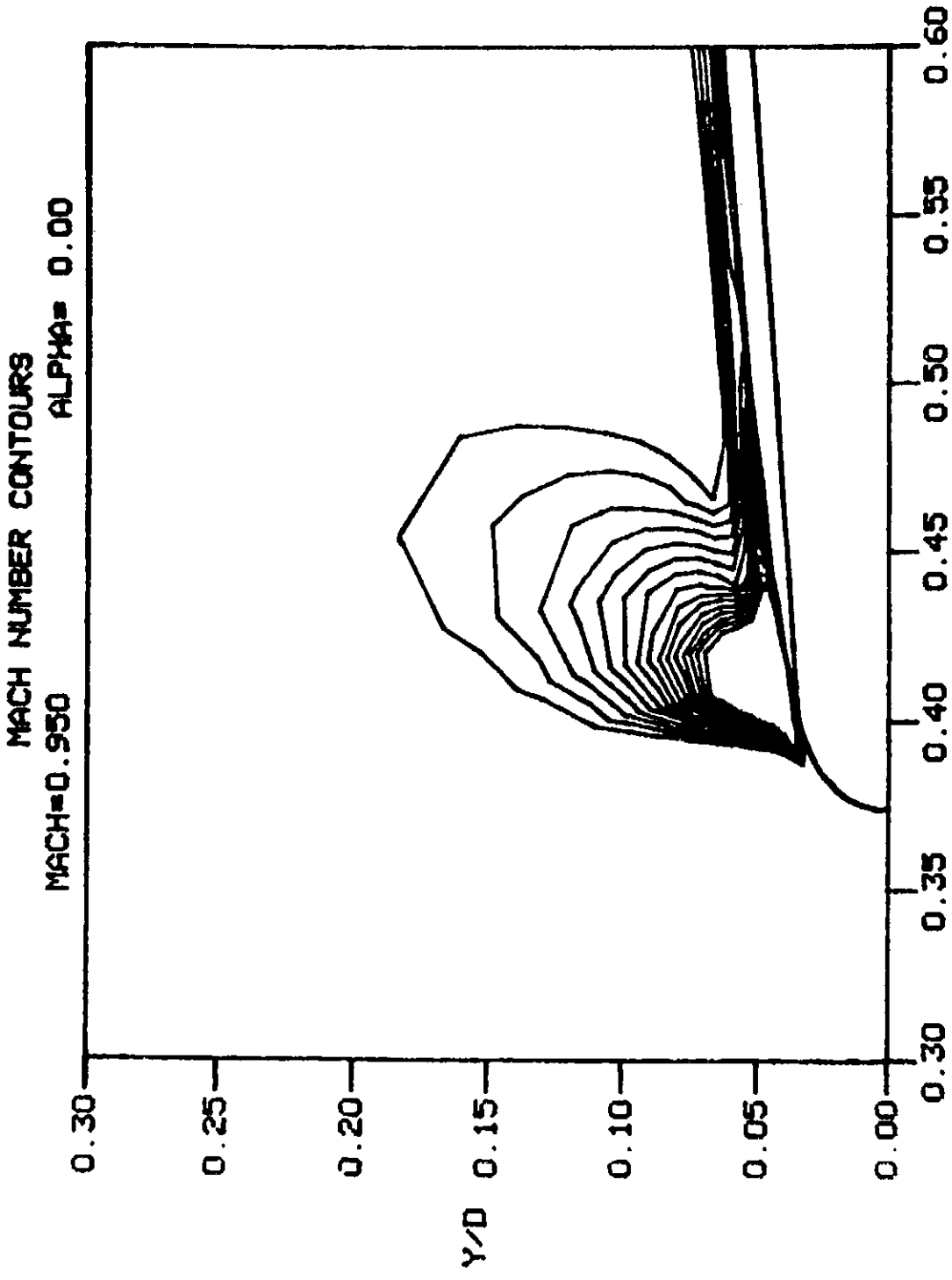

Figure B-3.

A second case was computed after the boundary-layer subroutine became operational. This case consists of a nose radius of 0.1 in., $M_\infty = 0.95$, $Re_{ft} = 3 \times 10^6$, $T_\infty = 490°R$, and $T_w = 530°R$. The pressure coefficients for this case are shown in Fig. B-4. The recompression followed by a second expansion is characteristic of a separated-flow region. The associated Mach contours are shown in Fig. B-5, and the coresponding streamlines are presented in Fig. B-6. This figure vividly illustrates the pocket of recirculating flow. A typical velocity profile within this separated region is presented in Fig. B-7, and a velocity profile slightly downstream of the separated zone is shown in Fig. B-8. The boundary-layer thickness in a separated region is defined to be measured from the point at which the velocity becomes positive.

The boundary-layer properties upto the beginning of separation are summarized for this case in Table B-1. The left and right-hand sides of Eq. (B-1) are also include in the last two columns of this table. There are a number of observations that should be noted from Table B-2. Firstly, the boundary-layer thickness oscillates but the displacement and momentum thickness (integral properties) are monotonic. The oscillations in δ could probably be eliminated by placing more grid points within this region of large and rapidly varying pressure gradients. Finally, equality between the left and right-hand sides of Eq. (B-1) first occurs between X/D values of 0.790 and 0.794. Unfortunately, the corresponding values of H are greater than 2.8 and thus violate the restriction on H imposed by Wazzan, et al.[32] The possible error this causes in the predicted location of transition-onset is presently unknown. However, the pressure gradient is small in this region, and the assumption of local similarity is probably valid.

Since transition onset occurs near X/D = 0.794, the flow field needs to be recalculated using this information. It is expected that the extent of the separated region will diminish considerably if not completely disappear. Unfortunately, the subject code does not presently have the capability to allow boundary-layer transition, i.e., the flow is either entirely laminar or entirely turbulent. This capability is needed in order to arrive at a satisfactory model of the complete flow.

In summary, the nose radius determines the wetted length and thereby the boundary thickness at the shock. A larger nose radius not only promotes boundary-layer transition at transonic speeds but can also lead to separation of a laminar boundary layer. As long as one is not too concerned about precise

absolute values, the model discussed herein appears to be appropriate for a comparative study of the effects of nose-bluntness at transonic speeds. If and when the parametric study is completed, the results will be reported elsewhere.

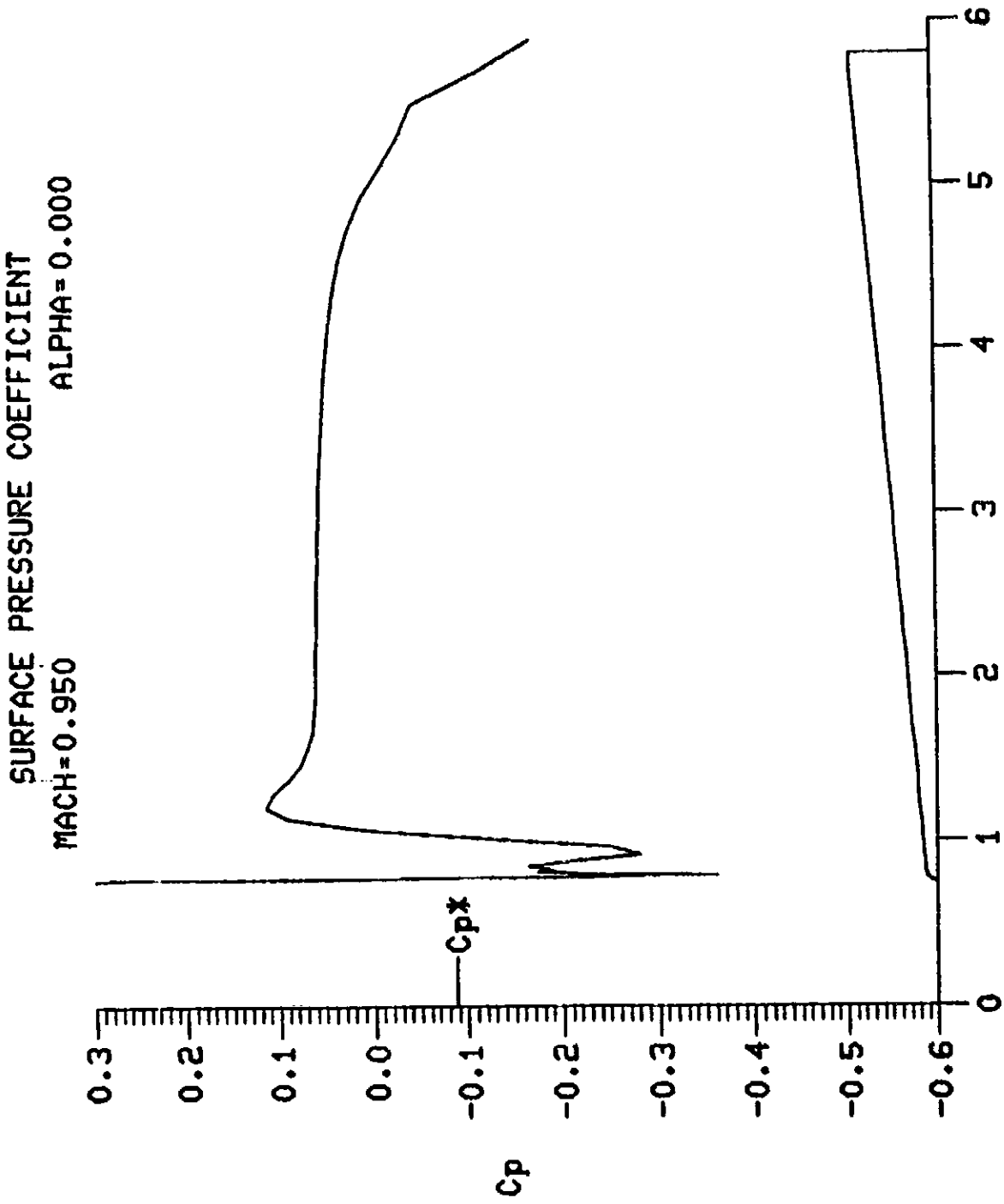

Figure B-4.

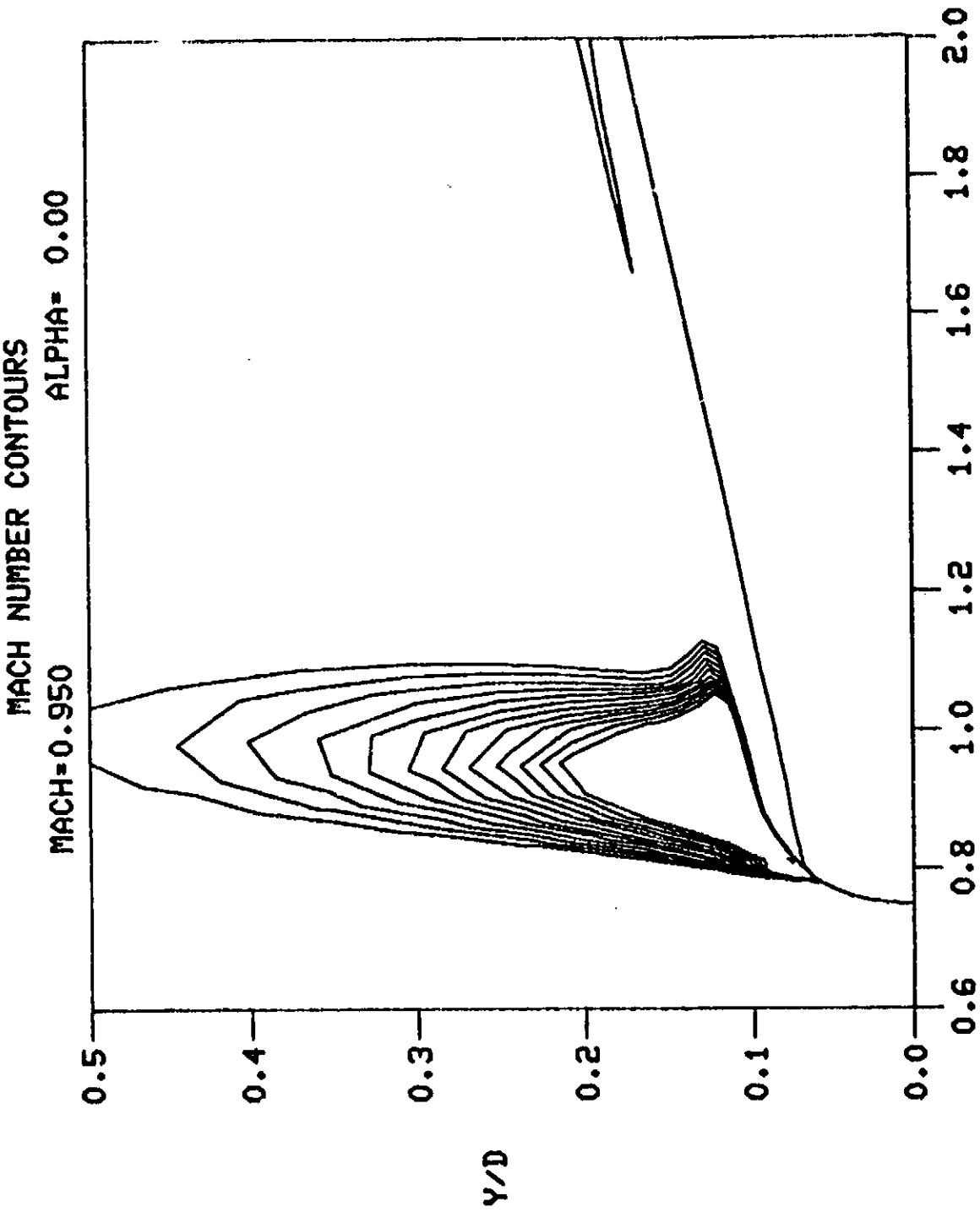

Figure B-5.

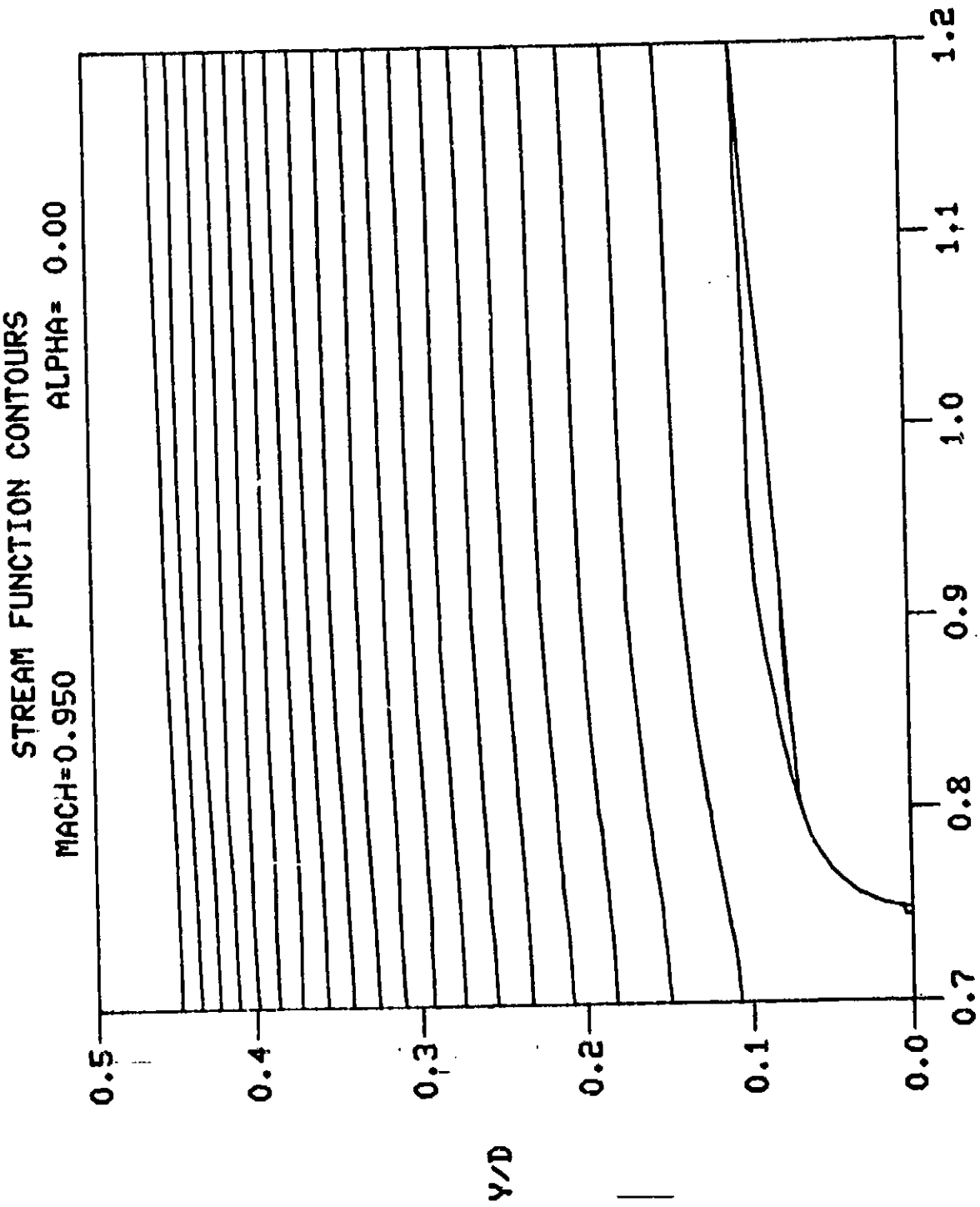

Figure B-6.

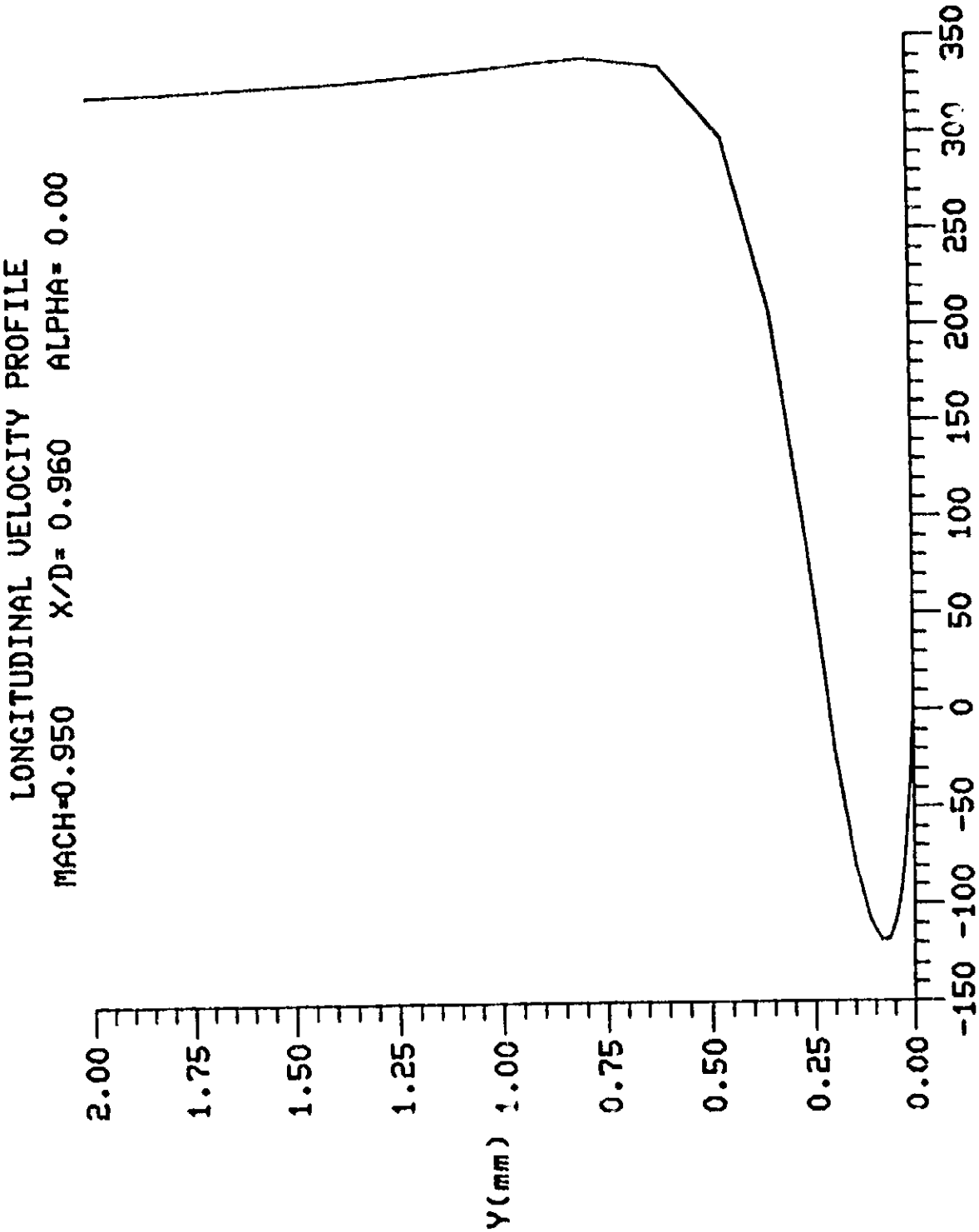

Figure B-7.

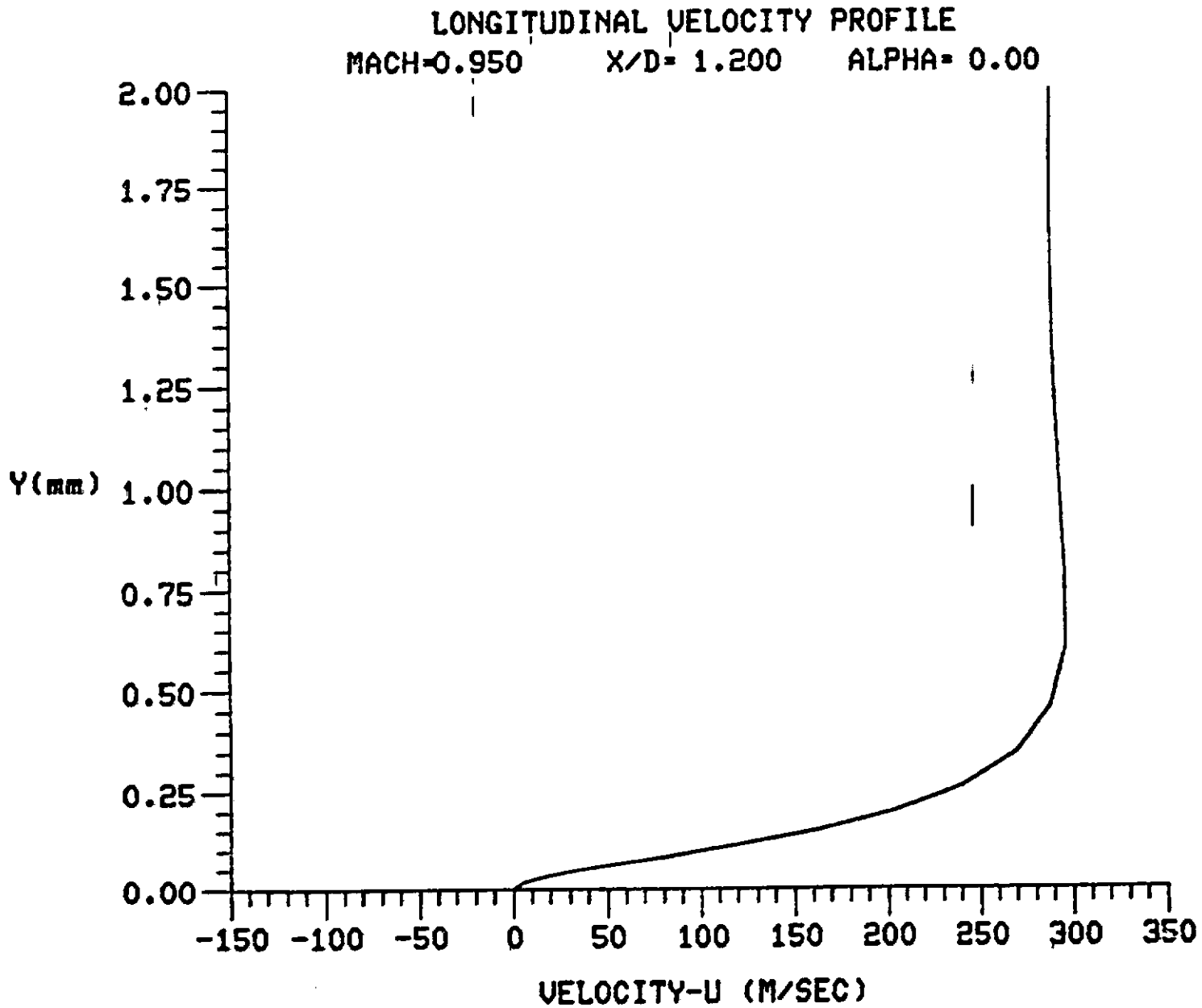
LONGITUDINAL VELOCITY PROFILE
MACH=0.950 X/D= 1.200 ALPHA= 0.00
Y(mm)
2.00
1.75
1.50
1.25
1.00
0.75
0.50
0.25
0.00
-150 -100 -50 0 50 100 150 200 250 300 350
VELOCITY-U (M/SEC)

Figure B-8.

TABLE B-1

SUMMARY OF COMPUTED BOUNDARY LAYER PROPERTIES FOR A CONE
WITH A NOSE RADIUS OF 0.1 in. and $M_\infty = 0.95$, $Re_{ft} = 3 \times 10^6$

X/D**	$P_w \times 10^{-3}$ (psf)	$\delta \times 10^{-4}$ (ft)	$\delta^* \times 10^{-4}$ (ft)	$\theta \times 10^{-5}$ (ft)	H	C_f	$\log_{10}(R_s^*)$	RHS of Eq. (B-1)
0.77144	1.017	0.8305	0.186	0.672	2.763	0.0306	4.247	5.697
0.77478	0.949	1.2783	0.230	0.822	2.801	0.0257	4.290	5.487
0.77831	0.884	1.0134	0.251	0.879	2.854	0.0224	4.320	5.200
0.78204	0.816	1.525	0.314	1.095	2.869	0.0193	4.355	5.124
0.78596	0.752	1.184	0.329	1.105	2.977	0.0173	4.372	4.597
0.79007	0.698	1.748	0.433	1.146	2.963	0.0137	4.402	4.657
0.79437	0.680	1.332	0.481	1.400	3.432	0.0089	4.405	3.548
0.79885	0.709	1.930	0.844	2.094	4.030	0.0022	4.449	7.555
0.80351	0.755	2.422	1.152	2.819	4.088	-.00091	4.476	8.406

**D = 1.4 in.